**Southeast Environmental Research Center**
FLORIDA INTERNATIONAL UNIVERSITY

# Annual Report: ecosystem dynamics in the White Zone: history, drivers, and restoration implications

**Task Agreement # P15AC01625**
**Cooperative Agreement # H5000-10-5040**

Period: October 4, 2016 to October 3, 2017

**Submitted to:**

**David Rudnick**
South Florida Natural Resources Center
Everglades and Dry Tortugas National Parks
950 N. Krome Ave., Homestead, FL 33030-4443
Tel. 305-338-3508, Fax. 305-224-4147
Email: David_Rudnick@nps.gov

**Mike Ross, Jack Meeder, Len Scinto, Jay Sah,**
**Susana Stoffella, Himadri Biswas, and Sean Charles**
Southeast Environmental Research Center
Florida International University, Miami FL 33199

2017

**Table of Contents**

EXECUTIVE SUMMARY

Much has been learned about the coastal ecosystems of the southeastern Everglades in Years 1 and 2 of the White Zone project, through studies of vegetation and soil processes operating in the present and the recent past. Section 1 of the Report indicates that during the two decades between the initial C111 study and the current one, coastal plant species have consistently integrated with and sometimes replaced more glycophytic species. The transition appears to be more pronounced in the wetland matrix than in the tree islands, suggesting some resilience in the latter. Inclusion of 17 tree islands sampled in 2018 and not yet included in the analysis will clarify the issue further. Invading red mangrove populations are strongly right-skewed (i.e., consist of many small and a few large individuals), and the invasion process is highly variable from east to west. Similarly, the zonal pattern evident in both marshes and tree islands differs sharply from the Biscayne Bay coast through the wetlands south of the C-111 Canal to those west of Taylor Slough. We expect these patterns to become interpretable as we link environmental drivers (salinity, nutrient availability, water regime) with the biotic communities, and integrate remote sensing study with our rich field data.

In Section 2, detailed examination of sediment cores illustrate the same marine transgressive sequence that we've seen in the vegetation during the last 20 years. In the sediment profiles, salt water encroachment is evidenced by a pattern in the transition from fresh water mollusk assemblages to marine species; across all transects studied so far, this transitions occurs at greater depth near the coast than far from it. The consistency of this pattern highlights the value of mollusks as indicators of the extent and rate of salt water encroachment. Changes in mollusk composition are paralleled by changes in the depositional environments expressed in the nature of the sediments. We recognize an interior-to-coast sequence of depositional environments, from peat formed under sawgrass cover, to marl formed under sparse sawgrass or scattered mangrove, to peat formed under full mangrove canopies. Recently published work (Meeder et al. 2017) and previously unpublished values presented in Section 3.2 call attention to the strong differences in sediment accumulation rates across depositional environments. $^{210}$Pb analyses for two cores in marl soils within the White Zone in this Report show that accumulation is extremely low in these environments, but those rates vary significantly at the decadal scale within a single core. We think that complementing rates from Sediment Elevation Tables with $^{210}$Pb analyses can aid greatly in interpretation of the capacity of coastal soils to keep up with sea-level rise.

At the scale of the local landscape, variation in soils between the marsh matrix and tree islands embedded within it is also substantial and important to consider. In Section 3.1, we report that nutrients, especially P, are concentrated in tree island soils, as they are in other parts of the Everglades. We expect to explore the linkage between the biogeochemical setting of the tree islands and their enhanced productivity further in the future. Currently, the finding that the relationships between nutrient concentrations and exoenzyme activity differ in tree island and adjacent marsh is intriguing, and signal that phosphorus availability may not limit production in tree islands, as it does in most Everglades wetland communities. Finally, in Section 3.3 the role of invading mangroves in organic matter production and soil stabilization is highlighted. Considering the full range of environments in the study area, mangrove cover proved to be the primary determinant of root biomass and ingrowth. It appears that the rate of response of mangroves to sea-level rise holds the key to the future of south Florida's coastal wetlands.

INTRODUCTION

North America's coastal wetlands have been in flux since the arrival of humans many millennia ago. In some places and times, wetland change resulted primarily from rapidly rising seas (Meeder and Parkinson 2017); in others, sea-level rise (SLR) was minimal, and the principal driver was direct human manipulation of coastal structure and process. Today, along the Atlantic and Gulf coasts, a combination of factors - rapid sea level rise, regulated water delivery, and reshaped and repurposed landscapes - have produced a dizzying assortment of wetland transitions that are difficult to integrate. A generalized framework of coastal ecosystem dynamics that would apply from Newfoundland to south Texas is certainly desirable, but such a model must also account for the local variations in climate, geology, tidal regime, watershed characteristics, and biotic diversity that constrain the transitions encountered in an individual region. Below we describe ecosystem dynamics in one such region, the marshes and swamps of the coastal Everglades south and east of the Miami Rock Ridge. Results from Year 2 of a three-year study in this region shows our research moving forward on many fronts. By the project's conclusion, we intend to arrive at and convey a holistic understanding of wetland transitions in the idiosyncratic south Florida environment. In the process, these results may strengthen the conceptual basis for a model of coastal wetland dynamics that could be applied anywhere.

STUDY DESIGN AND PROGRESS DURING 2016-2017

In 1994-96, an FIU research group led by Jack Meeder and Mike Ross undertook a study of the Southeast Saline Everglades (Egler 1952), i.e., the mainland wetlands flanking northeastern Florida Bay and southwestern Biscayne Bay. The FIU study (Meeder et al. 1996) demonstrated that both SLR and fresh-water discharge exerted important controls on plant and mollusk community dynamics, as well as on the relative proportions of organic and carbonate material in the coastal soils. Ecological changes consistent with saltwater intrusion were greatest in wetlands that had been cut off from upstream freshwater sources for many years, and least in wetlands still receiving fresh-water discharge. The Meeder et al. (1996) report and subsequent papers (Ross et al. 2000; Ross et al. 2002; Meeder et al. 2017) demonstrated that the interior border of the white zone – a zone of low productivity, in which a light-colored marl substrate is exposed by the low vegetation cover - is a broad but effective marker of coastal transgression. They also demonstrated that the composition of plant, mollusk, and diatom assemblages along the gradient are sensitive indicators of local conditions. Tree islands scattered across this landscape appeared to be somewhat more resistant to saltwater influence than surrounding plant communities in the marsh/swamp matrix, though they were distributed in a similar zonal arrangement relative to the coast (Ross et al. 2013). In the fall of 2015, the FIU research team began an expanded survey of southern Everglades coastal wetlands, intending (1) to document any changes that occurred during the ~20 year interval between surveys, and (2) to interpret such changes from the perspective that two decades of progress in coastal wetland science might provide. This Report describes progress made in the project so far, with emphasis on Year 2.

In the initial project, our group sampled vegetation and soils at 56 sites, extending as far as Taylor Slough on the west to the C-103 (Mowry) Canal on the east (Meeder et al. 1996). Sample locations were distributed along seven transects perpendicular to the Florida Bay or Biscayne Bay coastline. Vegetation cover ranged from pure mangrove swamp near the coast to

homogeneous sawgrass marsh in the interior. In the current project, we are resampling a subset of 28 of the original sites, while adding 11 sites in coastal marshes west of Taylor Slough, and another 9 sites north of Barnes Sound including three in the L-31E Pilot Project site whose sedimentary sequences were described in Meeder et al. (1996). We sample the marsh (or swamp) matrix and the closest well-developed tree island to the marsh plot center on separate excursions during October 2016 – May 2017 (**Figure 1; Tables 1 and2**).
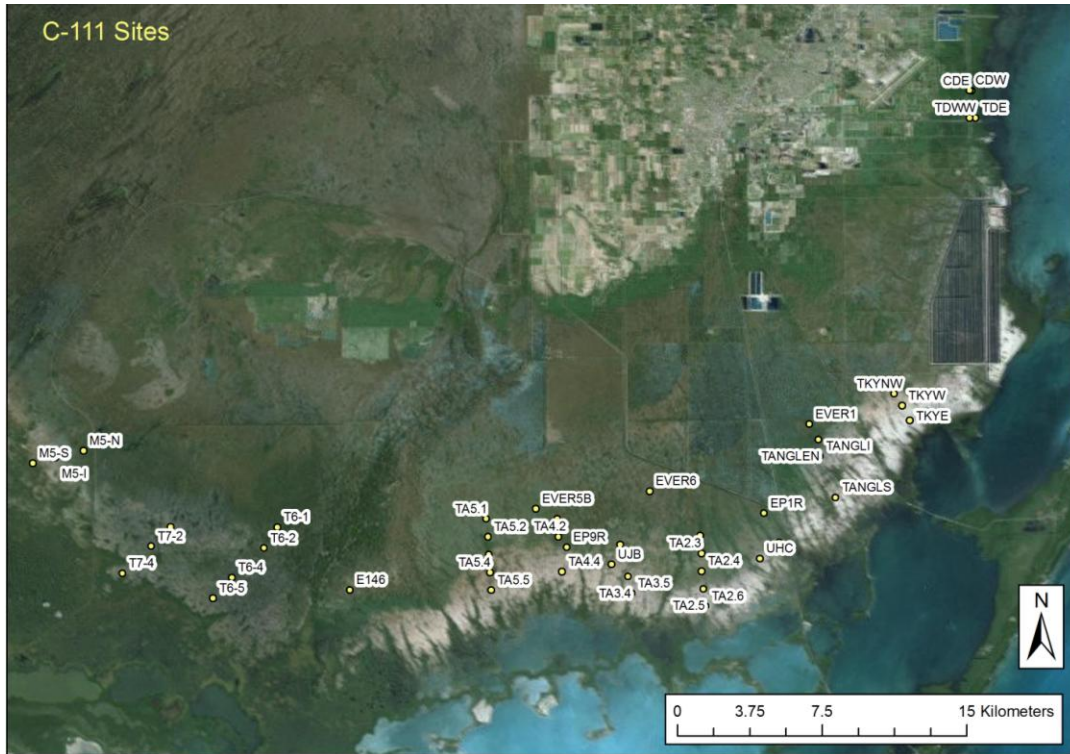


**Figure 1**: Map showing the location of sites proposed for vegetation sampling.

During the last year, we completed vegetation and soil sampling at 24 matrix sites and 17 tree islands. Below, we present results from our surveys of (1) matrix vegetation at all 48 sites sampled in 2016-17 and tree island composition at the 17 sites sampled in 2017, (2) spatial variation in mangrove structure in the marsh/swamp matrix east of Taylor Slough, (3) mollusk indicators of paleosalinity along 11 coastal transects not previously described, (4) soil characteristics at all matrix and tree island sampling locations, except for tree islands sampled in 2018 (5) soil accretion rates based on ^{210}Pb at two sites in the lower Everglades, and (6) root biomass and production in 24 matrix sites.

| Table 1: Marsh sites sampled in 1996 and 2016. | | | |
|---|---|---|---|
| **1990s Sites #** | Sites sampled in 1996 | 2016 Sites # | Sites sampled in 2016 |
| | | **1** | CDE |
| | | **2** | CDW |
| **1** | E146 | **3** | E146 |
| **2** | EP10 | **4** | EP10 |
| **3** | EP12R | **5** | EP12R |
| **4** | EP1R | **6** | EP1R |
| **5** | EP9R | **7** | EP9R |
| **6** | EVER1 | **8** | EVER1 |
| **7** | EVER5B | **9** | EVER5B |
| **8** | EVER6 | **10** | EVER6 |
| | | **11** | M5-I |
| | | **12** | M5-N |
| | | **13** | M5-S |
| | | **14** | T6.1 |
| | | **15** | T6.4 |
| | | **16** | T6.5 |
| | | **17** | T6.6 |
| | | **18** | T7.1 |
| | | **19** | T7.2 |
| | | **20** | T7.3 |
| | | **21** | T7.4 |
| **9** | TA2.2 | **22** | TA2.2 |
| **10** | TA2.3 | **23** | TA2.3 |
| **11** | TA2.4 | **24** | TA2.4 |
| **12** | TA2.5 | **25** | TA2.5 |
| **13** | TA2.6 | **26** | TA2.6 |
| **14** | TA3.3 | **27** | TA3.3 |
| **15** | TA3.4 | **28** | TA3.4 |
| **16** | TA3.5 | **29** | TA3.5 |
| **17** | TA4.1 | **30** | TA4.1 |
| **18** | TA4.2 | **31** | TA4.2 |
| **19** | TA4.4 | **32** | TA4.4 |
| **20** | TA5.1 | **33** | TA5.1 |
| **21** | TA5.2 | **34** | TA5.2 |
| **22** | TA5.3 | **35** | TA5.3 |
| **23** | TA5.4 | **36** | TA5.4 |
| **24** | TA5.5 | **37** | TA5.5 |
| | | **38** | TANGLEN |
| | | **39** | TANGLI |
| | | **40** | TANGLS |
| | | **41** | TDE |
| | | **42** | TDWW |
| **25** | TKYE | **43** | TKYE |
| **26** | TKYINT | **44** | TKYINT |
| | | **45** | TKYNW |
| | | **46** | TKYW |
| **27** | UHC | **47** | UHC |
| **28** | UJB | **48** | UJB |

| Table 2: Tree islands sites sampled in 1996 and 2016. | | | |
|---|---|---|---|
| **1990s Sites #** | Sites sampled in 1996 | 2016 Sites # | Sites sampled in 2016 |
| **1** | TI-EP12R | **1** | TI-EP12R |
| **2** | TI-EVER1 | **2** | TI-EVER1 |
| | | **3** | TI-M5N |
| **3** | TI-TA2.2 | **4** | TI-TA2.2 |
| **4** | TI-TA2.3 | **5** | TI-TA2.3 |
| **5** | TI-TA2.4 | **6** | TI-TA2.4 |
| **6** | TI-TA2.5 | **7** | TI-TA2.5 |
| **7** | TI-TA2.6 | **8** | TI-TA2.6 |
| **8** | TI-TA3.3 | **9** | TI-TA3.3 |
| **9** | TI-TA3.4 | **10** | TI-TA3.4 |
| **10** | TI-TA3.5 | **11** | TI-TA3.5 |
| | | **12** | TI-TANGLEN |
| | | **13** | TI-TANGLI |
| **11** | TI-UHC | **14** | TI-UHC |
| **12** | TI-UJB | **15** | TI-UJB |
| **13** | TI-TKYINT | **16** | TI-TKYINT |
| **14** | TI-TKYW | **17** | TI-TKYW |

RESULTS

## 1. Vegetation pattern, dynamics, and function

### 1.1. Vegetation change 1996-2016 in marsh/swamp matrix and tree island:

*Matrix vegetation:* In 2016 and 2017, shoot cover of each vascular plant species was estimated in 30 1 m$^2$ subplots distributed evenly along a $360^0$ arc at 50 m distance from the matrix plot center. The distribution of subplots was thus similar to the one used in the matrix sampling in 1994-96, but species cover was not estimated in the earlier study. To facilitate comparison between 1994-96 and 2015-17, we based our vegetation analyses on species frequencies (proportion of the 30 subplots in which each species was present). Temporal change in matrix vegetation were based on 28 plots common to the two studies, all of which are in the eastern portion of the study area (**Figure 1; Table 2**).

Multivariate techniques, including non-metric multidimensional scaling (NMS) ordination (McCune and Grace 2002), were used to examine vegetation:environment relationships in the matrix, and to illustrate temporal shifts in species composition along a distance-to-coast gradient. We also classified and characterized sites through application of an agglomerative hierarchical cluster method with flexible beta (−0.25) linkage (McCune and Mefford 2011). These analyses were applied to Site x Time combinations for the 28 sites sampled in both 1996 and 2016, plus the 20 sites sampled only in 2016 (**Table 1**). Data were species frequencies, relativized to the species maximum observed at any site. Species present in only one site were excluded from the analysis. A Mantel test (McCune and Grace 2002) was applied to assess the relationship between species composition and distance to the coast. In this procedure, the ordination axes were firmly rotated so that Axis 1 was aligned with distance to the coast, and the second axis was orthogonal to the first. In NMS ordination space, the direction of a shift in species composition at a site was indicated by an arrow between the 1994-96 and 2015-17 assemblages, and change across all sites was indicated by an arrow connecting centroids that represented the two sampling periods. Analysis of similarity (ANOSIM) (Clarke and Warwick 2001) was used to examine the significance of the difference in overall species composition between sampling periods, and paired t tests were used to test whether matching sites scores on Axis 1 differed between years. ANOSIM was also used to quantify differences among cluster derived groups.

*Tree islands*: Vegetation was sampled in 17 tree islands in 2017. 14 of these had also been sampled in 1994-96 (**Table 2**). In both periods, a single observer spent 30-60 minutes thoroughly searching each island for plant species. In both 1994-96 and 2017, species present in the tree islands were ranked based on canopy cover. Species ranked 1 to 4 were assigned an abundance of 10, those ranked 5 to 8 an abundance of 5, those ranked 9 to 12 an abundance of 2, and those ranked 13 or more an abundance of 1. Species abundances were relativized to the observed species' maximum, as in the original study. Ordination, vector fitting, and temporal comparisons were implemented as described above for the matrix vegetation.

## Results and Discussion

*Matrix vegetation composition*

NMS analysis (**Figure 1.1.1**) indicated that marsh vegetation was arranged primarily along a gradient of distance to the coast. Inland marsh sites to the right along Axis 1 are characterized by sawgrass (*C. jamaicense*) or spikerush (*Eleocharis cellulosa*) while in the center sites are dominated mainly by red mangrove (*Rhizosphora mangle*). The negative side of axis 1 is occupied by coastal sites dominated by halophytes like saltgrass (*Distichlis spicata*), black needle rush (*Juncus roemerianus*) and other mangrove species ((white mangrove (*Laguncularia racemosa*), black mangrove (*Avicennia germinans*), and buttonwood (*Conocarpus erectus*)). Variation in vegetation composition among all sites over the sampling period (1996-2016) was adequately summarized by a two dimensional NMS ordination (Stress = 0.16). Distance to coast was significantly correlated to species composition (Mantel test 999 permutations, r=0.16, p<0.01).
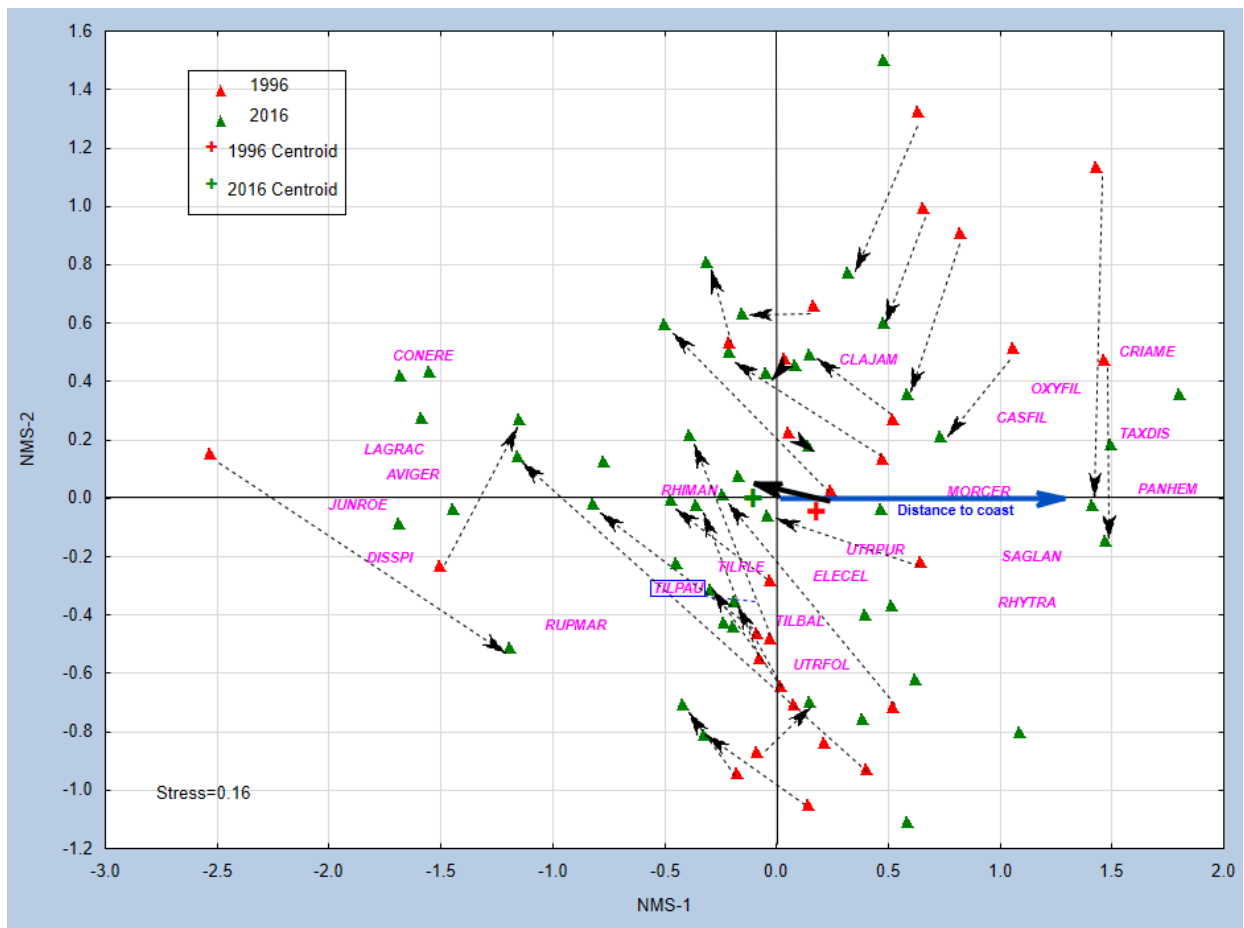


**Figure 1.1.1**:Non-metric Multidimensional Scaling (NMS) Ordination Axis-1 and 2 of marsh sites sampled in 1996 and 2016. Change direction for sites and group centroids between years are indicated by dotted and solid arrows respectively.

Cluster analysis resulted in sites grouped into three floristically distinctive units: Marl Marsh, Spikerush-Mangrove Scrub, and Mangrove Tidal Swamp (**Table 1.1.1**); in **Figure 1.1.1**, these units are arrayed from positive to negative along Axis 1. Significant differences among the groups were

| Table 1.1.1: Mean relative frequency of common matrix species (i.e. present in ≥ 3 sites) ordered by NMS-1 scores in three matrix vegetation types. | | | | |
|---|---|---|---|---|
| **Species Name** | Species Code | Marl Marsh | Spikerush-Mangrove Scrub | Mangrove Tidal Swamp |
| *Panicum virgatum* | PANVIR | 0.04 | | |
| *Crinum americanum* | CRIAME | 0.08 | | |
| *Panicum tenerum* | PANTEN | 0.06 | | |
| *Taxodium distichum* | TAXDIS | 0.07 | | |
| *Oxypolis filiformis* | OXYFIL | 0.10 | | |
| *Bacopa caroliniana* | BACCAR | 0.04 | | |
| *Symphyotrichum tenuifolium* | ASTTEN | 0.05 | | |
| *Sagittaria lancifolia* | SAGLAN | 0.10 | 0.04 | |
| *Cassytha filiformis* | CASFIL | 0.16 | | |
| *Rhynchospora tracyi* | RHYTRA | 0.09 | 0.09 | |
| *Morella cerifera* | MORCER | 0.05 | 0.05 | |
| *Cladium jamaicense* | CLAJAM | 0.94 | 0.14 | |
| *Eleocharis celulosa* | ELECEL | 0.48 | 0.87 | 0.09 |
| *Utricularia purpurea* | UTRPUR | 0.11 | 0.22 | |
| *Tillandsia flexuosa* | TILFLE | 0.06 | 0.10 | |
| *Utricularia foliosa* | UTRFOL | 0.01 | 0.08 | |
| *Tillandsia balbisiana* | TILBAL | 0.03 | 0.04 | |
| *Tillandsia pauciflora* | TILPAU | 0.05 | 0.19 | |
| *Tillandsia spp* | TILSPP | 0.03 | 0.03 | 0.04 |
| *Rhizosphora mangle* | RHIMAN | 0.36 | 0.52 | 0.81 |
| *Rupia maritima* | RUPMAR | | 0.05 | 0.18 |
| *Conocarpus erectus* | CONERE | | | 0.19 |
| *Avicennia germinans* | AVIGER | | | 0.42 |
| *Laguncularia racemosa* | LAGRAC | | | 0.42 |
| *Distichlis spicata* | DISSPI | | | 0.23 |
| *Juncus roemerianus* | JUNROE | | | 0.19 |

confirmed by ANOSIM (999 permutations, Global R = 0.724, p-value < 0.01), with Mangrove Tidal Swamp clearly the most distinct of the three, and Marl Marsh and Spikerush-Mangrove Scrub exhibiting some overlap (**Table 1.1.2**). Marl Marsh sampled in this study is characterized by sawgrass (*Cladium jamaicense)* accompanied by freshwater marsh species like arrowhead (*Sagittaria lancifolia*), love vine (*Cassytha filiformis*), beaksedge (*Rhynchospora tracyi*) and string-lili (*Crinum americanun*). Spikerush-Mangrove Scrub is distinguished by spikerush and

red mangrove, while all three mangrove species (*Rhizosphora mangle*, *Avicennia germinans* and *Laguncularia racemosa*) and halophytes like saltgrass (*Distichlis spicata*) and black needle rush (*Juncus roemerianus*) can be found in the Mangrove Tidal Swamp (**Table 1.1.1**). Species density (number of species per 1-m$^2$ subplot) was highest in the Marl Marsh (2.84±1.31), intermediate in the Mangrove Tidal Swamp was (2.37±1.27) and lowest in the Spikerush-Mangrove Scrub (2.09±0.40).

| **Table 1.1.2**: ANOSIM distances and significance (p-value) among 3 cluster derived groups. | | | |
|---|---|---|---|
| | Marl Marsh | Spikerush-Mangrove Scrub | Mangrove Tidal Swamp |
| Marl Marsh | - | 0.648 (<0.01) | 0.865 (<0.01) |
| Spikerush-Mangrove Scrub | | - | 0.834 (<0.01) |
| Mangrove Tidal Swamp | | | - |

The spatial arrangement of matrix vegetation sites is illustrated in the spatial distribution of the three floristic units among our sampling locations (**Figure 1.1.2**). Mangrove Tidal Swamp is characteristic of the easternmost portion of the study area, i.e., wetlands draining into Biscayne Bay; among sites classified in this unit, only UHC is located west of US 1. Within the C111 Basin between US 1 and Taylor Slough, Marl Marsh and Spikerush-Mangrove Swamp are arranged in interior and coastal bands, respectively. Further west, where freshwater flow is enhanced and the Buttonwood Embankment limits the input of tidal waters, the zonal arrangement of these units is no longer evident.
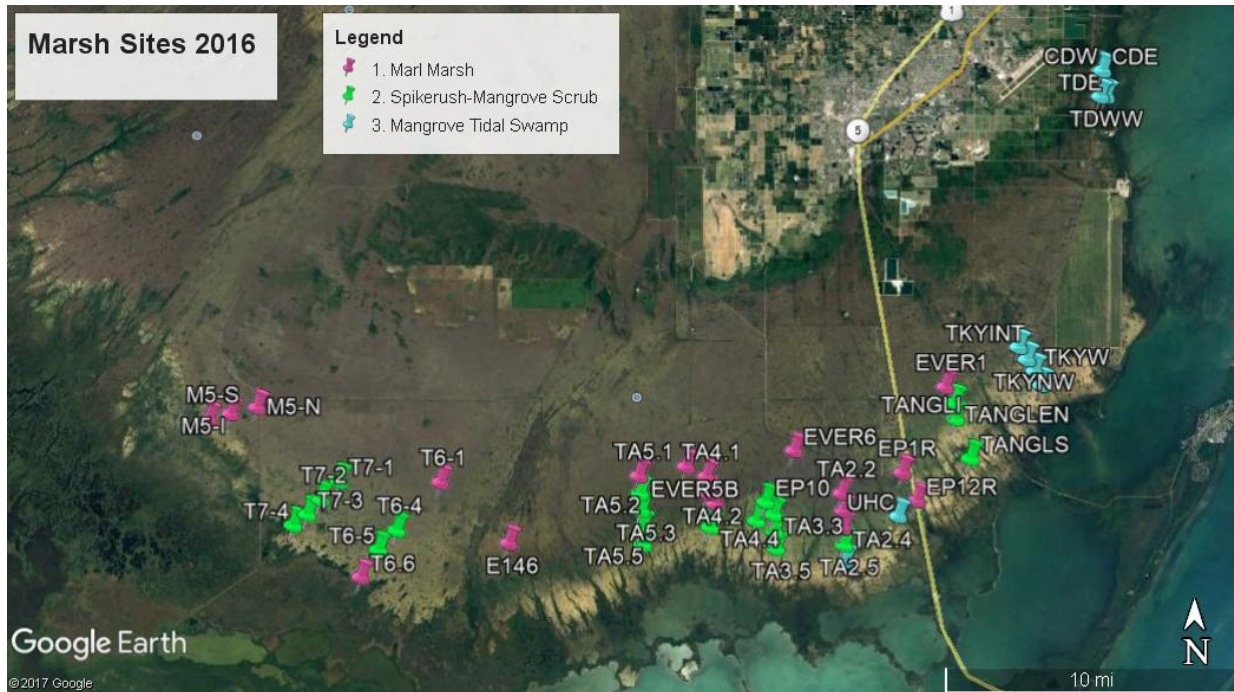


**Figure 1.1.2**: Map showing current distribution of 3 matrix vegetation floristic units.

*Matrix vegetation dynamics*

Considering the subset of sites sampled in both years (all in the Southeast Saline Everglades east of Taylor Slough), marsh sites located on the positive side of Axis 1 tended to move toward the negative pole over the 1996-2016 period. Vegetation change at individual sites (indicated by small arrows) and across the study area as a whole (indicated by the thick arrow linking the centroids for each year) was marked by a small but notable movement toward more coastal vegetation assemblages. Species composition (position along Axis 1, reflecting distance-to-coast) differed significantly between sampling years (t=3.07, df=27, p-value<0.01).

Among the 28 sites sampled in both 1996 and 2016, only four sites changed from one floristic unit to another. Three of the four transitioned to a more coastal assemblage (Site TA5.2, which changed from Marl Marsh to Spikerush-Mangrove Scrub, and Sites TA2.6 and UHC, which changed from Spikerush-Mangrove Marsh to Mangrove Tidal Swamp). Only Site EP12R changed in the opposite direction, from Spikerush-Mangrove Scrub to Marl Marsh.

*Tree island composition and dynamics*

**Figure 1.1.3** presents the NMS ordination based on the 17 islands sampled in 2017, along with equivalent data from 1996. The three dimensional ordination was characterized by a low level of stress (0.11). However, unlike the ordination of matrix vegetation presented in **Figure 1.1.1**, distance to coast was weakly related to species composition (Mantel test 999 permutations, r=0.025, p<0.26). ANOSIM revealed no difference across the data set among sampling years (ANOSIM; 999 permutations, R = 0.03, p-value < 0.21), and t-test comparing scores on Axis 1 in 1996 and 2016 likewise showed no significant change over time (t=1.44, df=13, p-value<0.07). Nevertheless, the ordination does place forests that include freshwater tree species like pond apple (*Annona glabra*) and strangler fig (*Ficus* spp) on the positive side of Axis 1, while salt tolerant tree species more characteristic of coastal areas (e.g., black mangrove (*Avicennia germinans*), joewood (*Jacquinia keyensis*), and christmasberry (*Lycium caroliniensis*)) occupy the negative side. These data suggest that a) tree island assemblages are not as zonally arranged relative to the coast as matrix vegetation, and b) tree islands may be buffered from some of the effects salt water encroachment that have likely driven change in the marsh matrix. Because the tree islands sampled in 2017 represent just over one-third of the complete set (17 of 48) to be sampled by the end of the project, vegetation analysis based on the full data set may lead to different conclusions.
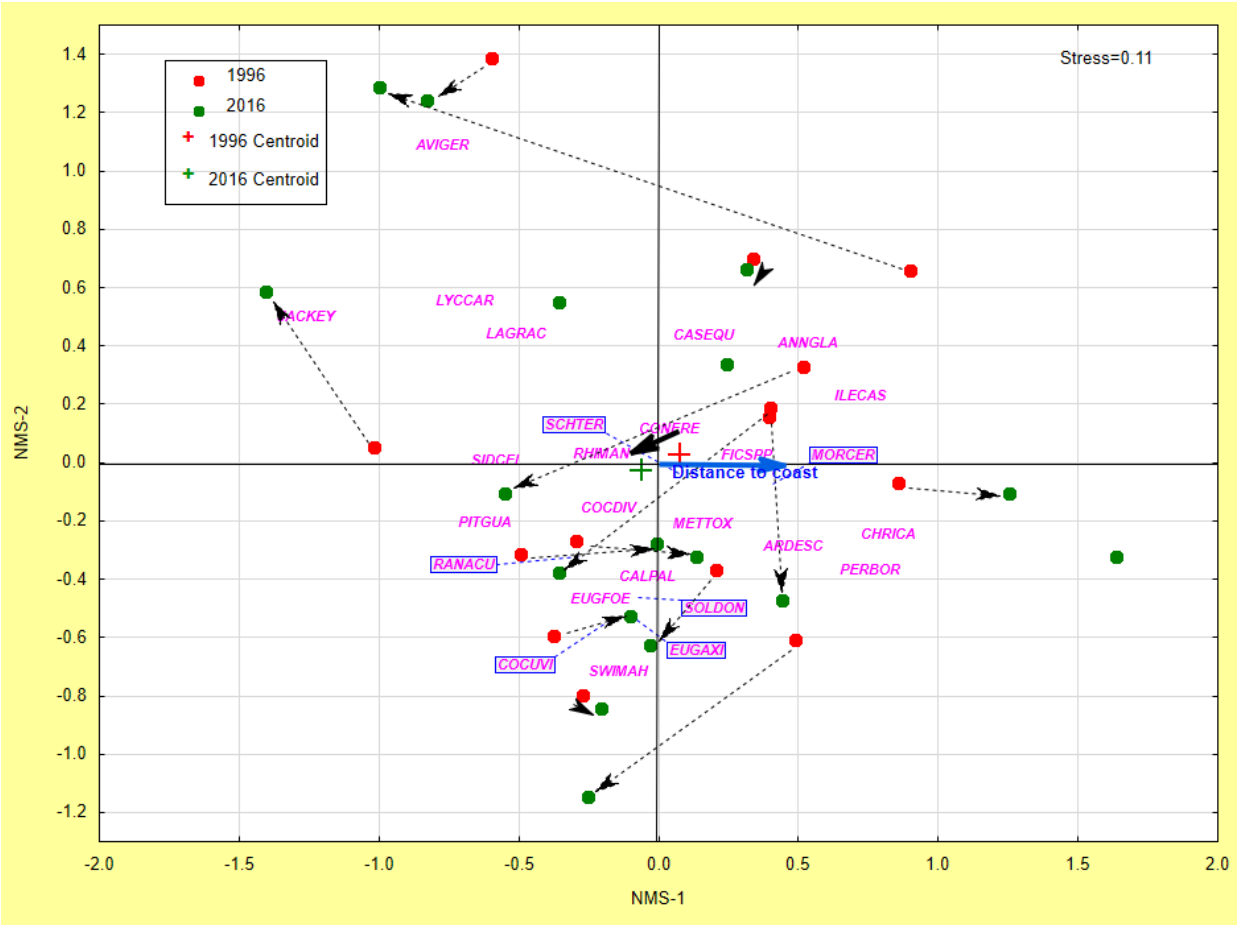
**Figure 1.1.3**:Non-metric Multidimensional Scaling (NMS) Ordination Axis-1 and 2 of tree islands sites. Change direction for sites and group centroids between years are indicated by dotted and solid arrows respectively.

### 1.2. Change in mangrove structure in the marsh/swamp matrix:

The objective of the study reported below is to gain an understanding of the spatial distribution of *Rhizophora mangle* (red mangrove) in the southern Everglades using georeferenced aerial images (orthophotographs) and Geographical Information System (GIS). By understanding the current distribution of *R. mangle*, we hope to gain insight into the processes driving the species' inland expansion from coastal areas into the freshwater marsh.

Manual remote sensing and GIS techniques were used. Though laborious, manual methods were deemed necessary in the early stage of our research on mangrove expansion. By forming a reliable baseline for pattern recognition, such analyses will aid us in transitioning to the use of advanced remote sensing and GIS techniques with medium-high resolution satellite images. Using orthophotgraphs on a GIS platform, we identified and counted individual mangrove shrubs, measured their crown diameters, and calculated average % crown cover and tree density. We envisioned the invasion process as a moving wave progressing inland, beginning with the establishment and growth of an initial cohort of mangroves relatively close to the coast. With time these colonists would produce new propagules that would be transported by tides toward the interior, where they would become established. In the zone of initial establishment, the coastal mangroves would grow larger, but due to competition for space and other resources, tree density would decrease. The more inland ones would be smaller shrubs with smaller crowns and higher tree density. Thus, we expected our analyses to show crown cover of red mangroves decreasing and tree density increasing from coast to interior.

**Study locations:** We collected data from 15 sites along five transects established in the project. These transects are south of Turkey Point (TKY_), in the triangular area between Card Sound Rd and South Dixie Highway (TANGL_), and three areas south of the C-111 Canal and west of US 1 (TA2_, TA3_, and TA5_) (**Figure 1.2.1**). Three sites were selected along each transect to examine whether the distribution of red mangroves from population to population along the same transect support the hypothesis stated above. Hereafter, we refer to the transect sites located nearest to the coast as Coastal, the sites in the middle as Intermediate, and the sites located most inland as Interior.

**Data and Methodology:** Orthophotographs were obtained from the Florida Department of Transportation for the year 2016 with a spatial resolutions of 0.25 and 0.8 foot. As higher resolution (0.25 foot) images were not available for all transects, we resampled the 0.25 foot resolution images to 0.8 foot resolution to maintain uniformity in counting and measurement of crown diameters. The methodology is described in detail in **Appendix 1.2.1**. The distribution of crown sizes, average % cover, and average tree density were calculated from 0.8 foot resolution images. Average % cover will hereafter be referred to as cover and average tree density as tree density, expressed as number of trees per hectare. Distances of the sites from the coast were also calculated. We evaluated if our methodology can be used with lower resolution (3 feet) orthophotographs. Data was processed in ESRI ArcGIS 10.5 platform. Data analysis was performed using MS Excel and R statistical software.
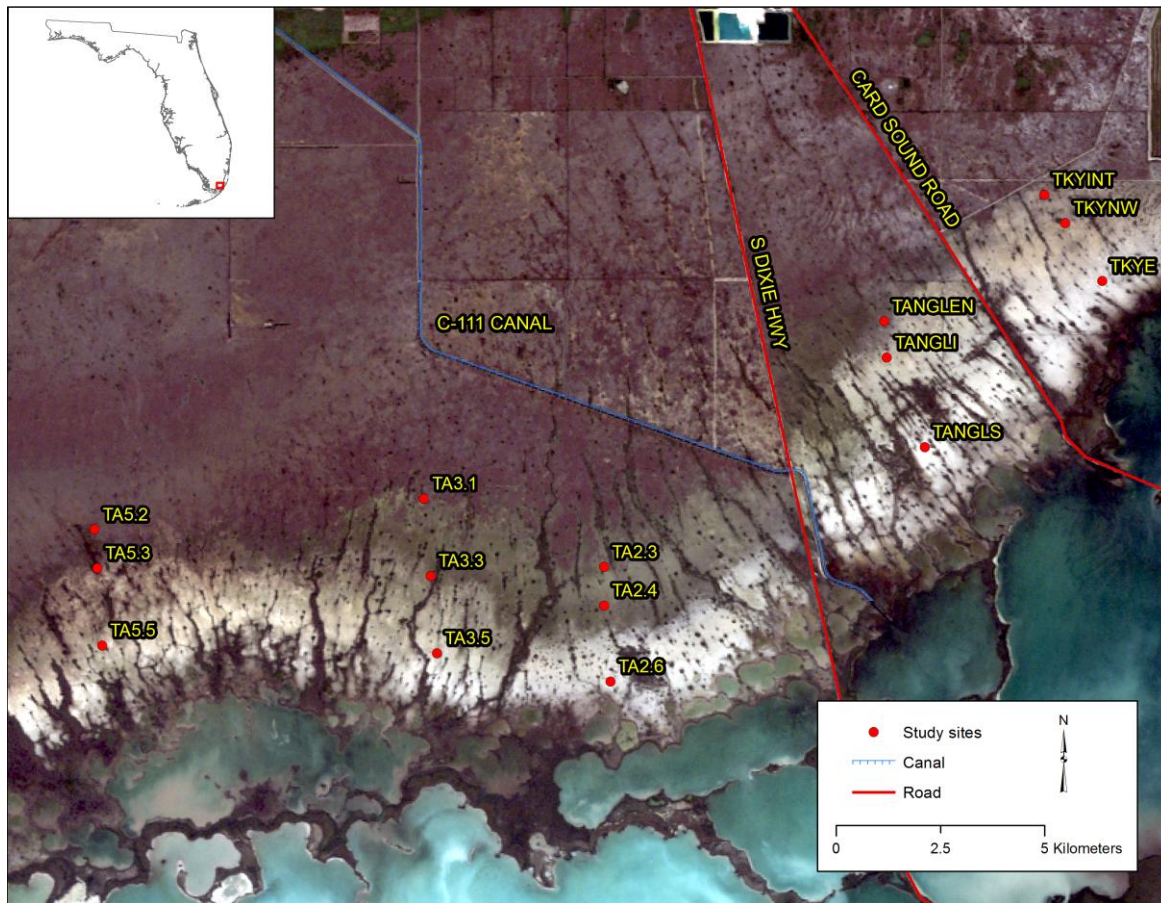
**Figure 1.2.1**. Location of study sites along transects.

To determine how well remote sensing data represent real world approximations, the remotely sensed sampling data of 0.8 foot resolution for all the 15 sites were compared with field sampled data. Beginning in 2016, extensive vegetation sampling was conducted by teams of technicians and students at each of the sites except TA3.1. The sites were visited by helicopter. Vegetation composition and structure were documented in 30 1 m$^2$ quadrats equally spaced at 50 m distance from the plot center.

## Results

### *Red mangrove population structure*

Crown size distributions are shown in **Table 1.2.1** and **Figure 1.2.2.** The right-skewness of all distributions is evident (**Figure 1.2.2**). As such, the means of crown sizes from all sites were higher than the median (**Table 1.2.1**). The skewness is mainly due to higher end values and outliers. With three exceptions, kurtosis values for crown sizes were positive; several were highly positive or leptokurtic, meaning that they had sharper peaks in comparison to a normal distribution. In the few sites with negative kurtosis, values were very close to 0. There appeared to be little relationship between median tree size and position along the transects. For example, the highest and lowest median tree sizes were both found at coastal sites (TA5.5, 1.78 m; and TKYE, 0.48 m).

14

**Table 1.2.1.** Summary statistics of crown sizes (m) for each site along transects from 0.8 foot resolution images.

| Sites | n | mean | std. dev | median | min | max | range | skew | kurtosis |
|---|---|---|---|---|---|---|---|---|---|
| | | | | | | | Statistic | | |
| TKYINT | 207 | 0.83 | 0.44 | 0.73 | 0.24 | 3.19 | 2.95 | 2.58 | 9.35 |
| TKYNW | 128 | 0.82 | 0.50 | 0.73 | 0.24 | 3.64 | 3.40 | 2.85 | 10.78 |
| TKYE | 209 | 0.55 | 0.26 | 0.48 | 0.24 | 1.44 | 1.20 | 0.85 | 0.43 |
| TANGLEN | 128 | 1.12 | 0.55 | 0.98 | 0.48 | 3.38 | 2.90 | 1.36 | 2.22 |
| TANGLI | 122 | 1.32 | 0.57 | 1.21 | 0.24 | 3.66 | 3.42 | 0.92 | 1.35 |
| TANGLS | 202 | 1.10 | 0.47 | 1.00 | 0.24 | 3.01 | 2.77 | 0.83 | 1.31 |
| TA2.3 | 109 | 0.97 | 0.56 | 0.80 | 0.37 | 3.74 | 3.37 | 2.66 | 8.40 |
| TA2.4 | 108 | 1.60 | 0.58 | 1.47 | 0.59 | 3.01 | 2.42 | 0.71 | -0.32 |
| TA2.6 | 90 | 0.85 | 0.35 | 0.79 | 0.34 | 1.93 | 1.59 | 0.79 | 0.28 |
| TA3.1 | 150 | 0.99 | 0.57 | 0.76 | 0.24 | 3.44 | 3.20 | 1.61 | 3.08 |
| TA3.3 | 122 | 1.17 | 0.57 | 1.03 | 0.34 | 3.77 | 3.43 | 2.05 | 6.22 |
| TA3.5 | 120 | 0.93 | 0.45 | 0.82 | 0.26 | 2.59 | 2.33 | 1.19 | 1.75 |
| TA5.2 | 163 | 0.96 | 0.56 | 0.75 | 0.26 | 4.09 | 3.83 | 1.75 | 5.04 |
| TA5.3 | 201 | 1.08 | 0.42 | 0.99 | 0.26 | 2.22 | 1.96 | 0.63 | -0.30 |
| TA5.5 | 72 | 1.75 | 0.84 | 1.78 | 0.26 | 3.83 | 3.57 | 0.21 | -0.52 |
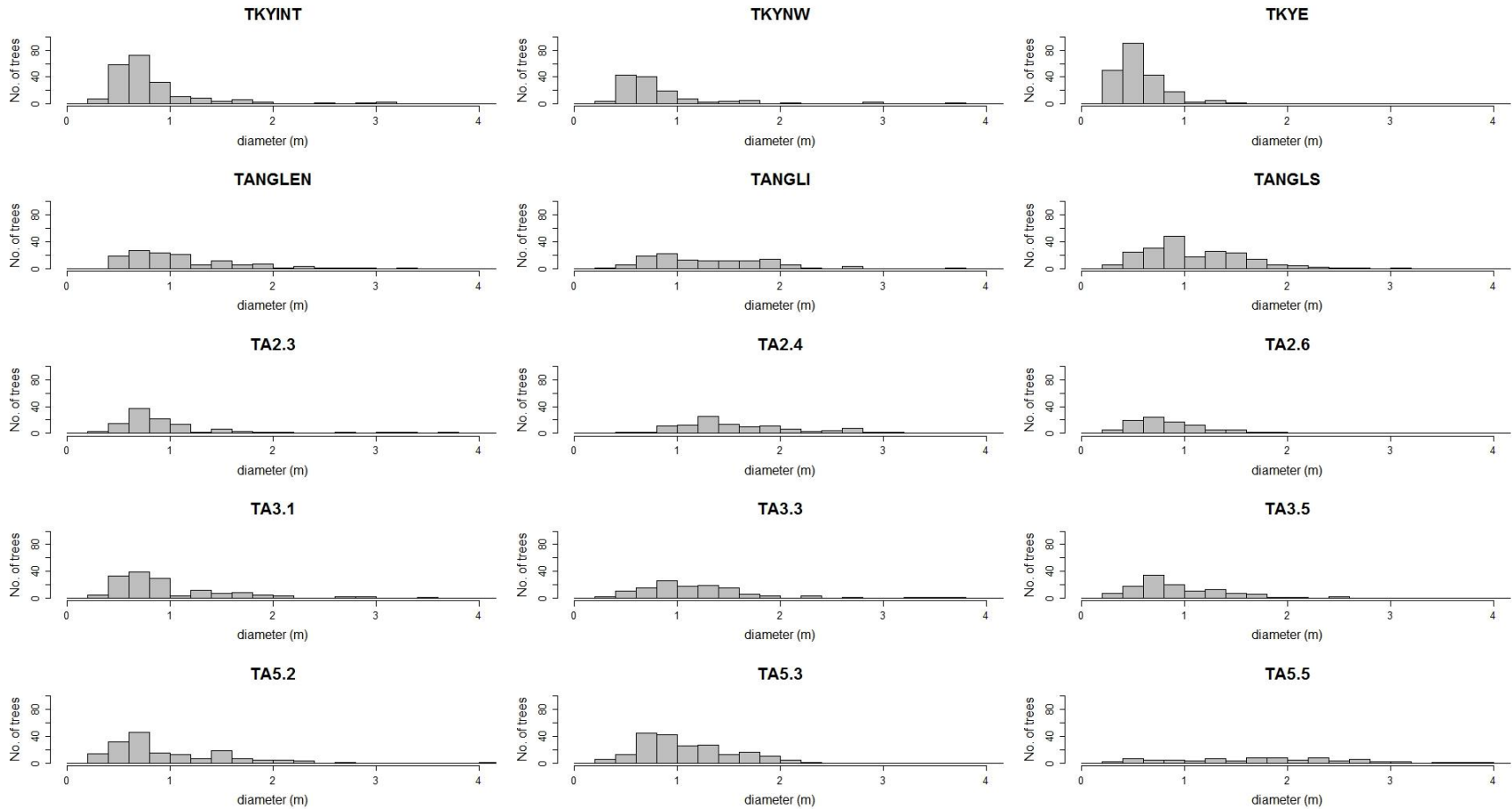
**Figure1.2.2.** Histogram of crown sizes (m) for all the 15 sites from 0.8 foot resolution orthophotographs.

*Red mangrove abundance*

Crown cover and tree density along transects vary from coast to interior sites and also among transects (**Figures 1.2.3, 1.2.4**, and Appendix 1.2.3: Figures A 1.2.1 and A 1.2.2). *R. mangle* mean crown area, tree density and cover for all 15 sites are presented in **Table 1.2.2**. Transect-wise is provided in Appendix 1.2.2.

| **Table1.2.2.** Mean crown area, tree density and cover from 0.8 feet resolution orthophotos. | | | |
|---|---|---|---|
| **Transect sites** | **Mean red mangrove crown area (m$^2$)** | **Red mangrove tree density (#/ha)** | **Total red mangrove cover (%)** |
| TKYINT | 0.38 | 2070 | 14.20 |
| TKYNW | 0.51 | 1280 | 9.28 |
| TKYE | 0.33 | 2090 | 5.96 |
| TANGLEN | 1.33 | 1280 | 15.52 |
| TANGLI | 1.87 | 1220 | 19.71 |
| TANGLS | 1.14 | 2020 | 22.63 |
| TA2.3 | 0.99 | 1090 | 10.76 |
| TA2.4 | 2.27 | 1080 | 21.86 |
| TA2.6 | 0.67 | 900 | 6.02 |
| TA3.1 | 1.15 | 1500 | 15.25 |
| TA3.3 | 1.33 | 1220 | 16.21 |
| TA3.5 | 0.84 | 1200 | 10.00 |
| TA5.2 | 0.97 | 1630 | 15.79 |
| TA5.3 | 1.06 | 2010 | 21.35 |
| TA5.5 | 2.96 | 720 | 21.30 |

Cover and tree density for each transect site were plotted against distance from the coast (**Figures 1.2.3, 1.2.4**) to identify if the crown cover and tree density change with distance from the coast. Although, the general trend suggested that crown cover increased and tree density decreased with distance from the coast, the regression slopes did not differ significantly from zero.
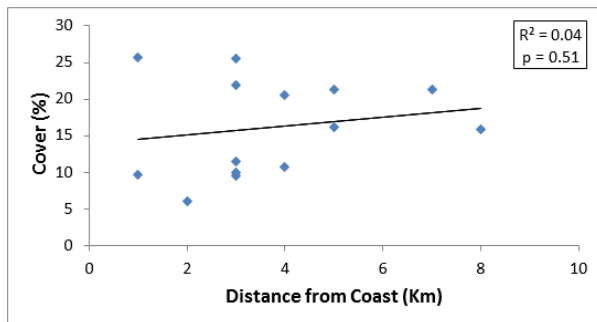


**Figure 1.2.3.** Cover with distance from coast**.**
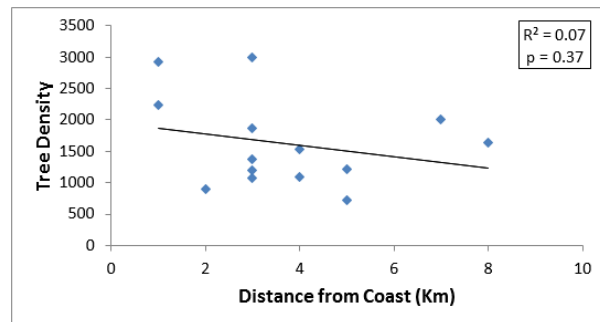
**Figure1.2.4.** Tree density with distance from coast.

*Evaluation of methodology if used with lower resolution orthoimages.*

Our results indicate one time distribution of mangrove shrubs, however, this information alone is not sufficient to understand the encroachment process. Thus, we intend to analyze orthophotos from the 1990s and/or 2000s using the same methodology to identify how mangrove structure and distribution have changed over time. Since the orthophotos from earlier periods are coarser in spatial resolution (3 feet, which will allow linear measurement of 1 m), we investigated if our methodology alone would be adequate to extract this information from these images (see Appendix 1.2.1). In sites where smaller shrubs dominate (in this case, crown diameters < 1 m), significant amounts of crown area will not be captured using 3 feet resolution images (Appendix 1.2.4: Table T 1.2.1). **Figure 1.2.5**, in which the cumulative percent of total mangrove area at Site TA3.5 is plotted against crown diameter, illustrates this data loss: 29% in trees smaller than the spatial resolution of historical aerial photos. Across the 15 sites examined, the % crown area < 1m diameter ranged from 2.6% - 82.3% (mean = 27.3%; standard error = 5.10; Appendix 4, Table T1.2.1). The assessment of historical dynamics in mangrove populations that we intend to do will need to be cognizant of this data limitation, and we will restrict our conclusions accordingly. Looking toward the future, use of more advanced remote sensing algorithms with high resolution satellite images as well as LIDAR data may allow more complete representations of mangrove dynamics.

*Comparison of cover from remotely sensed method with field estimates.*

The cover estimate for TKYE was remarkably low compared to field observation. TKYE was also the site where small stems were most important (82% of area in crowns < 1 m diameter). When we removed this outlier from the data set, the RMSE for cover estimated from remote sensing method and fieldwork was 8.62, with field observed cover underestimated, and especially in the most open stands (**Figure 1.2.6**).
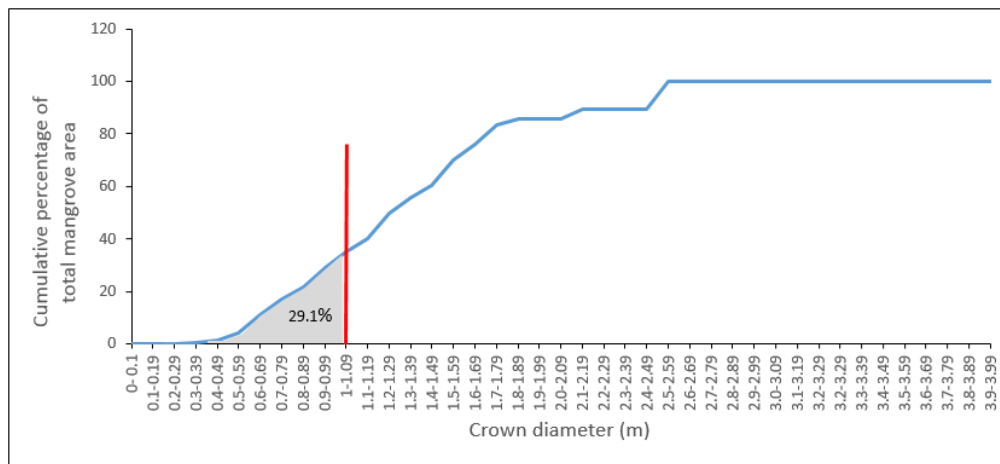


**Figure1.2.5.** Representation of data loss (area in grey color) at site TA3.5 if a 3 foot resolution orthophoto is used. The red line at 1m on x-axis indicates the diameter below which no measurements will be possible when 3 feet resolution orthoimage will be used. Consequently, over 29% of the crown area will not be captured.
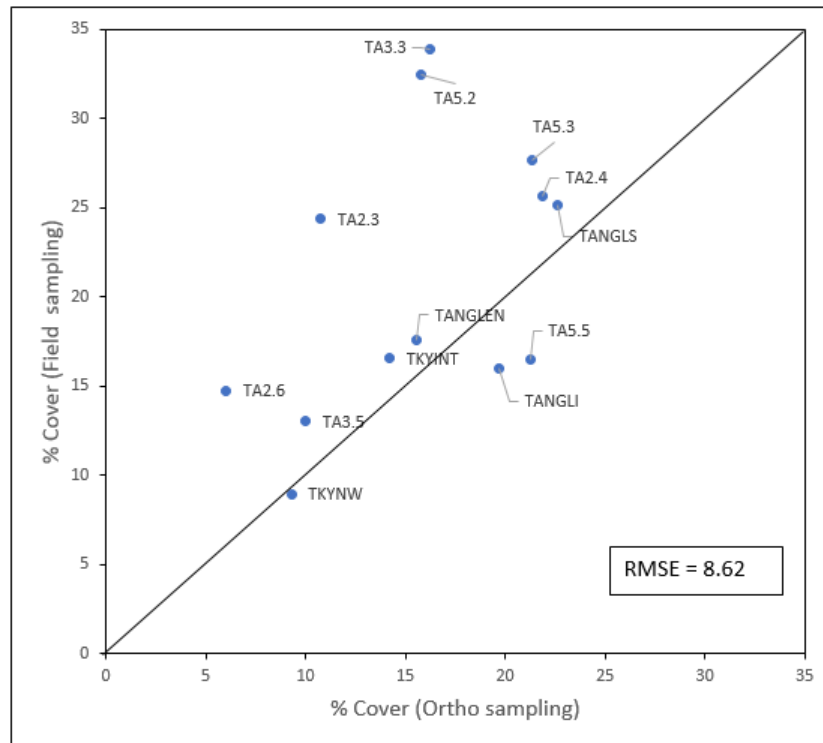
**Figure1.2.6.** Scatterplot of cover estimated from remote sensing method and fieldwork (Without site TKYE).

Our study has highlighted an important perspective on the distribution of red mangrove population in the southern Everglades. We have generated a dataset which could be used as a baseline data for pattern recognition and for comparison with either old remote sensing data or evolving very high resolution orthoimagery or satellite images in the future.

## Discussion

We have shown in this study the distribution of the *R. mangle* population. The distributions of crown cover and crown size have diverse pattern along transects from coastal to interior sites and among transects. We observed from the histograms of the crown sizes that they were right skewed and sometimes leptokurtic due to high end values or outliers. It could be that these trees with larger crowns are remnants from the first batch of red mangroves that arrived at those locations. These large crowned mangroves have to be investigated further to see how they have grown over the years and if they could yield useful information regarding the encroachment process. Compared to field estimated cover, our cover estimation was mostly low most notably for the site TKYE. This underestimation of cover could be a combination of the inherent properties of the orthophotos, such as their spatial resolution; error in identification of the mangroves due to mixed signature from surrounding vegetation; or positioning of the mangroves in the shadow zone. The high values in the field needs to be verified as well.

The trend and regression analysis of crown cover and tree density with distance from the coast did not show any definite pattern. The expectation that the points lying closer to the coast would have higher crown cover was observed only on two transects, TANGL and TA5. However, there is a striking dissimilarity between the two. The coastal site TA5.5 and the intermediate site TA5.3 on transect TA5 have same average crown cover but the tree density is considerably less

19

at the coastal site and tree size is higher; this is the combination that we expected and hypothesized. Even in the case of TANGL, where mangrove cover does decrease inland, the interior-ward decrease in cover from coast to intermediate site results from low tree density at the intermediate site, though that site supports relatively large trees. If tree size can be equated with age, then it appears that the intermediate site was colonized rapidly, but subsequent recruitment did not keep pace. The natural gradient which is expected along transects from coast to interior would have mature, older mangroves with large crown size at the coast and smaller, young shrubs with small crown size at the interior. But this is obviously not observed along other transects.

So what does it mean then? Shall we blatantly reject our hypothesis? The answer is complicated. First, the watershed is very complex. Transect TKY is located east of Card Sound Road, transect TANGL is situated between South Dixie Highway and Card Sound Road, and the remaining transects lie in the C111 basin. These areas differ in terms of freshwater input from the canals and how well surface water drains. Second, these three areas are influenced by different marine sources, either Biscayne Bay or Florida Bay. Biscayne Bay is a high energy system with stronger tides compared to Florida Bay which is gentler with less tidal effect. Third, cycles of establishment, growth, and mortality have to be considered. Establishment of new mangroves, growth, and mortality could be impacted by both natural and man-made influences. For example, coastal site TKYE has small shrubs with small crown diameter whereas coastal site TA5 have larger shrubs with larger diameter. Does that mean the older shrubs at TKYE have been replaced by newer shrubs after succumbing to some major disturbance, perhaps a cold temperature event or Hurricane Andrew? Can we expect a similar phenomenon at TA5? Perhaps these changes could be traced using remote sensing data from a different time period. Factors that contribute to mangrove establishment, growth, and mortality include salinity, freshwater input, hurricanes and tidal events. The effects of these factors have not been analyzed and is beyond the scope of this report. However, it must be mentioned that this study was successful in identifying some definite patterns in different parts of the watershed and raising some important questions, especially regarding how the populations we've described here have developed and changed over time. A time-series analysis using orthophotographs as well as satellite images from previous years would be more meaningful and it will give us a better understanding about the encroachment process. Older orthophotos will not be as high in resolution as the orthophotos used in this study and we expect that smaller crowns will not be detected in the older coarse resolution orthoimages. However, we believe that usage of sophisticated and advanced remote sensing methods such as principal component analysis, vegetation indices, etc., using medium-high resolution multispectral satellite images, and lidar data in conjunction with the methods used in this study using orthoimages will yield substantial information about the encroachment process of *R. mangle*.

## 2. Environmental and paleo-indicators

### 2.1. Diatom patterns in surface sediments:

Analysis of the diatom flora for the C-111 sites were initiated last year by Dr. Anna Wachnicka, and 17 marsh sites were completed and described in the 2016 report. Since that time, Dr. Wachnicka has moved on to a position at the South Florida Water Management, but is collaborating with Dr. Evelyn Gaiser's lab to complete the work. Eric Massa, a graduate student in the periphyton lab, has processed the samples as described below, and will soon initiate the diatom counts.

Periphyton samples were processed and subsampled for soft algae counts, diatom counts, nutrient analysis, chlorophyll a analysis, and ash-free dry mass. Samples were homogenized in a beaker and initial wet weight and dilution volume were recorded. Subsamples of 120 ml (nutrient analysis), 40 ml (ash-free dry mass), 10 ml (chlorophyll a), 10 ml (diatoms), and 1 ml (soft algae) were taken. Subsamples for nutrient analysis and ash-free dry mass were dried in an oven at 80° C before further processing. Chlorophyll a subsamples were diluted with an additional 90 ml of DI water before a 1 ml subsample of the mixture was vacuumed on a glass fiber filter. The filters with the diluted chlorophyll subsamples, as well as the subsamples for diatom and soft algae counts were frozen until further processing began.

The subsamples for ash-free dry mass were weighed before and after ashing so that the proportion of samples composed of mineral matter could be determined. Samples were ashed in a blast furnace at 500° C for 45 minutes. Dried nutrient analysis subsamples were ground using a mortar and pestle and stored in 7 ml glass vials for later analysis for total phosphorus.

Diatom subsamples were initially processed by adding ~20 ml of concentrated (35%) hydrochloric acid to subsamples and agitated. Subsamples were then oxidized with saturated potassium permanganate and acidified with saturated oxalic acid solution. Subsamples were returned to pH 7 (neutral) by decanting and refilling beakers with DI water every 6 to 8 hours. Cleaned diatom samples were stored in 7 ml glass vials. Several subsamples were not sufficiently cleaned by this method, and those diatom subsamples were decanted into clean beakers and cleaned again using nitric acid as below.

Remaining carbonate and organic materials were eliminated from diatom subsamples by adding ~20 ml of a concentrated (70%) nitric acid to the subsamples. The subsamples were left in acid under the fume hood overnight.  Next, the samples were returned to neutral pH by decanting and filling the beakers with DI water every 6 to 8 hours.  The cleaned diatom samples were stored in 7 ml glass vials.  Approximately 1 ml of each cleaned sample was placed on No.1 coverslips, air dried and permanently mounted onto glass slides using Naphrax®.

### 2.2. Mollusk composition in sediment profiles:

In the 2016 Annual Report, we reported on paleo-environmental conditions indicated in four sediment profiles along a transect north of C-103 (Mowry Canal) in the northeastern corner of the study area. In this section, we report on profiles of sediment salinity index (SI), organic matter content (OM), and rate of OM accumulation at an additional eleven southern Everglades sites that were analyzed completely in 2017. Four sites (TKYE, TKYW, TKYNW, and TKYINT) comprise a coast-to-interior transect south of Turkey Point Nuclear Power Plant (Figure 2.2.1). Two sites (TANGLS and TANGLIN) are found along a transect in the Triangle, between Card Sound Road and US 1. Three sites (TA2.6, TA2.5, TA2.2) extend north from the western end of Long Sound, 2 km west of Highway Creek. Finally, two sites (TA5.5 and TA6.4) are located east and west of the lower reaches of Taylor Slough, respectively (**Figure 2.2.1**). Our objective was to characterize the present depositional environment at these locations, as well as long-term changes in depositional environment, based on profile analysis.

*Description of sites*

*Turkey Point transect*. The Turkey Point transect is 3.5 km long and extends across ~ 50% of the coastal plain (as defined by the low lying area east of the Atlantic Coastal Ridge). The area to the west of the transect - separated from it by the L31E canal and levee - has been highly perturbed by agriculture, rock mining and urban development, with only a small fraction remaining as fresh water wetlands. Sawgrass is currently found in these wetlands, and, based upon sawgrass peat-marl sediments found east of the levee, this species once prevailed in at least half of the area between the L31E and the coast. The four sites that comprise the 2016 transect are offset from those examined in the Meeder et al. (1996) study by a few tens of meters to the north **(Figure 2.1)**. Along this transect, the White zone (Ross et al 2000) has retreated to within 50 m of the levee. Further retreat is inhibited by ground water seepage under the levee, as observed in 1996, and fresh water delivery through breaks in the levee placed in the last decade.
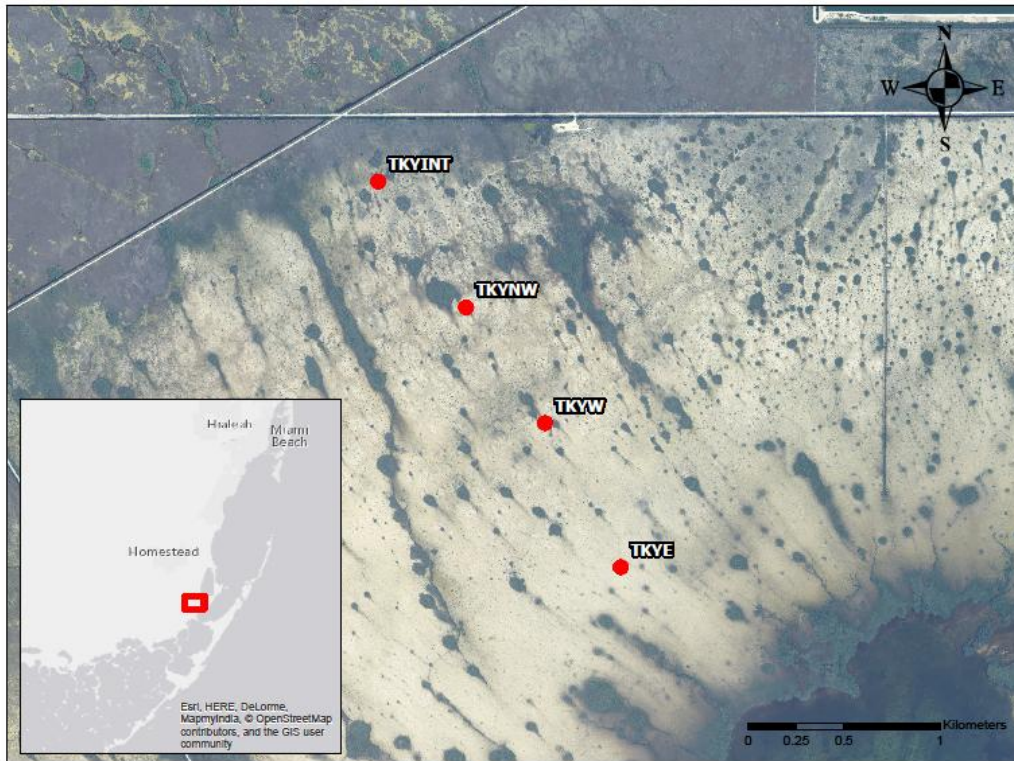
**Figure 2.2.1. Location** of Turkey Point Cores. Note the white zone reaches to the toe of the levee.

*Triangle transect.* The Triangle transect runs NNW-SSE, approximately midway between Card Sound Rd and US1 (**Figure 2.2.1**). Cores were collected at four locations, and analysis has been completed for cores from two sites: the second-most upslope (TANGLIN) and the closest to the coast (TANGLS). Along this reach of shoreline, as well as further west as far as Flamingo, the coastal land area is broken up by several round-to-ovoid water bodies. The margins of these "lakes" are likely old fringe mangrove habitats where the sediments maintained elevation with respect to rising sea level. In contrast, sediments in the interior of the lakes were not able to match SLR, and became submerged. Cottrell's (1984) study of sediments in Florida Bay suggested an analogous process took place there several millennia earlier. Today, no extensive well-defined mangrove fringe is found in this portion of the SESE, but large clumps of mangroves are found at some distance from the shoreline. Recently settled mangrove propagules can be found inland several km, well into the sparse saw grass.

*Transect TA-2.* Analyses of OM content and depositional rate have been completed for the three cores in this transect, but mollusk analysis is not yet complete. The transect extends from deep in the White zone north of Long Sound to sawgrass-dominated marsh within a few km of the C111 Canal (**Figure 2.2.1**).

*Transect TA-5.* Of the five cores from TA5, only Core TA5-5 has been worked up so far (**Figure 2.2.1**). The transect represents a stretch of coastal wetland between Taylor Slough and Joe Bay. Along this stretch, Core TA5-5 is located in the heart of the White zone.

23

*Transect T6*. This transect is located west of Taylor Slough, and is comprised of four cores (**Figure 2.2.1**). To date, Core T6-5 is the only core that has been worked up. This site is close to the interior edge of the mangroves, in an area where the White zone is not clearly defined.

### *Methods of sediment retrieval and analysis.*

Methods of sediment retrieval and analysis in 2017 were identical to those reported in our 2016 Annual Report, but procedures are briefly repeated here for clarity. Sediment cores collected with 3-cm diameter aluminum tubes were returned to the lab, frozen, and later sectioned frozen at 1 cm intervals. The core increments were weighed frozen to determine wet bulk density. After thawing, the sample was split into halves, and one half was used for sediment analysis. A 1 cc sample separated from each sample was used to determine dry bulk density, organic matter content (by Loss On Ignition: Dean 1967), and carbonate content (Meeder et al. 1996).

The second half of each sample was sieved and all invertebrates over 1mm in size were collected. Specimens were identified and counted. By applying a weighted averaging technique to mollusk composition, we calculated a Salinity Index (Meeder et al. 1996), by which we inferred historical salinity conditions. Both vertical and horizontal changes in SI were determined to document salt water encroachment history. Core sections with continuous or semi-continuous 1-cm intervals with SI≤1.5 were considered to represent a fresh water environment.

All sediment intervals were analyzed for SI, and for OM in g cm$^3$. Sediment accumulation rates estimated by ^{210}Pb were used to assess the rate of organic matter burial and the timing of salt water encroachment. OM in g m$^2$ yr$^{-1}$ was calculated from OM in g cm$^3$ by dividing by the accumulation rate for the local sediment type. Some OM values were discarded because of analytical problems and no substitute was calculated. In determining the time of salt water encroachment in cases where no mollusks were present or no sample existed, the SI value was determined by taking the average of the preceding and subsequent value. These analyses were limited to the upper 30 cm to avoid complications with compaction and decomposition.

We applied ^{210}Pb rates specific for each depositional environment, based on rates previously reported (**Table 2.2.1**). The following rates were used for different sediment types: mangrove peat 4.1, mangrove peat marl 3.2, marl 1.25 and saw grass peat marl 2.2 mm yr$^{-1}$. We also commissioned FIU's Applied Research Center (Dr. David Kadko) to determine accumulation rates in several cores. Those rates are reported in Section 3.2, but have not yet been incorporated in our analysis of the dynamics of deposition.

**Table 2.2.1.** Sediment core radiometric analysis (from Meeder et al. 2017)

| Core location | [b]Accumulation rate | [c]$R^2$ | Sediment type |
|---|---|---|---|
| CJB | 3.1 | 0.855 | Mangrove peat–marl |
| LJB | 1 | 0.887 | Marl |
| UJB | 1.6 | 0.9 | Marl |
| NUJB | 2.1 | 0.933 | Sawgrass peat–marl |
| CHC | 3.2 | 0.94 | Mangrove peat–marl |
| LHC | 1.4 | 0.909 | Marl |
| EP1R | 2.3 | 0.822 | Sawgrass peat–marl |
| CTP | 1.4 | 0.924 | Marl |
| Florida Keys | [c] 3.9–4.2 | | Mangrove peat |

[a]In mm yr^{-1}
[b]Coefficient of determination of best fit model of exponential decay.
[c]Florida Key sites are located in the riverine mangroves along the north-east
bank of Tavernier Creek on the Florida Bay side of US1 approximately 2.5 km
and from the fringing mangrove on the back side of Lignumvitae Key based
upon ^{137}Cs method

Photographs and brief descriptions of cores are presented in **Appendix 2.2.1**.

**Appendix 2.2.2** presents organic matter profiles from all cores analyzed for OM so far, including sites presented previously (2016 Annual Report) and sites in which mollusk-based SI profiles are not yet complete.

### *Depositional environments*

The stratification of depositional environments indicated by sediment profiles examined in 2016 and 2017 are summarized in **Table 2.2.2**.

| | Sediment type | Dominant plants |
|---|---|---|
| | **Table 2.2.2.** Relationships between sediment types and plant communities. | |
| 1 | Mangrove peat | *Rhizophora mangle* occasionally with *Avicennia germinans* and *Laguncularia racemosa* |
| 2 | Mangrove peat marl | *Rhizophora mangle*, *Eleocharis cellulosa* and periphyton |
| 3 | Marl | Periphyton and *Eleocharis cellulosa* |
| 4 | Saw grass peat marl | *Cladium jamaicensi*s, *Eleocharis cellulosa,* and periphyton |
| 5 | Saw grass peat | *Cladium jamaicensis* |

In **Table 2.2.3**, we present organic matter accumulation rates for depositional environments #1 - #4, which are based on ^{210}Pb analyses (**Table 2.2.1**) and sediment analysis of cores described below and in **Appendix 2.2.3**. The data indicate highest OM accumulation rates in mangrove peat, followed by mangrove peat-marl, sawgrass peat-marl, and marl. We expect to have data that would support similar estimates for sawgrass peat by the end of the study.

| Table 2.2.3.  Summary of OM $g/m^2/yr$ in different sediment types. | | | | |
|---|---|---|---|---|
| **Sediment type** | **N** | **Mean** | **Max** | **Min** |
| Mangrove peat | 58 | 520.22 | 1133.08 | 164.58 |
| Mangrove peat marl | 62 | 223.38 | 415.32 | 75.16 |
| Marl | 141 | 54.68 | 98.87 | 19.06 |
| Saw grass peat marl | 74 | 185.15 | 346.06 | 104.42 |

Though no single sediment profile we've analyzed to date displays all five of the depositional environments described in **Table 2.2.2**, the tendency is for the depositional environments to transition upward in the order #5, #4, …, →#1 (**Figure 2.2.2**).
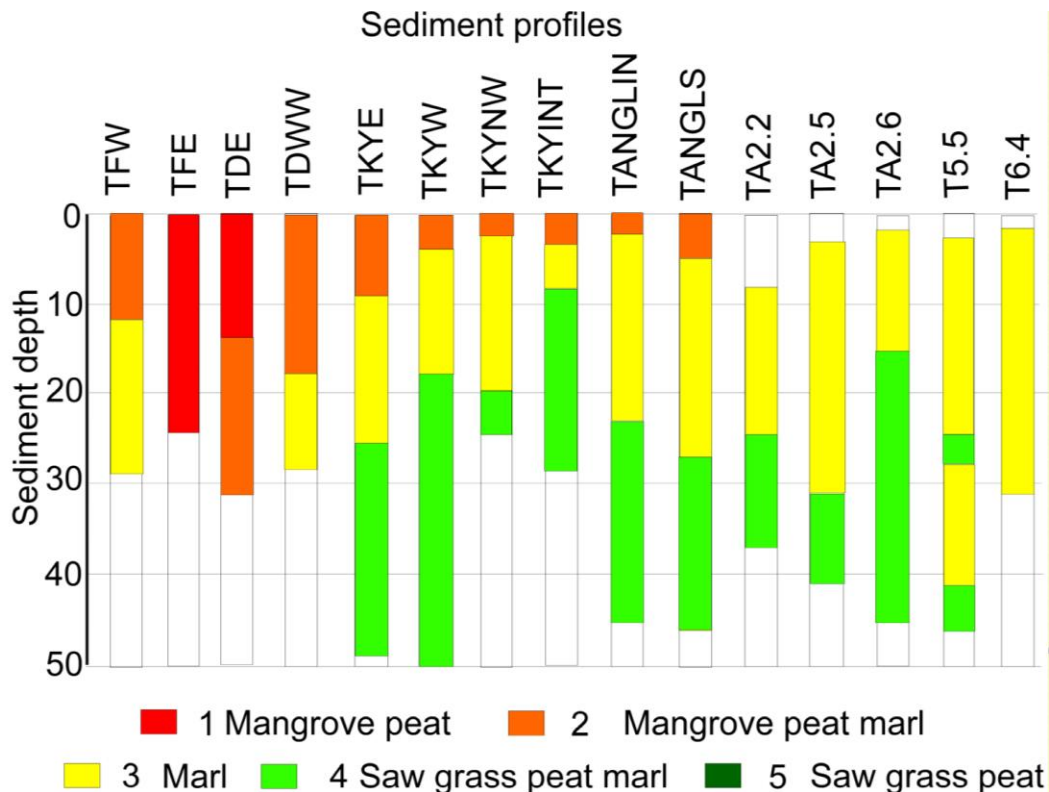


**Figure 2.2.2.** Sediment profiles (summary of Appendix B).

*Turkey Point transect.*

At Turkey Point, SI increased upward in all four cores, with the thickness of marine-influenced sediments generally increasing towards the coast (**Table 2.2.4**).

Table 2.2.4. Salinity indices for Turkey Point transect cores. Sites are arranged L-R from most coastward (TKYE) to furthest inland (TKYINT). Red typeface indicates intervals characterized by marine influence. Blank cells indicate no data for the interval.

| Depth (cm) | TKYE | TKYW | TKYNW | TKYINT |
|---|---|---|---|---|
| 0 | 3.39 | 2.40 | 3.45 | 1.60 |
| 1 | 2.18 | 2.72 | 1.92 | 1.94 |
| 2 | 3.08 | 1.91 | 1.42 | 2.00 |
| 3 | 3.39 | 1.33 | 1.5 | 1.67 |
| 4 | 2.88 | 1.60 | 1.08 | 1.34 |
| 5 | 2.21 | 1.38 | 1.42 | 1.42 |
| 6 | 3.00 | 1.32 | 1.43 | 1.32 |
| 7 | 1.98 | 1.92 | 1.46 | 1.55 |
| 8 | 1.68 | 1.00 | 1.41 | 1.31 |
| 9 | 1.94 | 1.29 | 1.38 | 1.18 |
| 10 | | 1.26 | 1.28 | 1.29 |
| 11 | | 1.46 | 1.39 | 1.29 |
| 12 | | 1.40 | 1.38 | 1.27 |
| 13 | | 1.47 | 1.36 | 1.34 |
| 14 | | 1.36 | 1.36 | 1.34 |
| 15 | | 1.46 | 1.37 | 1.43 |
| 16 | | 1.65 | 1.43 | 1.38 |
| 17 | | 1.39 | 1.38 | 1.43 |
| 18 | | 1.33 | 1.39 | 1.36 |
| 19 | 1.40 | 1.43 | 1.4 | 1.35 |
| 20 | 1.38 | 1.45 | 1.35 | 1.33 |
| 21 | 1.36 | 1.36 | 1.38 | 1.50 |
| 22 | 1.36 | 1.45 | 1.42 | |
| 23 | 1.50 | 1.41 | 1.32 | |
| 24 | 1.39 | | 1.39 | |
| 25 | 1.41 | 1.31 | | 1.50 |
| 26 | 1.41 | 1.33 | | 1.42 |
| 27 | 1.33 | 1.27 | | 0.83 |
| 28 | 1.36 | 1.24 | | 1.29 |
| 29 | 1.43 | 1.41 | | |
| | 1.38 | 1.32 | | |
| | 1.27 | 1.35 | | |

All cores along the Turkey Point transect exhibited higher OM accumulation rates (though not always higher OM content) in the upper core intervals (**Table 2.2.5**), where sediment change was from marl to mangrove peat marl (**Figure 2.2.2**). Mangrove material was generally limited to the upper intervals, and sediments containing mangrove roots and residues had higher OM (and SI) values. Sawgrass was observed in the lower sediment intervals of TKYNW and TKYINT, and was associated with low SI values but OM values much higher than in the overlying marl sediments (**Table 2.2.5; Figure 2.2.2**). Sawgrass peat-marl strata on this transect were the first examined in the 2015-2018 study to contain abundant sawgrass OM, though we expect to encounter sawgrass peats with higher OM values in the northern and western portions of the study area.

**Table 2.2.5.** Profiles of OM in g cm$^3$ and OM accumulation rate in g m$^2$ yr$^{-1}$ along the Turkey Point transect. Sites are arranged L-R from most coastward (TKYE) to furthest inland (TKYINT). TKYW was not processed. Blank cells indicate no data for the interval.

| Depth (cm) | TKYE OM (g cm$^3$) | TKYE OM (g m$^2$ yr$^{-1}$) | TKYNW OM (g cm$^3$) | TKYNW OM (g m$^2$ yr$^{-1}$) | TKYINT OM (g cm$^3$) | TKYINT OM (g m$^2$ yr$^{-1}$) |
|---|---|---|---|---|---|---|
| 0 | 0.038 | 245.83 | 0.038 | 122.92 | 0.048 | 152.55 |
| 1 | 0.046 | 297.11 | 0.023 | 75.16 | 0.052 | 165.22 |
| 2 | 0.040 | 254.49 | 0.030 | 37.25 | 0.050 | 160.74 |
| 3 | 0.029 | 186.86 | 0.026 | 31.87 | 0.055 | 175.48 |
| 4 | 0.045 | 287.82 | 0.046 | 57.56 | 0.055 | 68.50 |
| 5 | 0.033 | 210.90 | 0.041 | 51.75 | 0.060 | 74.62 |
| 6 | 0.055 | 355.45 | 0.036 | 45.50 | 0.073 | 91.31 |
| 7 | 0.043 | 272.76 | 0.049 | 61.28 | 0.051 | 64.06 |
| 8 | 0.047 | 301.60 | 0.041 | 51.81 | 0.071 | 88.94 |
| 9 | 0.045 | 285.26 | 0.051 | 64.06 | 0.099 | 228.01 |
| 10 | 0.042 | 26.06 | 0.067 | 83.87 | 0.111 | 256.13 |
| 11 | 0.061 | 37.84 | 0.076 | 94.69 | 0.114 | 264.58 |
| 12 | 0.040 | 24.84 | 0.067 | 84.37 | 0.091 | 210.99 |
| 13 | 0.063 | 39.12 | 0.073 | 91.37 | 0.106 | 244.68 |
| 14 | 0.078 | 48.87 | 0.086 | 198.26 | 5.069 | |
| 15 | 0.073 | 45.41 | 0.096 | 221.76 | 0.099 | 230.09 |
| 16 | 0.091 | 56.87 | | | 0.113 | 261.11 |
| 17 | 0.061 | 37.87 | 0.071 | 163.66 | 0.150 | 346.06 |
| 18 | 0.080 | 50.19 | 0.097 | 224.30 | 0.073 | 168.87 |
| 19 | 0.092 | 57.22 | 0.111 | 257.64 | 0.105 | 244.10 |
| 20 | 0.064 | 39.78 | 0.102 | 235.30 | | |
| 21 | 0.046 | 28.69 | | | | |
| 22 | 0.057 | 35.78 | | | | |
| 23 | 0.067 | 42.12 | | | | |
| 24 | 0.069 | 43.34 | | | | |
| 25 | 0.081 | 50.41 | | | | |
| 26 | 0.096 | 60.12 | | | | |
| 27 | 0.105 | 65.53 | | | | |
| 28 | 0.075 | 46.62 | | | | |
| 29 | 0.066 | 41.34 | | | | |
| 30 | 0.078 | 48.75 | | | | |
| 31 | 0.079 | 49.56 | | | | |

Analysis of the Turkey Point transect allows a better understanding of direct relationships between sediment type to plant community. Vegetation types described in this section differ from those defined in Section 1.1, but are based on the same data, i.e., those collected in both 2016 and 2017. In the analysis described below, plant community refers to the dominant plant species, as well as three sub-dominants, based on species frequency and abundance in 30 1 m$^2$ plots.

Surface sediments for TKYINT, TKYNW, and TKYW were a mangrove peat-marl depositional type, which was generally in agreement with the current vegetation assemblage (**Table 2.2.6**).

TKYE, the most coastal of the sites was characterized as mangrove peat environment, which again was consistent with the vegetation cover onsite, which was exclusively *R. mangle*.

| Table 2.2.6: Relative abundance of primary producers and sediment types along Turkey Point transect | | | | | | | | | |
|---|---|---|---|---|---|---|---|---|---|
| | Species[1] | | | | | | | | |
| Site | Rupmar | Rhiman | Aviger | Lagrac | Junroe | Disspi | Elecel | Periphyton | Sediment type |
| TKYINT | | 2 | 3 | 5 | 4 | 3 | 1 | Very heavy | Mangrove peat-marl |
| TKYNW | 4 | 1 | 2 | 5 | 3 | 6 | | None | Mangrove peat-marl |
| TKYW | 2 | 1 | 4 | 6 | 3 | 5 | | None | Mangrove peat-marl |
| TKYE | | 1 | | | | | | None | Mangrove peat |
| [1]Rupmar = *Ruppia maritima*; Rhiman = *Rhizophora mangle*; Aviger =*Avicennia germinans*; Lagrac = *Laguncularia racemosa*; Junroe = *Juncus romoerianua;* Disspi = *Distichlis spicata* and Elecel = *Eleocharis cellulose* | | | | | | | | | |

## Triangle Transect

The sediment profile for TANGLI, 4.23 km from the coast, transitioned from sawgrass peat-marl at the base (50 cm belowground) to marl (6 to 23 cm) to mangrove peat-marl at the surface (**Figure 2.2.2**). The Mangrove peat marl is poorly developed, minor mangrove contribution. $^{210}$Pb analysis for this core indicated an accretion rate of 0.63 mm yr$^{-1}$ TANGLS, which was closer (1.5 km) to Manatee Bay, changed from sawgrass peat-marl to marl at about 27 cm below the surface (**Figure 2.2.2**). The upper 4 cm is a poorly developed mangrove peat marl.

At TANGLI, SI indicated freshwater conditions from the base through 4 cm from the surface, but above that harbored marine-influenced mollusk species. At TANGLS, freshwater conditions prevailed from the base to 6 cm from the surface; mollusks were lacking from 7-10 cm depth, so no characterization was possible in this interval (**Table 2.2.7**).

| Table 2.2.7. SI, OM g cm$^3$ and OM g m$^2$ yr$^{-1}$ for Triangle sediment samples. Sites are arranged L-R from most coastward (TANGLS) to furthest inland (TANGLI). TANGLEN and EVER1 were not processed. Red typeface indicates intervals characterized by marine influence. Blank cells indicate no data for the interval. | | | | | | |
|---|---|---|---|---|---|---|
| | TANGLS | | | TANGLI | | |
| Depth | SI | OM (g cm$^3$) | OM (g m$^2$ yr$^{-1}$) | SI | OM (g cm$^3$) | OM (g m$^2$ yr$^{-1}$) |
| | | | | | | |
| 0 | 1.85 | 0.051 | 64.12 | 0.00 | 0.000 | 0.00 |
| 1 | 2.3 | 0.051 | 63.19 | 1.00 | 0.046 | 57.31 |
| 2 | 2.1 | 0.017 | 21.37 | 1.50 | 0.044 | 54.69 |
| 3 | 1.89 | 0.027 | 33.94 | 2.13 | 0.064 | 79.37 |
| 4 | 1.65 | 0.033 | 40.81 | 1.92 | 0.054 | 68.06 |
| 5 | 1.5 | 0.036 | 45.19 | 1.17 | 0.054 | 67.25 |
| 6 | 1.42 | 0.034 | 42.31 | 1.83 | 0.036 | 45.06 |
| 7 | 1.46 | 0.044 | 55.00 | 1.38 | 0.029 | 36.81 |
| 8 | | 0.044 | 54.75 | 1.32 | 0.024 | 29.50 |

*Continuation* **Table 2.2.7**

| | **TANGLS** | **TANGLI** | | **TANGLS** | **TANGLI** | |
|---|---|---|---|---|---|---|
| **Depth** | **SI** | **OM** $(g\ cm^3)$ | **Depth** | **SI** | **OM** $(g\ cm^3)$ | **Depth** |
| 9 | | 0.055 | 69.12 | 1.33 | 0.021 | 25.62 |
| 10 | 1.37 | 0.085 | 106.00 | 1.35 | 0.030 | 37.94 |
| 11 | 1.40 | 0.109 | 136.75 | 1.43 | 0.025 | 31.37 |
| 12 | 1.36 | 0.087 | 108.94 | 1.42 | 0.030 | 37.31 |
| 13 | 1.40 | 0.069 | 85.81 | 1.33 | 0.034 | 41.87 |
| 14 | 1.42 | 0.083 | 104.37 | 1.33 | 0.023 | 28.19 |
| 15 | 1.39 | 0.052 | 65.37 | 1.31 | 0.015 | 19.06 |
| 16 | 1.31 | -0.061 | | 1.38 | 0.021 | 26.81 |
| 17 | 1.34 | 0.058 | 72.62 | 1.42 | 0.029 | 35.62 |
| 18 | 1.27 | 0.042 | 52.00 | 1.28 | 0.031 | 38.19 |
| 19 | 1.46 | 0.044 | 54.75 | 1.44 | 0.032 | 40.37 |
| 20 | 1.29 | 0.541 | | 1.43 | 0.029 | 36.19 |
| 21 | 1.36 | 0.049 | 61.62 | 1.33 | 0.029 | 36.81 |
| 22 | 1.38 | 0.047 | 58.12 | 1.50 | 0.035 | 44.25 |
| 23 | 1.17 | 0.053 | 65.87 | 1.25 | 0.045 | 55.81 |
| 24 | 1.50 | 0.048 | 60.31 | 1.56 | 0.082 | 189.77 |
| 25 | 1.00 | 0.059 | 74.37 | 1.42 | 0.053 | 122.91 |
| 26 | 1.30 | 0.067 | 83.12 | 1.30 | 0.051 | 119.77 |
| 27 | 1.28 | 0.058 | 72.25 | 1.63 | 0.114 | 264.53 |
| 28 | 1.37 | 0.116 | | 1.33 | 0.070 | 162.79 |
| 29 | 1.35 | 0.092 | | 1.29 | 0.074 | 172.56 |
| 30 | 1.43 | 0.114 | | 1.42 | 0.051 | 119.30 |
| 31 | 1.36 | 0.145 | | 1.40 | 0.069 | 159.53 |
| 32 | 1.38 | 0.148 | | 1.45 | 0.075 | 173.72 |
| 33 | 1.50 | 0.422 | | 1.73 | 0.069 | 160.35 |
| 34 | 1.35 | 0.117 | | 1.42 | 0.073 | 169.53 |
| 35 | 1.23 | 0.178 | | 1.40 | 0.053 | 122.33 |
| 36 | 1.28 | 0.118 | | 1.73 | 0.061 | 140.93 |
| 37 | 1.22 | 0.092 | | 1.64 | 0.054 | 126.51 |
| 38 | 1.12 | 0.097 | | 1.38 | 0.070 | 162.33 |
| 39 | 1.25 | 0.103 | | 1.33 | 0.078 | 182.21 |
| 40 | 1.45 | 0.145 | | 1.44 | 0.061 | 142.09 |
| 41 | 1.36 | 0.130 | | 1.50 | 0.045 | 105.58 |
| 42 | 1.21 | 0.162 | | 1.15 | 0.061 | 141.51 |
| 43 | 1.28 | 0.181 | | 1.38 | 0.059 | 137.79 |
| 44 | 1.27 | 0.119 | | 1.50 | 0.068 | 157.44 |
| 45 | 1.23 | 0.135 | | 1.13 | 0.086 | 200.93 |
| 46 | 1.29 | 0.116 | | 1.43 | 0.057 | 132.67 |
| 47 | 1.36 | 0.125 | | 1.00 | 0.045 | 104.42 |
| 48 | | 0.084 | | 1.33 | 0.048 | 111.05 |
| 49 | | 0.074 | | 1.23 | 0.064 | 147.79 |
| 50 | | 0.091 | | 1.38 | 0.055 | 127.33 |
| 51 | | 0.073 | | 1.25 | 0.071 | 165.70 |
| 52 | | 0.082 | | 1.25 | 0.063 | 146.86 |
| 53 | | 0.060 | | 1.38 | 0.086 | 200.35 |

*Continuation* **Table 2.2.7**

| TANGLS SI | TANGLI OM (g cm³) | Depth | TANGLS SI | TANGLI OM (g cm³) | Depth | |
|---|---|---|---|---|---|---|
| 54 | | | | 1.17 | 0.062 | 144.77 |
| 55 | | | | 1.19 | 0.085 | 198.26 |
| 56 | | | | 1.17 | 0.103 | 238.37 |
| 57 | | | | 1.2 | 0.071 | 165.93 |

Both cores described above exhibit high SI values at the top but do not contain OM values normally associated with higher SI values. This appears to be a product of the slow buildup of mangrove populations, perhaps due to limited propagule transport, despite the extensive saltwater encroachment (SWE) evident in the mollusk assemblages. The mangroves present on site are too sparsely distributed to have built an organic-rich sediment. OM values and the rate of OM accumulation are low for the marl intervals, most of both cores, but are elevated with the presence of abundant sawgrass material between 25 and 57 cm in TANGLI. This suggests that SWE has affected TANGLI area for considerably less time than TANGLS, resulting in sawgrass dominance. The White zone, usually marl sediments, has moved northward, creating the difference between the two cores.

### Transect TA2 (Highway Creek watershed)

Salinity indices have not yet been completed for cores in this transect, but organic matter profiles are presented in **Table 2.2.8**.

| **Table 2.2.8:** Profiles of OM in g cm³ and OM accumulation rate in g m² yr⁻¹ along Transect TA2. Sites are arranged L-R from most coastward (TA2.6) to furthest inland (TA2.2). Blank cells indicate no data for the interval. | | | | | | |
|---|---|---|---|---|---|---|
| **Depth** | **TA2.6** | | **TA2.5** | | **TA2.2** | |
| | OM (g cm³) | OM (g m² yr⁻¹) | OM (g cm³) | OM (g m² yr⁻¹) | OM (g cm³) | OM (g m² yr⁻¹) |
| 0-1 | 0.039 | 0.00 | 0.045 | 0.00 | 0.060 | periphyton |
| 1 | 0.041 | 0.00 | 0.047 | 0.00 | 0.055 | |
| 2 | 0.044 | 54.75 | 0.061 | 0.00 | 0.068 | |
| 3 | 0.041 | 51.31 | 0.044 | 55.50 | 0.077 | |
| 4 | 0.043 | 53.37 | 0.060 | 74.87 | 0.071 | |
| 5 | | | 0.067 | 83.25 | 0.069 | |
| 6 | 0.048 | 59.69 | 0.058 | 73.06 | 0.090 | |
| 7 | 0.041 | 51.50 | 0.053 | 66.31 | 0.085 | |
| 8 | 0.048 | 60.06 | 0.043 | 53.44 | 0.076 | 112.62 |
| 9 | 0.050 | 62.37 | -0.194 | | 0.051 | 105.94 |
| 10 | 0.050 | 62.62 | 0.025 | 31.00 | 0.062 | 94.87 |
| 11 | 0.070 | 87.56 | 0.033 | 41.56 | 0.063 | 63.37 |
| 12 | 0.070 | 88.06 | 0.037 | 46.56 | 0.070 | 77.87 |
| 13 | 0.055 | 68.44 | 0.038 | 47.56 | 0.065 | 78.69 |
| 14 | 0.068 | 85.37 | 0.035 | 44.37 | | |
| 15 | 0.057 | 71.25 | 0.053 | 65.94 | 0.064 | 81.37 |
| 16 | 0.071 | 88.56 | 0.063 | 79.25 | 0.035 | |

*Continuation* **Table 2.2.8**

| Depth | TA2.6 OM (g cm$^3$) | TA2.5 OM (g m$^2$ yr$^{-1}$) | TA2.2 OM (g cm$^3$) | Depth | TA2.6 OM (g cm$^3$) | TA2.5 OM (g m$^2$ yr$^{-1}$) |
|---|---|---|---|---|---|---|
| 17 | 0.092 | 214.07 | 0.068 | 84.94 | 0.040 | 80.00 |
| 18 | 0.096 | 223.60 | 0.063 | 78.62 | 0.045 | 43.75 |
| 19 | 0.097 | 225.35 | 0.061 | 75.87 | 0.043 | 50.50 |
| 20 | 0.111 | 258.14 | 0.077 | 96.00 | 0.053 | 56.75 |
| 21 | | | 0.071 | 88.25 | 0.038 | 53.62 |
| 22 | 0.106 | 246.05 | 0.093 | 116.44 | 0.027 | 66.25 |
| 23 | 0.110 | 255.93 | 0.045 | 56.62 | 0.033 | 48.06 |
| 24 | 0.113 | 263.60 | 0.044 | 54.44 | 0.000 | 33.25 |
| 25 | 0.096 | 224.42 | 0.054 | 67.56 | 0.000 | 41.69 |
| 26 | | | 0.042 | 52.25 | 0.000 | 0.00 |
| 27 | 0.109 | 252.33 | 0.048 | 60.44 | 0.000 | 0.00 |
| 28 | 0.086 | 200.35 | 0.042 | 52.31 | 0.000 | 0.00 |
| 29 | 0.103 | 240.35 | 0.050 | 62.19 | 0.000 | 0.00 |
| 30 | 0.069 | 160.12 | 0.076 | 94.62 | 0.000 | 0.00 |
| 31 | 0.078 | 180.58 | 0.071 | 88.19 | 0.000 | 0.00 |
| 32 | 0.078 | 181.05 | 0.079 | 183.49 | 0.000 | 0.00 |
| 33 | 0.090 | 208.26 | 0.081 | 188.02 | 0.000 | 0.00 |
| 34 | 0.124 | 288.60 | 0.069 | 160.58 | 0.000 | 0.00 |
| 35 | 0.117 | 272.44 | 0.088 | 204.19 | 0.000 | 0.00 |
| 36 | 0.102 | 236.63 | 0.105 | 243.02 | 0.000 | 0.00 |
| 37 | 0.104 | | 0.091 | 212.21 | 0.000 | 0.00 |
| 38 | 0.102 | | 0.072 | 168.37 | | 0.00 |
| 39 | 0.100 | | 0.075 | 174.65 | | 0.00 |
| 40 | 0.117 | | 0.069 | 161.28 | | |
| 41 | 0.120 | | 0.075 | 174.88 | | |
| 42 | 0.129 | | -0.430 | | | |
| 43 | 0.120 | | 0.082 | 189.65 | | |
| 44 | 0.094 | | 0.080 | 185.58 | | |
| 45 | 0.098 | | 0.090 | 208.84 | | |
| 46 | 0.127 | | 0.063 | 145.93 | | |
| 47 | 0.113 | | 0.069 | 159.53 | | |
| 48 | 0.137 | | 0.065 | 151.86 | | |
| 49 | 0.137 | | 0.070 | 162.79 | | |
| 50 | 0.119 | | 0.095 | 221.86 | | |
| 51 | 0.124 | | 0.077 | 179.88 | | |
| 52 | 0.122 | | 0.101 | 234.88 | | |
| 53 | 0.108 | | 0.111 | 258.26 | | |
| 54 | 0.126 | | 0.095 | 221.39 | | |
| 55 | 0.114 | | 0.134 | 310.93 | | |
| 56 | 0.121 | | 0.138 | 321.28 | | |
| 57 | 0.118 | | 0.093 | 216.63 | | |
| 58 | 0.127 | | 0.099 | 230.23 | | |
| 59 | 0.132 | | 0.102 | 237.09 | | |
| 60 | 0.119 | | 0.096 | 223.37 | | |
| 61 | 0.138 | | 0.068 | 158.60 | | |

| Depth | TA2.6 | TA2.5 | TA2.2 | Depth | TA2.6 | TA2.5 |
|---|---|---|---|---|---|---|
| | OM (g cm$^3$) | OM (g m$^2$ yr$^{-1}$) | OM (g cm$^3$) | | OM (g cm$^3$) | OM (g m$^2$ yr$^{-1}$) |
| 62 | 0.109 | | 0.081 | 188.95 | | |

## TA 5

One site (TA 5.5) has been analyzed for SI and OM content and accumulation rate. SI remains low except for an interval at 7-11 cm depth, which is marine influenced.  Low SI values in strata at 3-6 cm depth may be attributable to an increase in fresh water delivery to the Taylor Slough drainage basin (**Table 2.2.9**). OM and rate of OM accumulation was low in the marl interval 3 to 25 cm but nearly decreased by 50% upwards, perhaps associated with decreased periphyton productivity.  The interval 26 to 42 is variable but generally increasing because of sawgrass material until characteristic sawgrass peat marl with higher OM values was reached at 43 cm.

| Depth (cm) | TA5.5 | | |
|---|---|---|---|
| | SI | OM (g cm$^3$) | OM (g m$^2$ yr$^{-1}$) |

**Table 2.2.9**.  SI, OM g cm$^3$ and OM g m$^2$ yr$^{-1}$ for TA 5.5. Red typeface indicates intervals characterized by marine influence. Blank cells indicate no data for the interval**.**

| Depth (cm) | SI | OM (g cm$^3$) | OM (g m$^2$ yr$^{-1}$) |
|---|---|---|---|
| 0 | | 0.000 | 0.000 |
| 1 | | 0.000 | 0.000 |
| 2 | | 0.000 | 0.000 |
| 3 | 1.25 | 0.018 | 23.062 |
| 4 | | 0.018 | 22.375 |
| 5 | 1.33 | 0.026 | 32.062 |
| 6 | 1.25 | 0.025 | 31.125 |
| 7 | 1.57 | 0.033 | 41.438 |
| 8 | 1.80 | 0.044 | 54.812 |
| 9 | 1.98 | 0.041 | 50.750 |
| 10 | 1.81 | 0.055 | 68.875 |
| 11 | 1.67 | 0.035 | 44.125 |
| 12 | 1.17 | 0.042 | 52.250 |
| 13 | 1.17 | 0.039 | 48.938 |
| 14 | 1.30 | 0.042 | 52.375 |
| 15 | 1.20 | 0.539 | |
| 16 | 1.07 | 0.043 | 53.438 |
| 17 | 1.13 | 0.045 | 56.500 |
| 18 | 1.21 | 0.069 | 86.813 |
| 19 | 1.36 | 0.061 | 75.813 |
| 20 | 1.23 | 0.061 | 76.875 |
| 21 | 1.32 | 0.057 | 70.875 |
| 22 | 1.18 | 0.069 | 86.625 |
| 23 | 1.27 | 0.067 | 83.688 |
| 24 | 1.10 | 0.051 | 63.437 |
| 25 | 1.31 | 0.070 | 87.500 |

| Depth (cm) | TA5.5 | | |
|---|---|---|---|
| | SI | OM (g cm$^3$) | OM (g m$^2$ yr$^{-1}$) |
| 26 | 1.29 | 0.080 | 194.390 |
| 27 | 1.26 | 0.080 | 196.098 |
| 28 | 1.20 | 0.085 | 206.341 |
| 29 | 1.17 | 0.064 | 79.875 |
| 30 | 1.29 | 0.064 | 80.438 |
| 31 | 1.29 | 0.057 | 71.250 |
| 32 | 1.22 | 0.057 | 71.500 |
| 33 | 1.25 | 0.052 | 65.562 |
| 34 | 1.21 | 0.055 | 68.563 |
| 35 | 1.21 | 0.072 | 90.312 |
| 36 | 1.17 | 0.069 | 86.375 |
| 37 | 1.23 | 0.075 | 93.437 |
| 38 | 1.27 | 0.075 | 93.313 |
| 39 | 1.23 | 0.073 | 91.000 |
| 40 | 1.33 | 0.081 | 100.937 |
| 41 | 1.25 | 0.071 | 88.563 |
| 42 | 1.34 | 0.076 | 185.976 |
| 43 | 1.26 | 0.069 | 167.683 |
| 44 | 1.20 | 0.062 | 151.220 |
| 45 | 1.34 | 0.068 | 165.366 |
| 46 | 1.20 | 0.067 | 163.293 |
| 47 | 1.13 | 0.051 | 124.390 |
| 48 | 1.19 | 0.067 | 163.293 |
| 49 | 1.22 | 0.058 | 140.732 |
| 50 | 1.20 | 0.065 | 159.512 |
| 51 | 1.30 | 0.053 | 129.756 |
| 52 | 1.33 | 0.077 | 188.049 |
| 53 | 1.26 | 0.090 | 219.512 |
| 54 | 1.30 | 0.099 | 240.976 |
| 55 | 1.27 | 0.108 | 262.439 |
| 56 | 1.27 | 0.110 | 267.073 |
| 57 | 1.21 | 0.112 | 274.268 |
| 58 | 1.39 | 0.089 | 217.683 |
| 59 | 1.00 | 0.084 | 205.610 |
| 60 | 1.23 | 0.082 | 199.756 |
| 61 | 1.25 | 0.093 | 226.585 |
| 62 | | 0.073 | 177.805 |

## T6

Of the four cores on this transect, only T6-4 has been analyzed at this time. Sediment accretion rate determined from ^{210}Pb was 0.56 mm yr$^{-1}$ at this site.

Salinity indices for all subsamples are presented in **Table 2.2.10.** The SI is low and varies little suggesting a long fresh water history. Organic matter levels were likewise low in T6-4 and varied little (Table 2.9). Many OM accumulation rates are above average for marl sediments and seem to cycle (see red marked values Table 2.9). Assuming OM accumulation rates are related to vegetation productivity, this suggest ecosystem cycles in productivity.

**Table 2.2.10**. SI and OM data from T6-4. Red typeface in this table indicates peaks of putative high productivity intervals, which appear to repeat themselves three times over the time period represented in the core. Blank cells indicate no data for the interval, hyphen indicates no mollusks present in interval.

| Depth (cm) | Sed type | T6.4 | | |
|---|---|---|---|---|
| | | SI | OM (g cm$^3$) | OM (g m$^2$ yr$^{-1}$) |
| 0 | floc | | | |
| 1 | floc | - | 0.021 | 26.312 |
| 2 | floc | - | 0.021 | 25.688 |
| 3 | marl | - | 0.037 | 46.000 |
| 4 | marl | - | 0.066 | 82.812 |
| 5 | marl | - | 0.079 | 98.875 |
| 6 | marl | - | 0.064 | 80.250 |
| 7 | marl | 1.00 | 0.050 | 63.000 |
| 8 | marl | - | 0.060 | 75.062 |
| 9 | marl | 1.30 | 0.057 | 70.813 |
| 10 | marl | 1.30 | 0.050 | 62.250 |
| 11 | marl | 1.30 | 0.068 | 84.875 |
| 12 | marl | 1.40 | 0.068 | 84.750 |
| 13 | marl | 1.31 | 0.070 | 87.375 |
| 14 | marl | 1.30 | 0.048 | 59.625 |
| 15 | marl | 1.20 | 0.047 | 58.875 |
| 16 | marl | 1.00 | 0.044 | 54.500 |
| 17 | marl | 1.10 | 0.038 | 47.687 |
| 18 | marl | 1.30 | 0.040 | 49.875 |
| 19 | marl | 1.50 | 0.045 | 56.812 |
| 20 | marl | 1.20 | 0.038 | 48.000 |
| 21 | marl | 1.20 | 0.045 | 56.250 |
| 22 | marl | 1.32 | 0.040 | 50.000 |
| 23 | marl | 1.20 | 0.542 | |
| 24 | marl | 1.10 | 0.067 | 84.062 |
| 25 | marl | 1.35 | 0.070 | 88.063 |
| 26 | marl | 1.40 | 0.071 | 88.875 |
| 27 | marl | 1.30 | 0.066 | 82.937 |
| 28 | marl | 1.50 | 0.033 | 41.375 |
| 29 | marl | - | 0.060 | 74.437 |
| 30 | marl | - | 0.034 | 42.375 |
| 31 | marl | - | 0.040 | 49.812 |

## Discussion

We have identified several important trends in sedimentation patterns in the first two years of the White zone project. In general, SI in the coastal Everglades, especially in the SESE, increases upwards in sediment cores, and the sediment interval of marine influenced sediment decreases in thickness away from the coast. Sediments with elevated SI values contain higher OM values and exhibit higher rates of OM accumulation. Marl soils have the lowest OM content and the lowest rate of OM accumulation, in contrast to mangrove peat with the highest OM content and greatest rate of OM accumulation. These trends document active saltwater encroachment in the Mowry transect (presented in 2016), and in the Turkey Point, Triangle and T2 transects, all associated with rapid change in state along the marine to fresh water gradient. Below we expand on these points in reference to the Turkey Point and Triangle transects we analyzed in 2017.

### Turkey Point Transect

**Plant community and sediment type.** Salt tolerant species dominate all core locations except the most westward, TKYINT. TKYINT is the only site that maintains the important freshwater species *Eleocharis cellulosa*, in association with a continuous periphyton layer. Even at this site, mangrove species and salt tolerant plants make up the largest portion of the vegetation, and a mangrove peat-marl sediment has supplanted the underlying marl, suggesting that saltwater encroachment (SWE) has reached the vicinity of the L31E levee. Not only has SWE advanced, but *Ruppia maritima* has invaded the transect at Sites TKYW and TKYNW (**Table 2.2.6**), illustrating that the period of inundation has become long enough to support normally submerged aquatic plants.

**SI dynamics and their relationship to OM accumulation.** SI profiles from cores extracted at similar locations and distances from the coast in 1996 and 2016 are presented in **Figure 2.2.3**. The most pertinent data comes from Site TKYINT, where a marine-influenced stratum of 4 cm depth has appeared, indicating an advancement of the SWE front of 350-1000 m in the last 20 yr (see black arrow in **Figure 2.2.3**), or a rate of 15-50 m yr$^{-1}$. This advancement has occurred despite restoration efforts to increase fresh water delivery into the coastal wetland through culverts from the L31E canal.
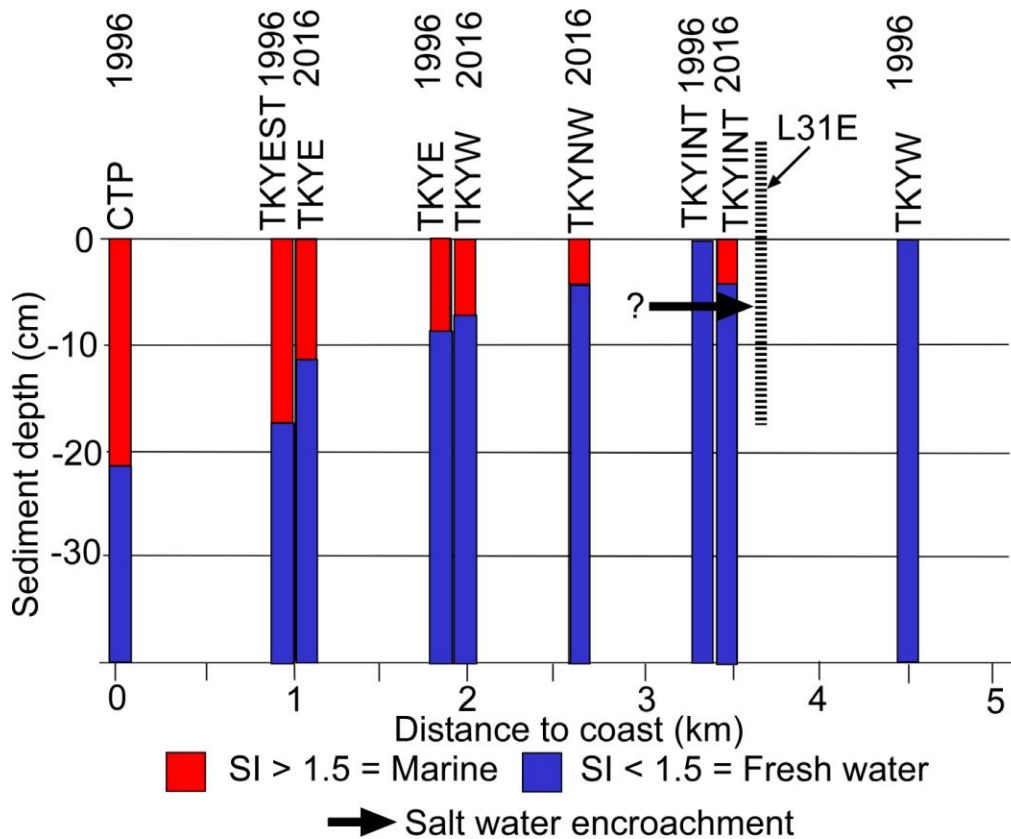
**Figure 2.2.3.** 1996 and 2016 SI profiles for the Turkey Point transect. Saltwater encroachment has advanced the zone of marine influence by 350 to 1000 m inland during the last two decades.

In order to better visualize the relationship of SI to OM accumulation rates, **Table 2.2.11** combines data previously presented in **Tables 2.2.4 and 2.2.5**. It is clear that higher SI values are associated with higher OM accumulation values, with a prominent exception: low SI values associated with sawgrass peat-marl intervals, which usually occur relatively low in the sediment profile.

| | TKYE | | TKYW | | TKYNW | | TKYINT | |
|---|---|---|---|---|---|---|---|---|
| Depth | SI | OM/yr/m$^2$ | SI | OM/yr/m$^2$ | SI | OM/yr/m$^2$ | SI | OM/yr/m$^2$ |
| 0 | 3.39 | 245.833 | 2.40 | not done | 3.45 | 122.917 | 1.60 | 152.548 |
| 1 | 2.18 | 297.115 | 2.72 | | 1.92 | 75.160 | 1.94 | 165.224 |
| 2 | 3.08 | 254.487 | 1.91 | | 1.42 | 37.250 | 2.00 | 160.737 |
| 3 | 3.39 | 186.859 | 1.33 | | 1.5 | 31.875 | 1.67 | 175.481 |
| 4 | 2.88 | 287.821 | 1.60 | | 1.08 | 57.563 | 1.34 | 68.500 |
| 5 | 2.21 | 210.897 | 1.38 | | 1.42 | 51.750 | 1.42 | 74.625 |
| 6 | 3.00 | 355.449 | 1.32 | | 1.43 | 45.500 | 1.32 | 91.313 |
| 7 | 1.98 | 272.756 | 1.92 | | 1.46 | 61.281 | 1.55 | 64.063 |
| 8 | 1.68 | 301.603 | 1.00 | | 1.41 | 51.813 | 1.31 | 88.938 |
| 9 | 1.94 | 285.256 | 1.29 | | 1.38 | 64.062 | 1.18 | 228.009 |

Table caption:

**Table 2.2.11.** Profiles of SI and OM accumulation rate in g m$^2$ yr$^{-1}$ along the Turkey Point transect. Sites are arranged L-R from most coastward (TKYE) to furthest inland (TKYINT). Red typeface indicates intervals characterized by marine influence. Blank cells indicate no data for the interval.

37

*Continuation* **Table 2.2.11**

| Depth | TKYE SI | TKYE OM/yr/m² | TKYW SI | TKYW OM/yr/m² | TKYNW SI | TKYNW OM/yr/m² | TKYINT SI | TKYINT OM/yr/m² |
|---|---|---|---|---|---|---|---|---|
| 10 | | 26.063 | 1.26 | | 1.28 | 83.875 | 1.29 | 256.134 |
| 11 | | 37.844 | 1.46 | | 1.39 | 94.688 | 1.29 | 264.583 |
| 12 | | 24.844 | 1.40 | | 1.38 | 84.375 | 1.27 | 210.995 |
| 13 | | 39.125 | 1.47 | | 1.36 | 91.375 | 1.34 | 244.676 |
| 14 | | 48.875 | 1.36 | | 1.36 | 198.264 | 1.34 | |
| 15 | | 45.406 | 1.46 | | 1.37 | 221.759 | 1.43 | 230.093 |
| 16 | | 56.875 | 1.65 | | 1.43 | | 1.38 | 261.111 |
| 17 | | 37.875 | 1.39 | | 1.38 | 163.657 | 1.43 | 346.065 |
| 18 | | 50.187 | 1.33 | | 1.39 | 224.306 | 1.36 | 168.866 |
| 19 | 1.40 | 57.219 | 1.43 | | 1.4 | 257.639 | 1.35 | 244.097 |
| 20 | 1.38 | 39.781 | 1.45 | | 1.35 | 235.301 | 1.33 | |
| 21 | 1.36 | 28.687 | 1.36 | | 1.38 | | 1.50 | |
| 22 | 1.36 | 35.781 | 1.45 | | 1.42 | | | |
| 23 | 1.50 | 42.125 | 1.41 | | 1.32 | | | |
| 24 | 1.39 | 43.344 | | | 1.39 | | | |
| 25 | 1.41 | 50.406 | 1.31 | | | | 1.50 | |
| 26 | 1.41 | 60.125 | 1.33 | | | | 1.42 | |
| 27 | 1.33 | 65.531 | 1.27 | | | | 0.83 | |
| 28 | 1.36 | 46.625 | 1.24 | | | | 1.29 | |
| 29 | 1.43 | 41.344 | 1.41 | | | | | |
| | 1.38 | 48.750 | 1.32 | | | | | |
| | 1.27 | 49.563 | 1.35 | | | | | |
| | | | 1.36 | | | | | |
| | | | 1.28 | | | | | |

**Summary.** The Turkey Point transect is a marine transgressive stratigraphic sequence associated with SWE and sea level rise. Rising sea level produces a change in state as both plant composition and resultant sediment type change along the marine-to-fresh water gradient. All cores demonstrate an increase in SI towards the surface and the thickness of the marine influenced sediment thickens towards the coast, the result of the increased length of time under marine influence. Mangrove sediments with higher rates of OM accumulation are retreating over and replacing, marl sediments with very low OM storage. At this early point in the transgression along the Turkey Point transect, conditions for greater OM storage are being created.

**Triangle Transect**

Salt water encroachment has reached TANGLIN (upper 6 cm) and TANGLS (upper 4 cm) at this time (**Table 2.2.6**). Initial SWE occurred about 18 yr before present based upon mangrove peat-marl accumulation rate of 3.2 mm yr^{-1} (Meeder et al. 2017). However this peat marl is poorly developed and the accretion rate likely less than the average 3.2 mm yr^{-1}, making the appearance of salt water encroachment somewhat earlier. In both cores mangrove peat marl intervals overlie marl intervals which in turn overlie saw grass peat marl. These cores document a marine transgressive stratigraphic sequence that seems to apply all along the southeast Florida coast (Meeder et al 2017, Meeder and Parkinson 2017).

### 3. Soils

#### 3.1. Soil structure and properties:

#### Materials and methods

We collected soil samples from different ecological gradients of C111 sites including organic rich tree island sites (n=34) and marsh sites (n=48) dominated by inorganic materials. The samples described in this report were collected during 2016-17, across a wide range of flooding conditions. The 17 tree island samples collected in Winter 2018 are not reported on here, but will be incorporated in data analyses for the Final report.

Soil core samples were collected in individual plastic fiber core liners, and subsequently capped on both sides. Short soil cores (variable diameter and core length) were then delivered to FIU freshwater biogeochemistry laboratory (FWBGCL) for chemical and microbiological analyses. The cores were sectioned at different depths depending on the obvious color differences and stored in plastic bags. Soil cores were sectioned up to 30 cm depth whenever possible; otherwise, the results were calculated on a 30 cm hypothetical core for this study. Photographic images and a short description of visual characteristics of the core profiles were recorded. Physiochemical properties, i.e., pH, water soluble P or bioavailable P (WSP), $NaHCO_3$ extractable P (soluble reactive P, SRP) and enzyme assay were determined from fresh wet soils. Fresh soil cores were thoroughly mixed and a representative subsample was used for wet chemical analyses. Other chemical properties including TP, TN, TC, and field bulk density (FBD) were analyzed on dried and ground soil samples. Details of the chemical and microbiological analyses are described below.

Fresh soil samples (nominally 4.5 gm) were weighed into 50 ml centrifuge tubes and 20 ml (known volume) of DDI $H_2O$ was added to obtain soil to water ratio of 1:20, on a dry mass basis, which is a modification of commonly used standard method for WSP (Kuo, 1996). The samples were then shaken continuously on a reciprocating table shaker for 1 h. The speed of the shaker was adjusted to ensure suspension of soil particles in the extracting solution. After one hour the samples were filtered through 0.45 µm membrane filters, and the filtered solutions were stored in a refrigerator (4°C) until the colorimetric analysis of WSP and SRP was done.

Sodium bicarbonate soil samples were also extracted at a 1:20 dry mass soil to solution ratio with 0.5M $NaHCO_3$ (pH 8.5) for 16 hours (Olsen et al., 1954; Olsen and Sommers, 1982; Sims, 2009). Equivalents of 1 g oven dried weight of wet soil (after centrifuging) were placed in 50 ml centrifuge tubes to which 20 ml of extracting solution was added. The suspensions were then shaken for 16 hours on a reciprocating shaker and filtered through 0.45µm membrane filter papers. Filtered solutions were stored afterwards in a refrigerator (4°C) until the analysis for soluble P was done. One set of samples was fumigated with $CHCl_3$ vapor in a sealed desiccator for 24 hours and then extracted by the above mentioned method using 0.5M $NaHCO_3$ solution.

Total carbon (TC) and total nitrogen (TN) of oven dried soil samples were analyzed by the high-temperature dry combustion method using a Carlo-Erba NA-1500 CNS Analyzer (Nelson and Sommers, 1996). Determination of total P was done by oxidation (dry combustion) and hydrolysis of the P-containing compounds in the sample to soluble forms (soluble reactive,

ortho-P; SRP) using $MgSO_4/H_2SO_4$ and HCl (Solórzano and Sharp, 1980), and then followed by standard colorimetric analysis of the resultant SRP (USEPA 1996, method 365.1).

Surficial soils (0-2 cm) were subjected to two assays that seek to characterize soil microbial activity. The first is a rapid extracellular enzyme assay. These assays provide insight into nutrient enrichment, availability, and mineralization (Wright and Reddy, 2001; Prenger and Reddy, 2004). Enzymatic analysis has also been used to assess the decomposition rates of organic matter and detritus, or litter (Sinsabaugh, 1994; Wright and Reddy, 2001; Rejmánková and Sirová, 2007). The second is an assay to determine the lability of soil organic matter as measured by the generation of $CO_2$ in aerobic incubations (Pisani et al. 2015). Both of these assays quantify microbial activity, one of the first processes thought to be influenced by changing environmental conditions. Enzyme assays were conducted to determine the activity of the β-glucosidase and phosphatase enzymes. Soil microbes produce β-glucosidase or phosphatase enzymes to cleave the esterase bond between complex organic molecules and the glucose or phosphate, respectively, thus allowing these compounds to become more available for uptake, degrading the organic compound in the process. Activity was determined by adding moieties of the fluorogenic substrate, 4-methylumbelliferyl (MUF; either -β-glucoside -MUF-C or MUF-phosphatase- MUF-P) to floc or soil slurries. Nominally one gram (known mass) of fresh weight soil was mixed with 1 ml of distilled, deionized, water ($DDIH_2O$) to create a 1:1 (soil:solution) slurry. Slurries were then diluted sequentially by addition of 9 ml $DDIH_2O$ to 1 ml of soil slurry and homogenized to get a ten times dilution ($10^{-1}$) of the soil slurry. This process was completed two more times to end with a final $10^{-3}$ dilution of slurry for enzyme activity analysis. Diluted samples (200 µl) were pipetted into 8 wells (one column) of a 96-well plate to which 50 µl of either MUF-P or MUF-C substrates were added to obtain final MUF-X concentrations of 10 µM. Plates were then incubated in the dark for 2 hrs (MUF-P) or 24 h (MUF-C). Substrates were added to replicate cells after incubation and immediately before fluorometric analysis to determine initial fluorescence (i.e. $t_0$). No substrate was added to rows/columns containing standards or background blanks. A Synergy HT microplate reader was used for fluorometric determination with excitation at $360 \pm 40$ nm and emission at $460 \pm 40$ nm. Enzyme activity was calculated using regressions of standard curves and expressed in µmol per gram of dry weight per hour (µmol $g^{-1}$ $h^{-1}$) soil samples.

Florida International University laboratory maintains strict Quality Assurance and Quality Control procedures. Calibration curves are analyzed and summarized at the beginning of all analytical runs according to method specification. Standards, either citrus or apple leaves, are digested or combusted for all TP and TN/TC analysis. All standards are accepted within the analytical range as defined by the National Bureau of Standards (NBS). Analytical duplicate samples are analyzed (10% of total samples) in all analysis runs. Acceptable duplicate analysis is $\pm 15\%$ relative percent difference (RPD). Matrix spikes are analyzed at 5% of total samples in all analytical runs and are accepted at $\pm 20\%$ recovery. Additionally analytical blanks are (5% of total samples) analyzed in all runs. All QA/QC results are included with combined data file. The Freshwater Biogeochemistry Laboratory (FIU FWBGCL) utilized Chain of Custody forms to insure all samples and analysis are accounted for and tracked.

# Results and Discussion

We found that physiochemical properties of soils collected at C111 sites are highly variable and thus we ran principal component analysis to test the data variability. Principal components (PC) 1 and 2 cumulatively explained about 70% of the total variability of the data (**Table 3.1.1**). PC1 and PC2 were therefore used to plot the results of the analyses.

When all physiochemical parameters are considered, it appears that field bulk density (FBD) and organic matter (OM) played the most significant roles in defining soil characteristics (**Table 3.1.2**).

**Table 3.1.1.** Principal component analysis of different physicochemical parameters of all the soils collected at C111 site.

| Eigenvalues of the Correlation Matrix | | | | |
|---|---|---|---|---|
| **Principal component** | **Eigenvalue** | **Difference** | **Proportion** | **Cumulative** |
| 1 | 6.4866 | 4.82362815 | 0.5897 | 0.5559 |
| 2 | 1.6630 | 0.73498233 | 0.1511 | 0.7003 |
| 3 | 0.9281 | 0.23666580 | 0.1031 | 0.8034 |
| 4 | 0.6914 | 0.19456362 | 0.0768 | 0.8802 |
| 5 | 0.4969 | 0.17592564 | 0.0552 | 0.9355 |
| 6 | 0.3210 | 0.20661392 | 0.0357 | 0.9711 |
| 7 | 0.1143 | 0.02137719 | 0.0127 | 0.9838 |
| 8 | 0.0930 | 0.04050385 | 0.0103 | 0.9942 |
| 9 | 0.0525 | | 0.0058 | 1.0000 |

**Table 3.1.2.** PCA analysis with PC1 and PC2 showing factor weightings for C111 soil samples

| Parameters | PCA1 | PCA2 |
|---|---|---|
| FBD | -0.32110 | 0.34564 |
| pH | -0.205754 | -.146876 |
| OM | 0.36725 | 0.17839 |
| Soil Moisture | 0.330708 | -.478279 |
| TN | 0.401946 | 0.050230 |
| TP | 0.342694 | 0.277780 |
| TC | 0.416212 | 0.181855 |
| WSP | 0.290544 | 0.315143 |
| SRP | 0.120189 | -.602585 |

A biplot was constructed using all the variables (**Fig. 3.1.1**). The cosine angle between vectors determine the degree of correlation between them. Narrow cosine angle between two vectors indicates that they are highly correlated. Orthogonal vectors are unrelated with each other. When the directions of the vectors are opposite, then they are negatively correlated (Cuin et al., 2010). Hence, from the vector orientation it can be observed that water content and fraction dry are negatively correlated, while TP, TN, TC, and OM that are positively correlated with each other.

Biplot analysis of all parameters show that most soils, including nearly all marsh soils, fall in the 2nd and 3rd quadrants (Figure 1). However, many tree island soil samples were concentrated in the 1st quadrant, representing a distinct group of organic- and nutrient-rich samples.
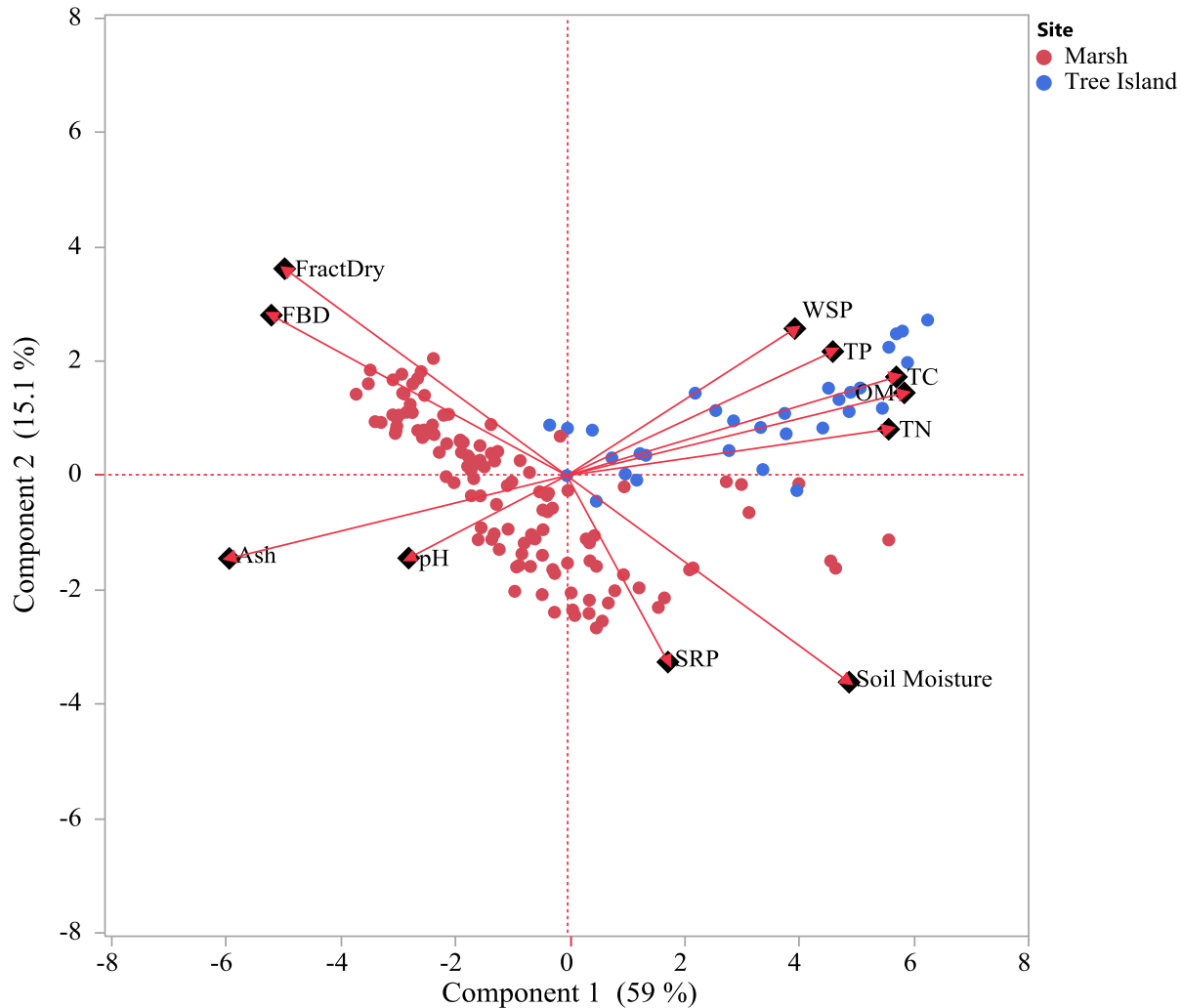


**Figure 3.1.1.** Biplot of the first two components of the PCA model for a) all soil parameters and b) FBD and OM parameters for all C111 samples.

Many of the marsh core samples contained inclusions of black peat or brown peat soil and sometimes roots or leaves, and these additional organic components or peat soil fractions may have influenced the categorization of the soil samples. A better assessment of those soil categories are needed for all the soil samples collected at C111 sites. So, depending on the FBD and OM content of the samples we categorize the samples in 4 different types 1) marl soil 2) marly peat soil 3) peaty marl soil and 4) peat soil. Peat and peaty marl soil were black or dark brown in color, with some fibrous roots and/or leaves, whereas marl and marly peat soils appeared grey, light grey, or light brown in color, with occasional root content. Detailed characteristics of these 4 soil types are described below.

*1) Marl soil (n = 69)*
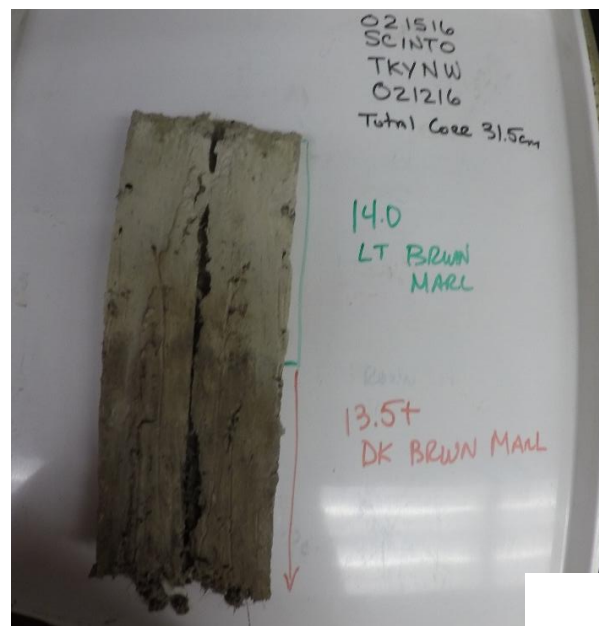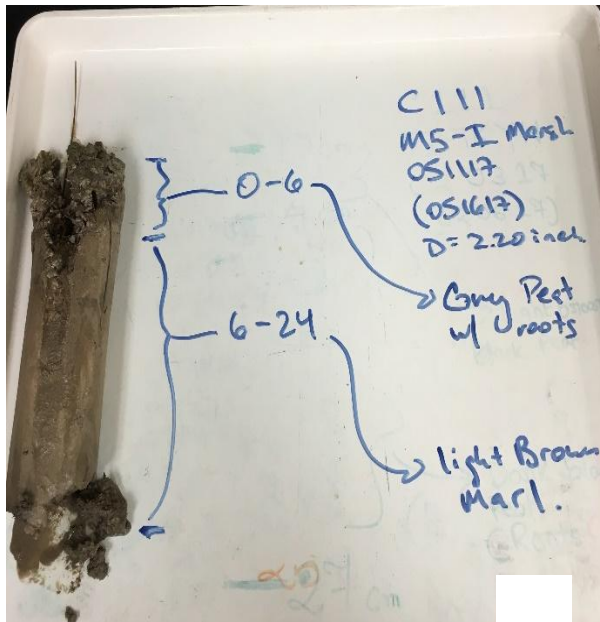


Organic matter content: average is 10% with a range of 5-14% (on dry weight basis)
Field bulk density: average is 0.45, with a range of 0.13-1.02 gm DW cm$^{-3}$
Total P content: average is 71.8, with a range of 26-132.5 µg gm$^{-1}$ DW of soil
TN/TC ratio: average is 0.03, with a range of 0.01-0.05

*2) Marly peat soil (n = 32)*
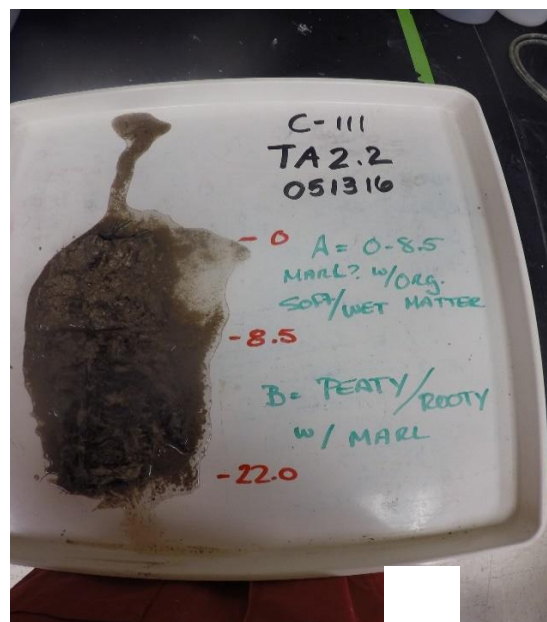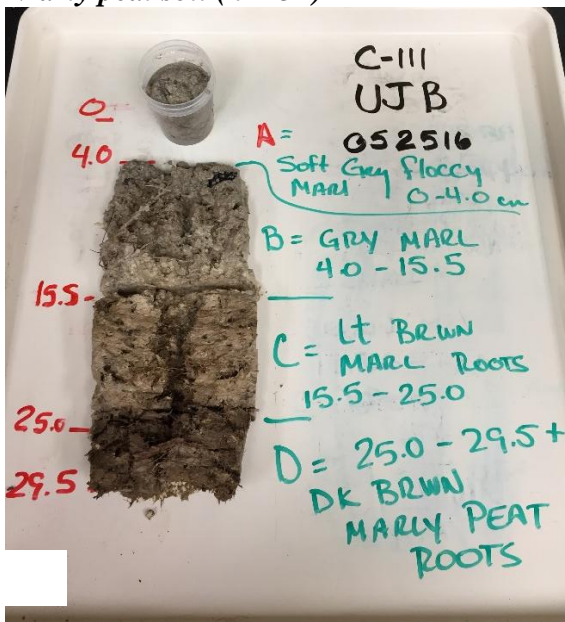


Organic matter content: average is 18% with a range of 15-24% (on dry weight basis)
Field bulk density: average is 0.25, with a range of 0.10-0.43 gm DW cm$^{-3}$
Total P content: average is 82, with a range of 28-214 µg gm$^{-1}$ DW of soil
TN/TC ratio: average is 0.05, with a range of 0.03-0.06

### 3) Peaty marl soil (n = 19)
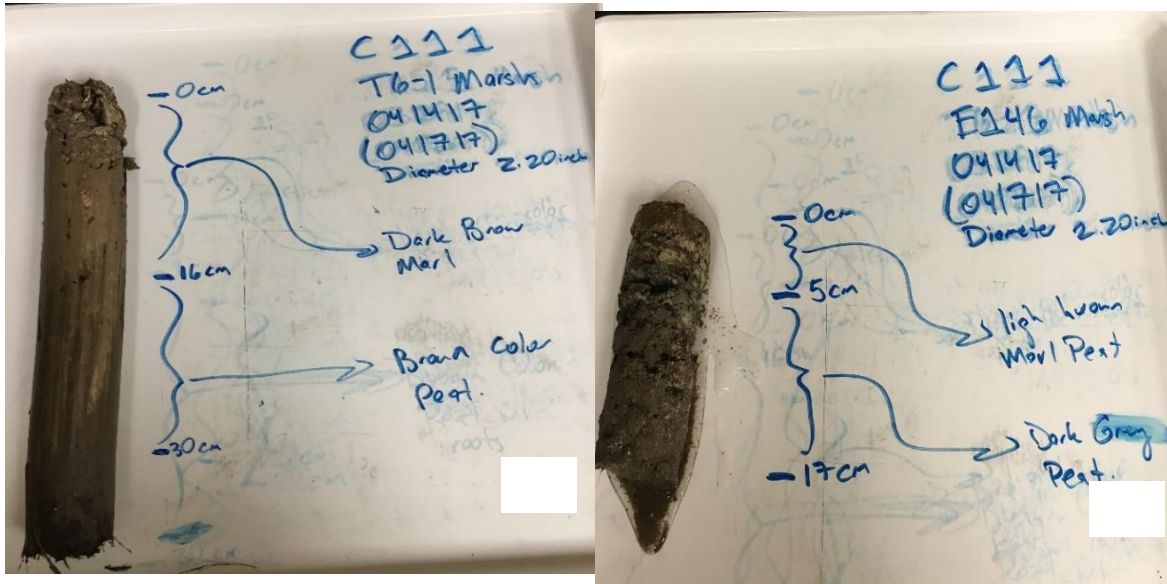


Organic matter content: average is 30% with a range of 25-38% (on dry weight basis)
Field bulk density: average is 0.13, with a range of 0.03-0.33 gm DW cm$^{-3}$
Total P content: average is 117.6, with a range of 43-419 µg gm$^{-1}$ DW of soil
TN/TC ratio: average is 0.05, with a range of 0.02-0.08

### 4) Peat soil (n = 36)
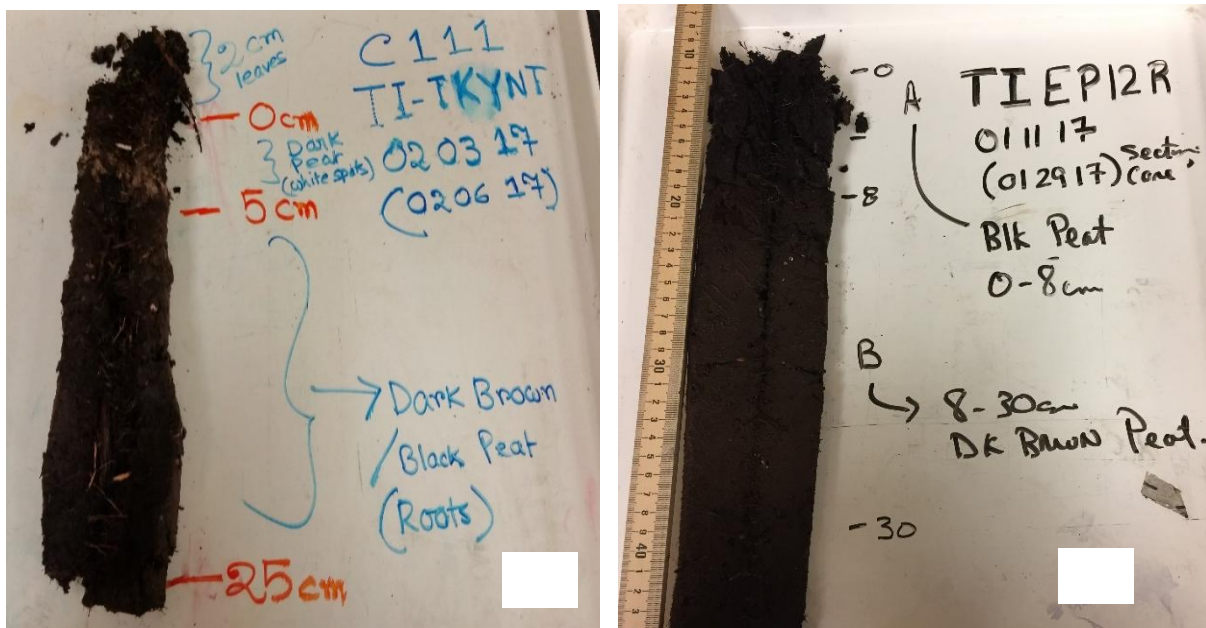


Organic matter content: average is 70% with a range of 39-89% (on dry weight basis)
Field bulk density: average is 0.12, with a range of 0.04-0.37 gm DW cm$^{-3}$
Total P content: average is 450.9, with a range of 132-1017 µg gm$^{-1}$ DW of soil
TN/TC ratio: average is 0.05, with a range of 0.04-0.09

As there was a considerable overlap between tree island and marsh soils (**Fig. 3.1.1**), separate box plots were constructed for comparison of N and P across samples (**Fig. 3.1.2 and 3.1.3**). Marl and marly peat soil contained the least TP while peat soils were highest in TP (μg/gm dry soil basis) (**Fig. 3.1.2**). This is at least in part because the marl soil has higher FBD as compared to the peat soil.
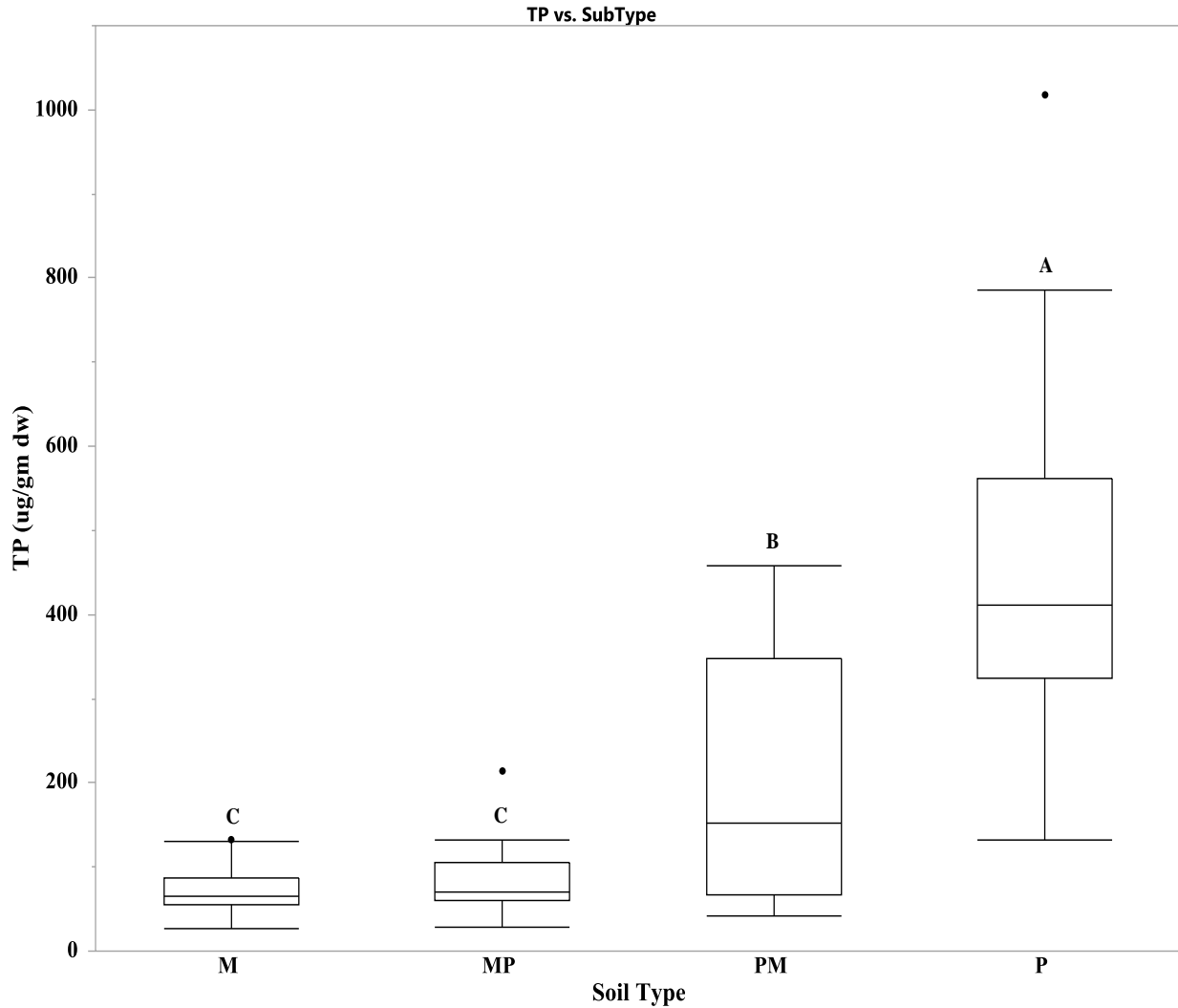


**Figure 3.1.2**. Boxplot analysis (with ANOVA) for Total P (TP) concentrations of 4 different soils types such as marl (M), marly peat (MP), peaty marl (PM) and peat (P) of C111 samples.
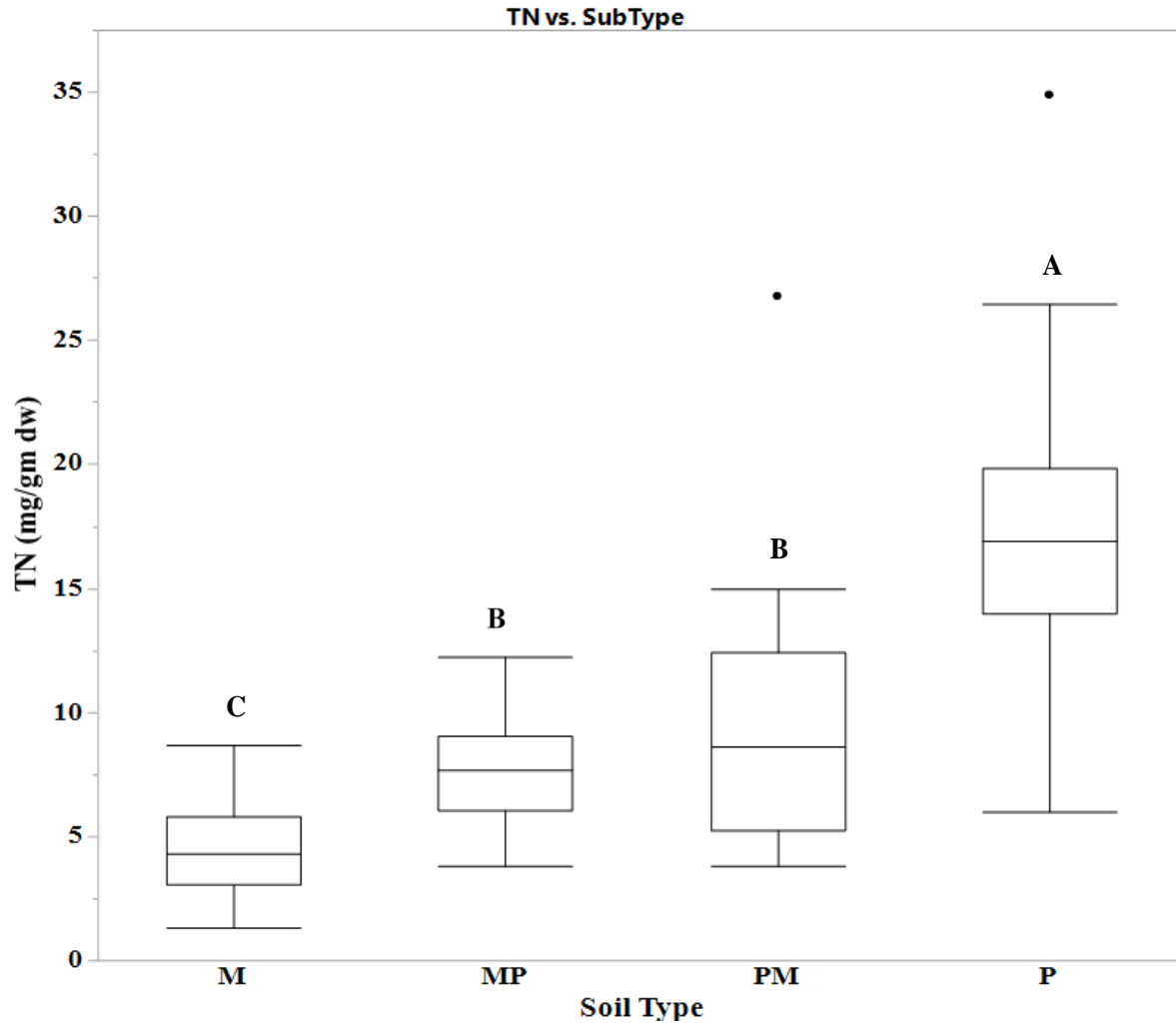
**Figure 3.1.3**. Boxplot analysis (with ANOVA) for Total N (TN) concentrations of 4 different soils types such as marl (M), marly peat (MP), peaty marl (PM) and peat (P) of C111 samples.

Marl soil contains the lowest TN (mg/gm dry soil basis) and peat soil the highest among the four soil types (**Fig. 3.1.3**). Marl soils are mostly oxidized mineral soil with shorter hydroperiod while peat soils are forming under wetter conditions. As it is in many situations, high TN content is associated with high organic matter content in the C111 basin.

$$TP = 87.29 + 673.98e^{-2.86 \, x \, Near \, Distance}$$
$$R^2 = 0.40$$
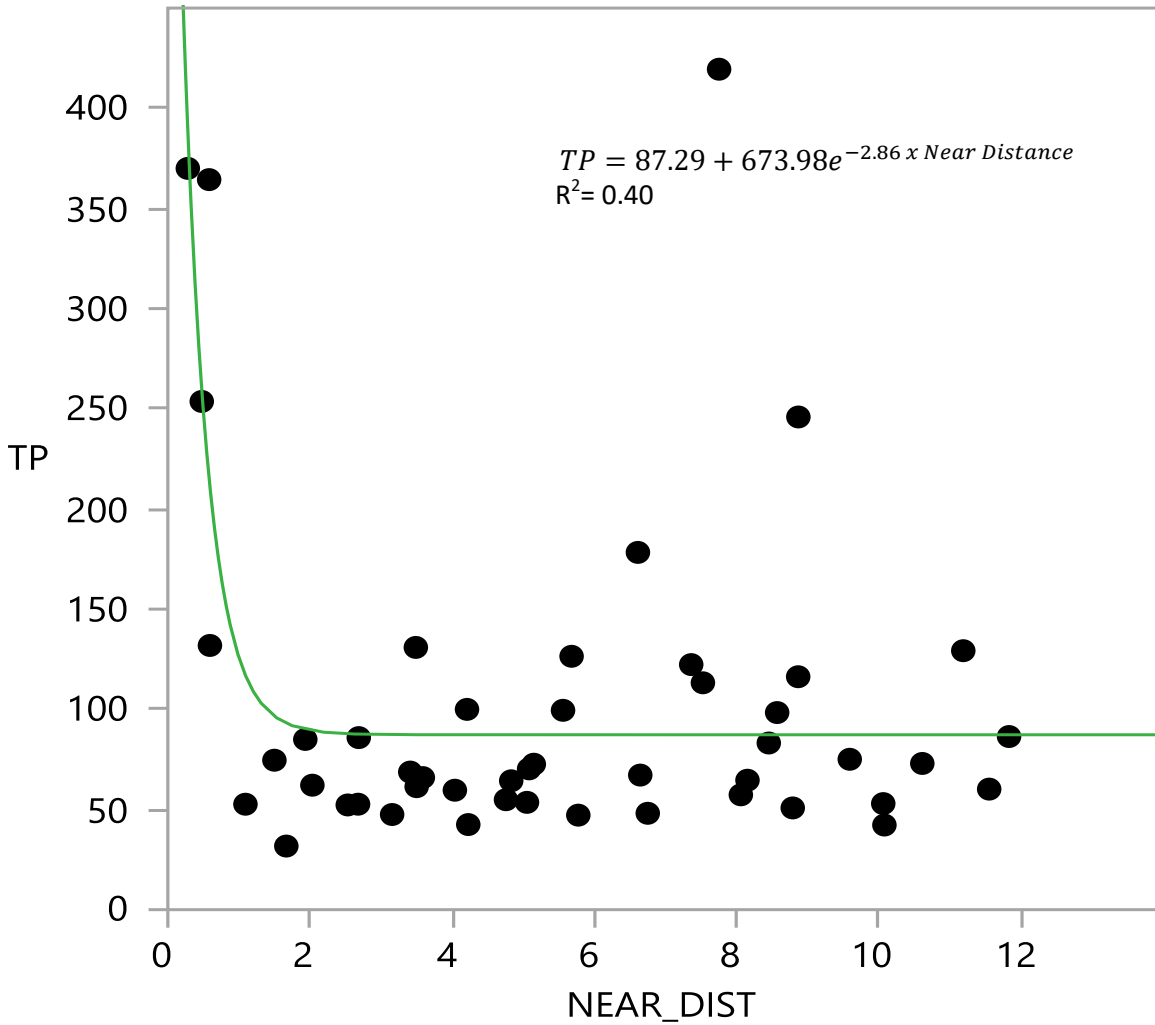
**Figure 3.1.4**. Curve fitting analysis of total P with the distance from the canal for marsh soil samples of C111.

TP exhibits a reasonably good fit to an exponential decline with distance from the C-111 Canal (**Fig. 3.1.4**). However, the presence of several high P sites at considerable distances from the Canal make it difficult to interpret the pattern as evidence of a source effect. In other parts of the Everglades ecosystem, soil P has been demonstrated to decline gradually downstream of structures delivering water directly into the marsh.
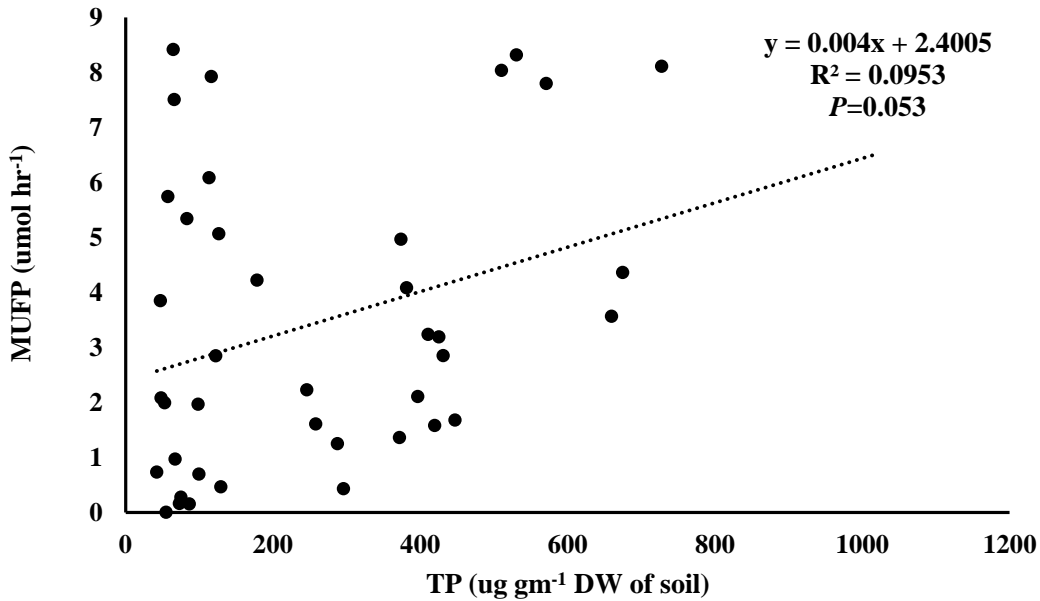
**Figure 3.1.5**. Relation between MUFP activity and TP content of surface soils (0-2 cm) collected from C111 sites

When analysis was applied across all sites, the MUFP activity showed a weak positive relationship with TP content (**Fig.3.1.5**). This was an unexpected result, as phosphatase activity typically is highest where P is most limited. To get a better explanation of the data, two separate graphs were prepared for tree island and marsh soils (**Fig 3.1.6 and 7** respectively).
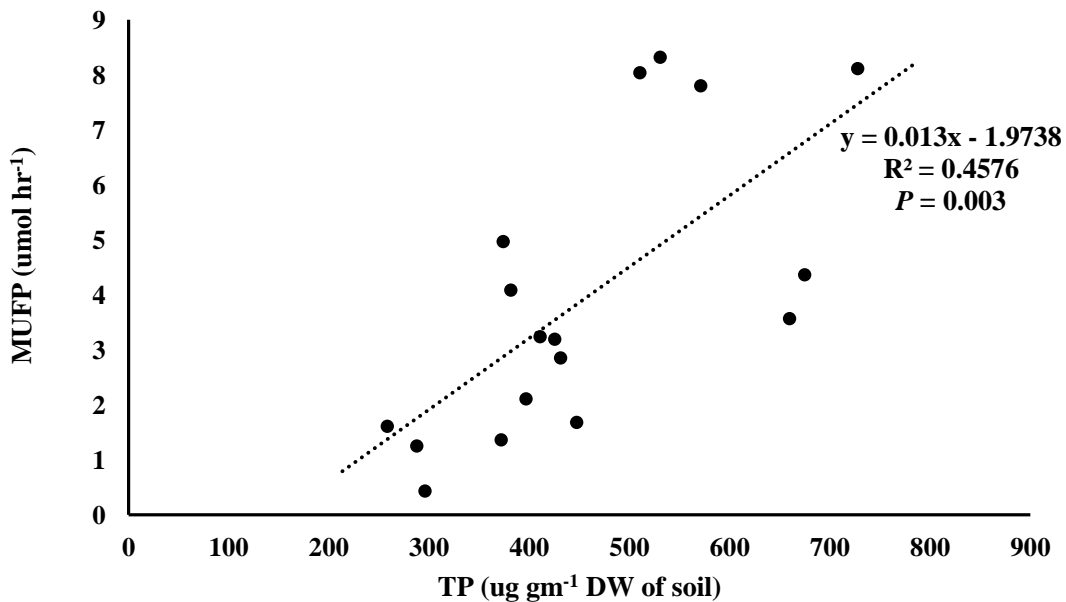


**Figure 3.1.6**. Relation between MUFP activity and TP content of surface soils (0-2 cm) collected only from tree island sites of C111.

Tree islands show a strong positive correlation between soil TP concentration and MUFP enzyme activity (**Fig.3.1.6**). As mentioned above, this is the reverse of the expected pattern. We hypothesize that this pattern is linked to high microbe populations in the tree island soils. It may be that the availability of TP is lower than the microbial demand in these forests, resulting in high phosphatase enzyme activity. Marsh sites follow the common relation between TP content and MUFP activity, although the negative correlation is very weak and in fact non-significant (**Fig 3.1.7**).
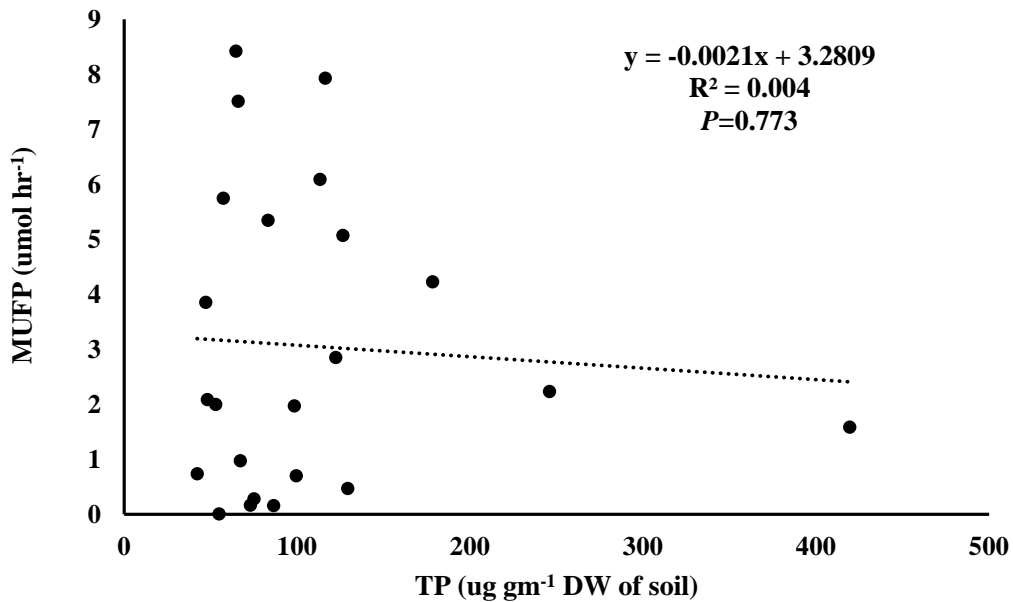


**Figure 3.1.7**. Relation between MUFP activity and TP content of surface soils (0-2 cm) collected only from marsh sites of C111.
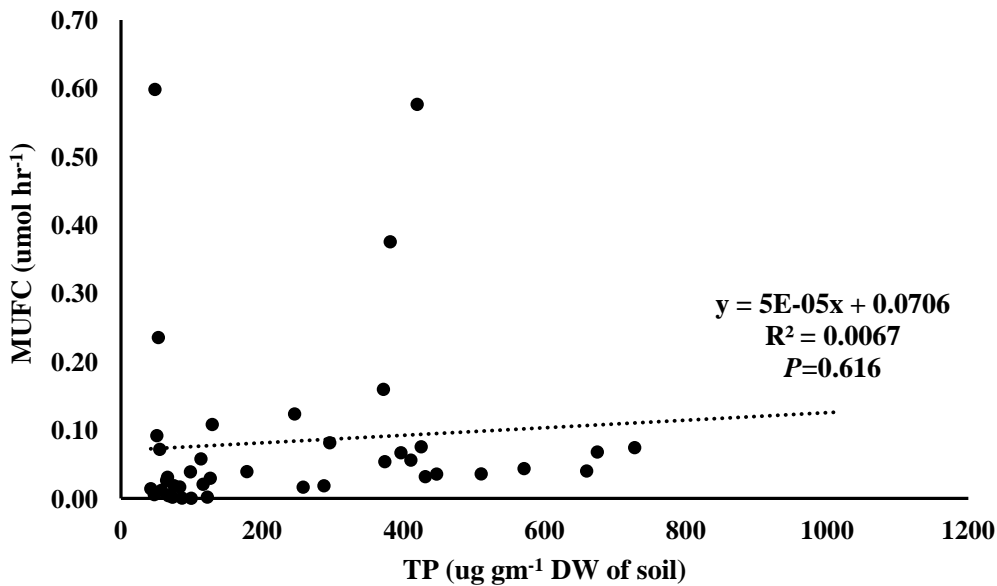


**Figure 3.1.8**. Relation between MUFC activity and TP content of surface soils (0-2 cm) collected from C111 sites

In **Fig. 3.1.8**, the relationship between MUFC activity and TP content is non-significant across all sites. To get better interpretability we again constructed separate graphs for tree island and marsh sites (**Fig. 3.1.9 and 10** respectively). Tree island sites showed very weak negative relation between TP and β-glucosidase activity. However marsh sites showed a significant positive relation between TP and MUFC enzymes activity ($P$=0.019) (**Fig. 3.1.10**). We reason that in the marsh sites where P is generally strongly limiting, sites of higher phosphorus availability have relatively high microbial populations, resulting in higher MUFC activity.
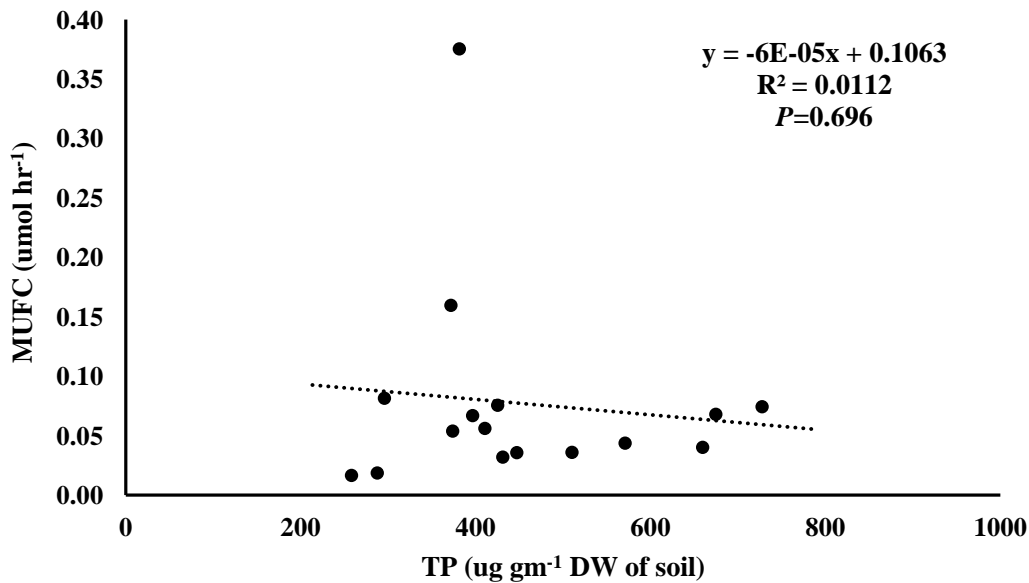


**Figure 3.1.9**. Relation between MUFC activity and TP content of surface soils (0-2 cm) collected only from tree island sites of C111.
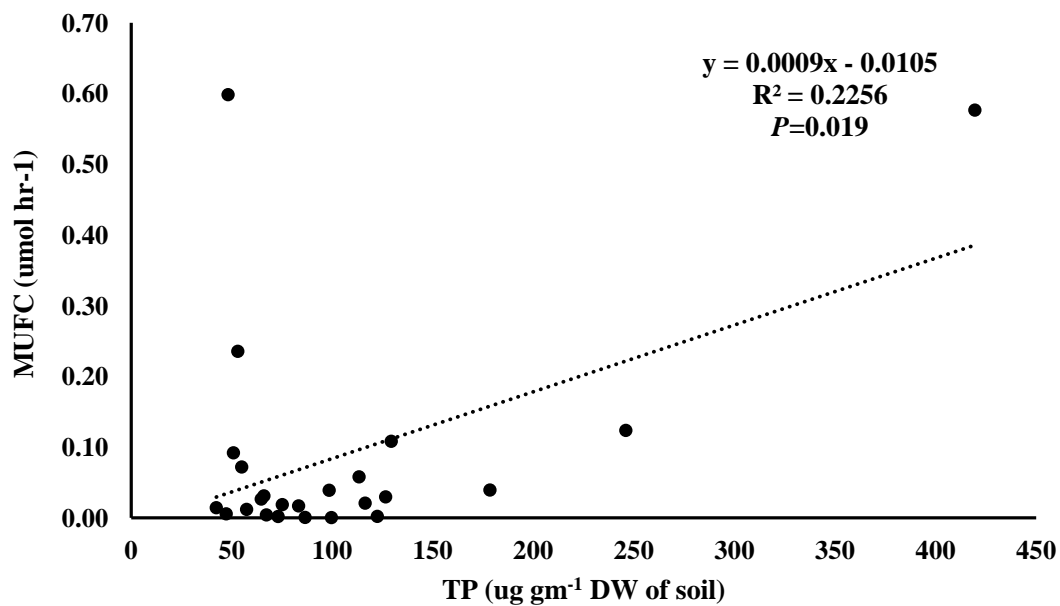


**Figure 3.1.10**. Relation between MUFC activity and TP content of surface soils (0-2 cm) collected only from marsh sites of C111

50

## 3.2. Sediment accumulation rates by $^{210}$Pb dating

Accretion rates were determined by $^{210}$Pb dating for two C-111 sites: T6.4, west of Taylor Slough, and TANGLI, 4 km from the coast in the middle of the white zone in wetlands between US 1 and Card Sound Road. The soil at T6.4 is a marl, while soil at TANGLI is marl from 6-23 cm depth, and peaty marl above. Soil accretion rates at the two sites range from 0.57 to 1.2 mm per yr at T6.4, and from 0.67 – 2.32 at TANGLI, depending on the depth considered, as well as the assumptions of the accretion models used. Variation of accretion with depth, and details of the calculations are described below. Raw data used for calculations is shown in **Appendix 3.2.1.**



**CORE T6-4**

$$\ln{}^{210}Pb_{xs} = (-\lambda/s)Z + \ln{}^{210}Pb_{xsinitial}$$

$$\ln{}^{210}Pb_{xs} = (-.2963)Z + 4.1569$$
S=1.0 mm/y (5.5-12.5 cm)
$R^2 = 0.89$

$$\ln{}^{210}Pb_{xs} = (-.4364)Z + 5.2795$$
S=0.71 mm/y (5.5 -15.5 cm)
$R^2 = 0.92$
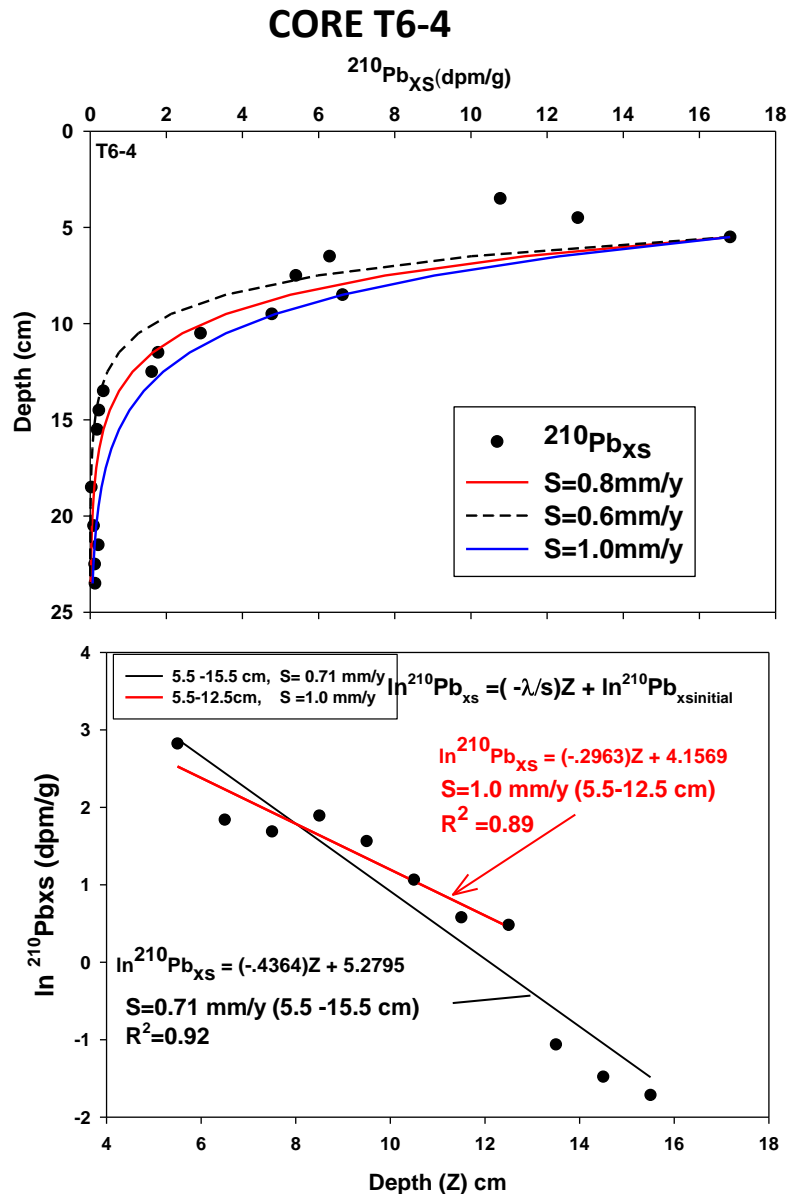
**Figure 3.2.1**. CIC (constant initial concentration) model that relies on the slope. The upper 5.5 cm cannot be used in this case as there is no slope, i.e. the sediment is mixed. The top figure shows the model fits ranging for 0.6 and 1.0 mm/y for depths $\geq$ 5.5 cm. The bottom figure shows the log plot. The average sedimentation rate for the **upper 5.5-12.5 cm is 1.0 mm/y** and over the depth range 5.5 – 15.5 cm is 0.71 mm/y.

**Constant Flux model**

T6-4

S = 0.57 mm/y
(10.5 -15.5 cm)
R²□= 0.965

S=1.2mm/y
(3.5 - 9.5cm)
R² = 0.961

S=0.70 mm/y
(3.5 - 20.5cm)
R² =0.715

| | 3.5 - 20.5 cm, | S =0.70 mm/y |
| 3.5 - 9.5 cm, | S=1.2 mm/y |
| 10.5 -15.5 cm, | S=0.57 mm/y |
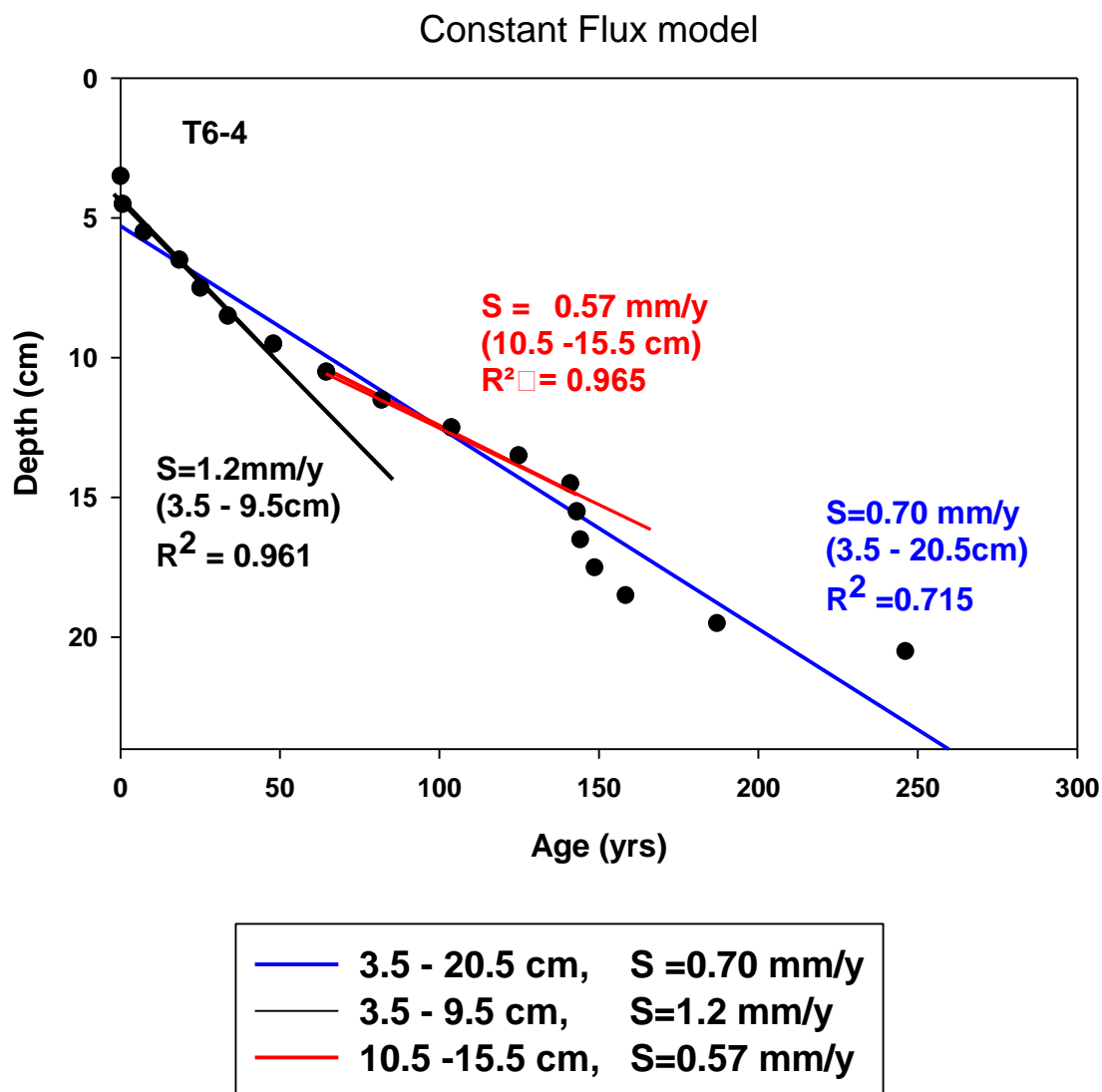
**Figure 3.2.2**. Where sediment accumulation is not constant, unsupported 210Pb activity will vary with depth in a complicated way (e.g. scatter) and 210Pb profiles (plotted logarithmically) will be non-linear (see figure 1). Then the CRS (constant rate of supply) model is used which relies on the depth distribution of the 210Pb inventory, and allows the age profile to be calculated. Note that ages can be assigned to the upper core which is mixed. Here, a sedimentation rate of 1.2 mm/y is calculated for the depth 3.5 – 9.5 cm. This is close to the CIC model in figure 1. For depths 10.5 – 15.5 cm, a sedimentation rate of 0.57 mm/y is calculated, and for 3.5 – 20.5 cm, a sedimentation rate of 0.70 mm/y is calculated.

# CORE TANGLI
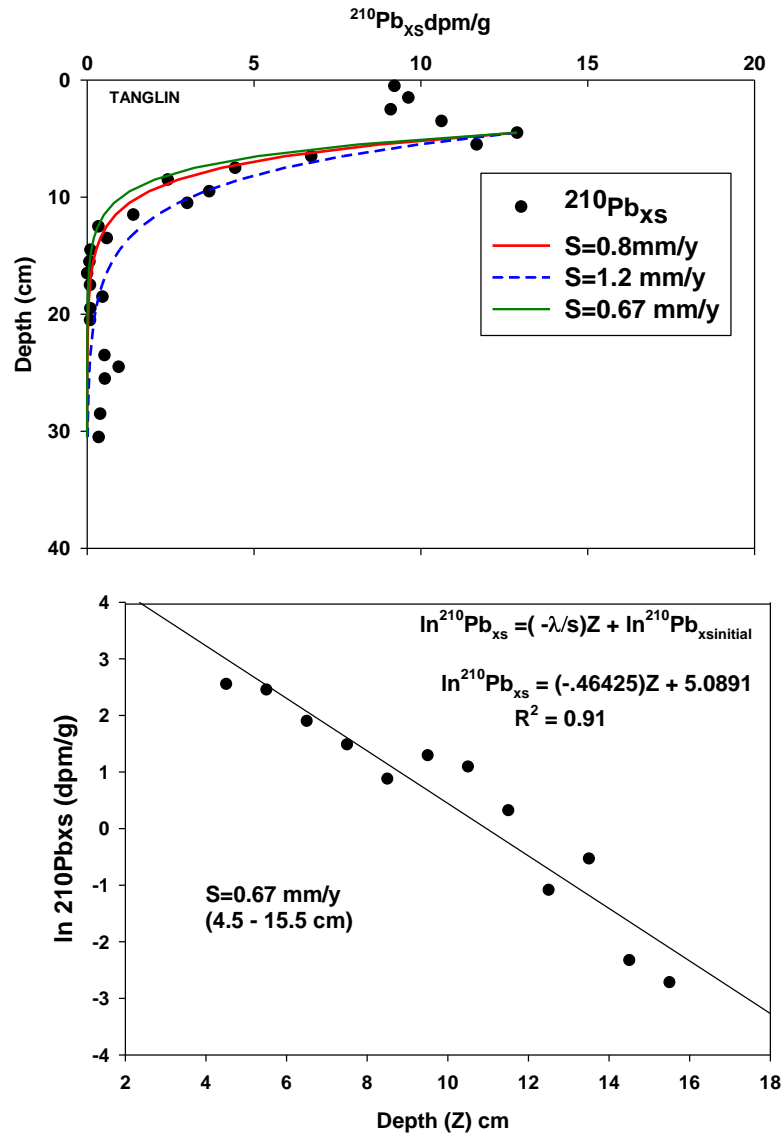


**Figure 3.2.3**. CIC (constant initial concentration) model that relies on the slope. The upper 4.5 cm cannot be used in this case as there is no slope, i.e. the sediment is mixed. The top figure shows the model fits ranging between 0.67 and 1.2 mm/y for depths $\geq$ 4.5 cm. The bottom figure shows the log plot. The average sedimentation rate over the depth range 4.5 – 15.5 cm is 0.67 mm/y, but note the scatter.
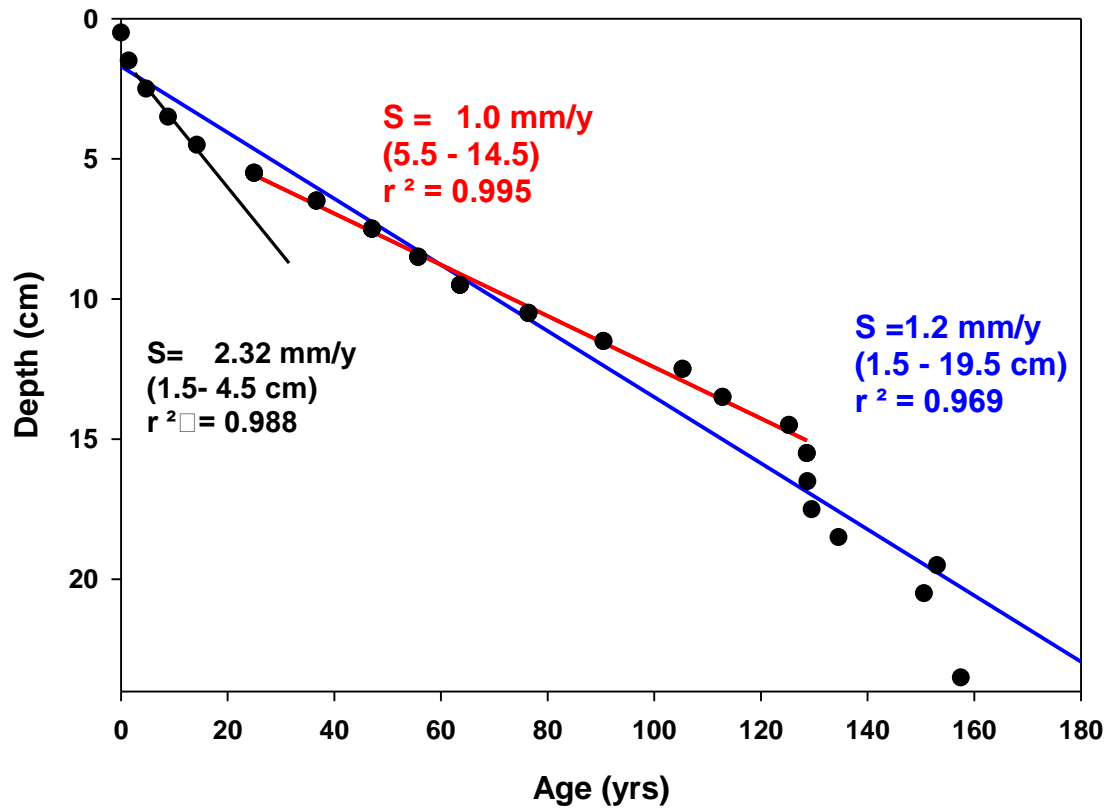
**Figure 3.2.4.** Where sediment accumulation is not constant, unsupported 210Pb activity will vary with depth in a complicated way (e.g. scatter) and 210Pb profiles (plotted logarithmically) will be non-linear (see figure 3). Then the CRS (constant rate of supply) model is used which relies on the depth distribution of the 210Pb inventory, and allows the age profile to be calculated. Note that ages can be assigned to the upper core which is mixed. Here, a sedimentation rate of 2.32 mm/y is calculated for the depth 1.5 – 4.5 cm. For depths 5.5 – 14.5 cm, a sedimentation rate of 1.0 mm/y is calculated, and for 1.5 – 19.5 cm, a sedimentation rate of 1.2 mm/y is calculated.

### 3.3. Belowground carbon dynamics:

### Introduction

Accelerated sea level rise (SLR) is causing drastic changes to the structure and function of coastal wetlands. Saltwater intrusion is expected in many freshwater ecosystems as SLR increases (Rahmstorf 2007; Milne et al. 2009), climate change alters temperature and precipitation patterns (Smith et al. 2005; Mily et al. 2005), and anthropogenic alterations upstream continue to reduce freshwater flow (Meehl et al. 2007). Additionally, global changes are causing major shifts in plant communities worldwide (Chen et al. 2011) and saltwater intrusion is expected to lead to the replacement of freshwater marsh communities with halophytic species (Sutter et al. 2013). In tropical and subtropical ecosystems, saltwater intrusion can cause mangroves to move inland and displace herbaceous marshes, as has been observed in Australia (Rogers et al. 2000, 2006; Winn et al. 2006), Mexico (Lopez-Medellin et al. 2011), and the United States (Ross et al. 2000; Krauss et al. 2011; Smith et al. 2013). Any shifts in coastal wetland C storage associated with these changes will have profound impacts locally on marsh resilience, and globally on the sequestration of $CO_2$, yet we lack a clear understanding of the impact of shifts in hydrologic conditions and foundation plant species.

Shifts between plant communities with drastically different traits are likely to alter ecosystem function (Ellison et al. 2005; Kominoski et al. 2013). One of the most obvious vegetation shifts across the landscape is the encroachment of woody vegetation into grasslands, a phenomenon occurring globally (Van Auken 2000; Frelich and Reich 2010; Knapp et al. 2008; Saintilan et al. 2015). Vegetation changes may influence C cycling through effects on productivity, litter chemistry, microclimate, capture of allochthonous inputs and soil aeration (Furukawa et al. 1997; Bowman et al. 2004; Lovett et al. 2004; Wittman et al. 2004; Fagherazzi et al. 2006), and in terrestrial ecosystems woody encroachment generally leads to increased soil carbon storage (Elridge et al. 2011). In coastal wetlands, differences in the capacities of marsh and mangrove to store C is uncertain (Kelleway et al. 2017), but any shift in C cycling associated with vegetation change may alter climate forcing, sediment accretion and wetland stability (Chen and Twilley 1999; Turner et al. 2004; McKee et al. 2007), as well as local water quality (Boto and Wellington 1988; Childers et al. 2002; Brinson et al. 2006). In a mineral-poor sedimentary environment like the Everglades interior, organic matter dynamics drive elevation change, particularly through the production and accumulation of roots (Hatten et al. 1983; Nyman et al. 1993; Turner et al. 2001; Delaune and Pezeshki 2002).

While shrub expansion into terrestrial ecosystems generally increases soil C storage (Elridge et al. 2011), there is still debate about whether mangrove encroachment is likely to increase soil C, particularly when driven by saltwater intrusion. Globally, mangrove and saltmarsh ecosystems store similar amounts of soil carbon (Chmura et al. 2013), and when adjacent mangrove and saltmarsh ecosystems have been compared, several studies have found greater soil C storage capacity in mangroves (Bianchi et al. 2013; Bianchi et al. 2013; Yando and others 2016; Charles et al. in review), while others have found no difference (Perry and Mendelssohn 2009; Henry and Twilley 2013; Doughty and others 2015). Driven by saltwater intrusion, landward mangrove encroachment often replaces freshwater and brackish marsh species. With or without mangrove expansion, saltwater intrusion can drive loss of soil OC by decreasing plant productivity and

biomass with salt stress (e.g., Krauss et al. 2009; Neubauer 2008), and cause major biogeochemical changes that often lead to enhanced breakdown of soil organic matter (Weston et al. 2006; Neubauer 2013; Chambers et al. 2013). However, in oligotrophic estuaries, like the Florida Everglades, saltwater intrusion may provide nutrients and stimulate productivity (Childers et al. 2006).  Saltwater intrusion may have drastically different impacts when accompanied by vegetation shifts.

The Florida Everglades are particularly susceptible to saltwater intrusion from sea level rise due to its low elevation (Titus and Richman 2001). This wetland is underlain by porous limestone bedrock, and a series of 2500 km of canals and water control structures greatly reduce natural freshwater availability (Sklar et al. 2000; McVoy et al. 2011). Within the coastal area, Everglades plant communities are oriented in zones according to their salinity tolerances. Glycophytic communities dominated by *Cladium jamaicense* occupy inland areas through competitive advantages in freshwater environments, mangrove species dominated by *Rhizophora mangle* prevail nearer to the coast due to salt tolerance, and the ecotone between the two is occupied by mixed graminoid-mangrove communities (Egler 1952; Koch 1996; Ross et al. 2000). Between 1940 and 1994, the mixed graminoid-mangrove community in the southeastern Everglades moved inland 3.3 km and was replaced by stands of *R. mangle* (Ross et al. 2000), a pattern identified elsewhere in the Everglades as well (Krauss et al. 2011; Smith et al. 2013). Additionally, an interior band of sparse vegetation  - the "white zone" (Egler 1952) - has expanded into what was previously denser-canopied freshwater marsh. Saltwater intrusion along the Everglades ecotone has also increased P availability (Sandoval et al. 2016), often temporarily increasing sawgrass productivity, but salinity stress ultimately reduces sawgrass productivity (Ewel et al. 2006; Troxler et al. 2014).

The Southeast Saline Everglades provides a unique opportunity to understand the functional implications of interacting saltwater intrusion and marsh-to-mangrove vegetation state change. As salinity intrudes, mangrove colonization of the landscape is spatially variable and heterogeneous, providing an ideal opportunity to understand the impacts of saltwater intrusion with and without the presence of mangroves. Furthermore, the Comprehensive Everglades Restoration Plan promises to increase the flow of freshwater to the southern Everglades in the coming years, potentially altering the march of coastal biotic and abiotic conditions toward the Everglades interior (Sklar et al. 2000). Quantifying the drivers of C storage in coastal wetlands will help identify vulnerability and shape management decisions in coastal wetlands.

We sampled five transects (24 sites) in the Southeast Saline Everglades to establish changes in plant communities over a 20-year interval (Ross et al. 2000). Within each site, we measured stocks (root biomass) and fluxes (root productivity and OM breakdown) of soil OC to determine how shifting vegetation (species, cover, height), environmental characteristics (soil depth, type, nutrient and organic matter content) and distance to the coast (a proxy for shifting marine connectivity) interact to influence C stocks and fluxes across the landscape. These findings will help to pinpoint areas and conditions that contribute to wetland vulnerability to loss of organic C and inundation by rising seas.  Moreover, our results may serve to distinguish the functional differences driven by vegetation dynamics from those driven by larger scale biogeochemical changes associated with saltwater intrusion.

**Methods**

We created transects across the Southeast Saline Everglades that provide a gradient across the marsh-mangrove ecotone. Included in the gradient are the lower and upper portions of the white zone, the "incipient" white zone (Ross et al. 2000; 2002) and the distal edge of the freshwater marsh for a total of 24 sites (Figure 1).

*Aboveground Vegetation.* At each site we estimated the shoot cover of vascular plant species rooted within 30 1-m$^2$ plots distributed along a 360 degree arc, each 50 m from the plot center (Ross et al 2000). The design allowed us to identify larger vegetation patterns, as well as heterogeneity within the larger landscape. Species abundance at each site was characterized based on its relative frequency within the 1m$^2$ vegetation plots. We also calculated averages of total cover, red mangrove cover and graminoid cover for each site.

*Root Biomass and productivity.* Within each site, we took three root biomass cores from the coastal to inland edge of our sites (generally North-South). Additionally, we extracted one 7.5-cm diameter × 30-cm deep soil core from the center of each site and transported it to the lab, where living roots were separated from the bulk soil, dried at 50° C and measured for biomass and organic C content as loss on ignition. Next, a mesh bag filled with commercial peat moss was placed in each hole vacated by belowground biomass cores (McKee et al. 2007). Root ingrowth bags were retrieved after 6-12 months in the field, based on access to sites (helicopter scheduling). Roots were separated from the ingrowth bags, dried and weighed. Root productivity was standardized to represent root growth per year.

*Organic Matter Breakdown.* We tested breakdown rates for labile (cellulose) and recalcitrant (wood) OM, using standard substrates. Adjacent to each root ingrowth experiment, we measured the breakdown of wood and cellulose standard substrates on the soil surface, and at 10-15 cm and 15-30 cm depths in the soil. After incubation in the field for 8-16 months, we returned all OM breakdown samples to the laboratory on ice, rinsed them of sediment, and dried the samples at 60$^0$C until their mass stabilized. We estimated breakdown rate, $k$, using a linear regression of the ln-transformed fraction of AFDM remaining vs. time (negative exponential model; sensu Benfield 2006). The specific model used was $M_d = M_0 \bullet e^{-kt}$, where $M_0$ is the initial litter mass, $M_t$ is the litter mass on a given sampling day, and $d$ is number of days of incubation). In addition, we used data from a NOAA local temperature station (N 25. 3903°, W -80.6803) to determine average daily temperature and degree days (days of incubation $\bullet$ degree C) over the incubation period. To examine breakdown as a function of temperature, we also calculated breakdown as $M_{dd} = M_0 \bullet e^{-kdd}$, where $dd$ is degree days. To examine the nutrient relations in the roots, we measured carbon (C), nitrogen (N), and phosphorus (P) concentrations as described for soils, and calculated molar ratios on initial (n=5 of each material) and final root and litter breakdown material.

*Environmental variables.* A the center of each site, we extracted one soil core (15 cm diameter $\bullet$ 30 cm deep) to determine soil nutrient dynamics. Additionally cores were taken to the lab and sectioned based on visually apparent horizon shifts. All samples were dried at 60°C to constant weight to determine dry mass, and then ground using an 8000-D ball mill (Spex SamplePrep, Metuchen, New Jersey, USA). Soil cores were subsampled based on soil horizons, for

determination of organic matter content (%OM), total phosphorus (%TP), total nitrogen (%TN) and total carbon (TC). We combined soil layers to report mean soil characteristics from 0-15, 15-30 and 0-30 cm (surface soil, subsoil, and total soil, respectively).   %OM was calculated from ash free dry mass (AFDM) as loss on ignition in a muffle furnace at 550°C for 5.5 h (Karam 1993), and converted to OC by dividing by 2 (Pribyl and others 2010). Carbon and nitrogen content were determined using a Carlo Erba NA 1500 CHN Analyzer (Carlo Erba, Milan, Italy). Phosphorus content was determined by the ash/acid extraction method (Allen 1974), followed by spectrophotometric analysis.  C:N, C:P, and N:P were calculated as molar ratios.

*Data analysis.* We measured linear relationships between each response variable (root biomass, root ingrowth, breakdown of recalcitrant of labile organic matter) and a suite of vegetation (cover of each species, cover of mangrove, cover of marsh and total cover) and soil characteristics (%OM, %P, %N, %C, CP, CN, NP and soil depth). We report all significant relationships ($p < 0.05$). In addition, we used generalized linear models to identify relationships between soil OC storage, vegetation type, soil physicochemical properties, and distance from coast.  We identified best fitting models using backward stepwise  maximal models of the form
*Response = Mangrove cover • Distance to coast •%P • %N •% OM •CP •CN •NP*
We then used backward stepwise model simplification to identify the best fitting model through Akaike's Information Criterion for finite sample size (Hurvich and Tsai 1989).

## Results

### Distance to coast, mangrove cover and soil phosphorus

Distance to coast was negatively correlated to % mangrove cover (**Figure 3.3.2a**, *P* = 0.03; $R^2$= 0.29). Distance to coast bore no relationship to soil TN, TP, TC, AFDM or C:N ratio, though TP was elevated at several sites within 0.75 km of the coast (**Figure 3.2.2b**).
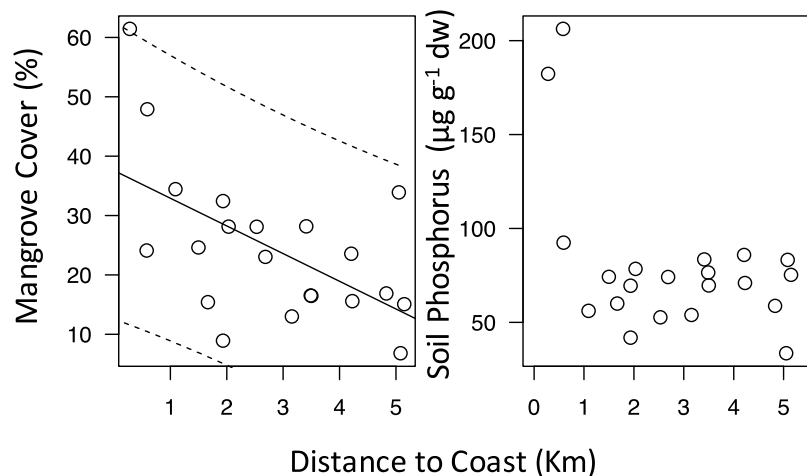


**Figure 3.2.2. a)** Mangrove cover had a negative relationship with distance to coast. **b)** Soil Phosphorus was higher within 1 km of the coast, but further from the coast there was no relationship between soil P and distance to the coast.

*Root biomass and productivity*

Total root biomass (0- 30 cm) was positively related to red mangrove cover ($R^2$= 0.39; $P <$ 0.001; **Figure 3.2.3a**), and showed a quadratic relationship with distance to the coast ($R^2 = 0.41$; $P < 0.001$ ; **Figure 3.2.3b**), i.e., decreasing sharply within the first kilometer of the coast, then stabilizing at greater distances at values less than 0.5 kg·m$^{-2}$. Root biomass was positively related to %TP ($R^2 = 0.25$; $P = 0.01$) and %OM in the surface soil ($R^2 = 0.14$; $P = 0.05$). Root biomass was positively related to total soil C:N ratio ($R^2 = 0.41$; $P < 0.001$) and negatively related to N:P ratio ($R^2 = 0.24$; $P = 0.01$). The model that best predicted root biomass was:

*Total belowground biomass=0 .0084 (Red mangrove cover) + 0.0083 (total soil C:N ratio) + 0.003 (surface soil TP) – 0.56 ($p < 0.001$; $R^2 = 0.89$).*

Root productivity was positively related to red mangrove cover ($R^2 = 0.28$; $P = 0.001$; **Figure 3.2.4a**), but showed no significant relationship with distance to coast (**Figure 3.2.4b**). While root productivity did not have a relationship with any individual soil nutrient, ($P > 0.05$), root ingrowth was negatively related to N:P ratios in the soil ($P = 0.04$). The model that best predicted root productivity was:

*Root productivity = 20.584 (Mangrove cover) – 0.001 (Mangrove cover:Distance to coast) – 0.001 ($p = 0.005$; $R^2 = 0.263$).*
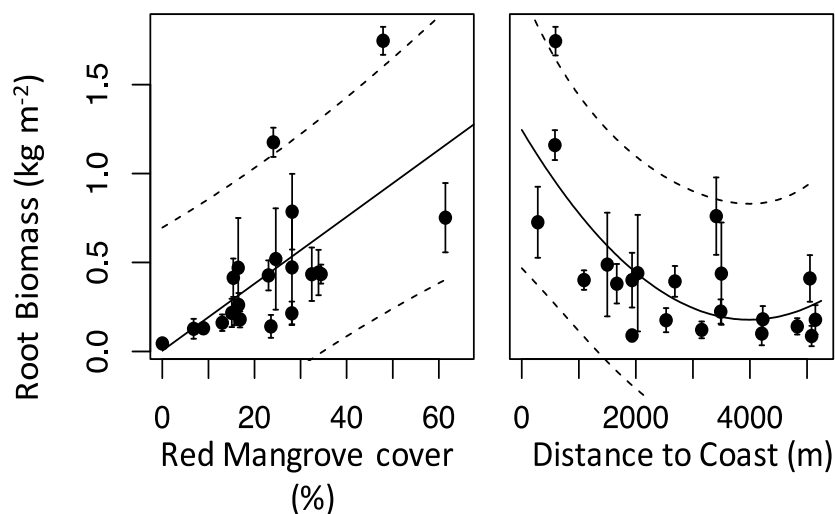


**Figure 3.2.3. a)** Root biomass is positively related to red mangrove cover. **b)** Root biomass has a negative quadratic relationship to distance to coast.
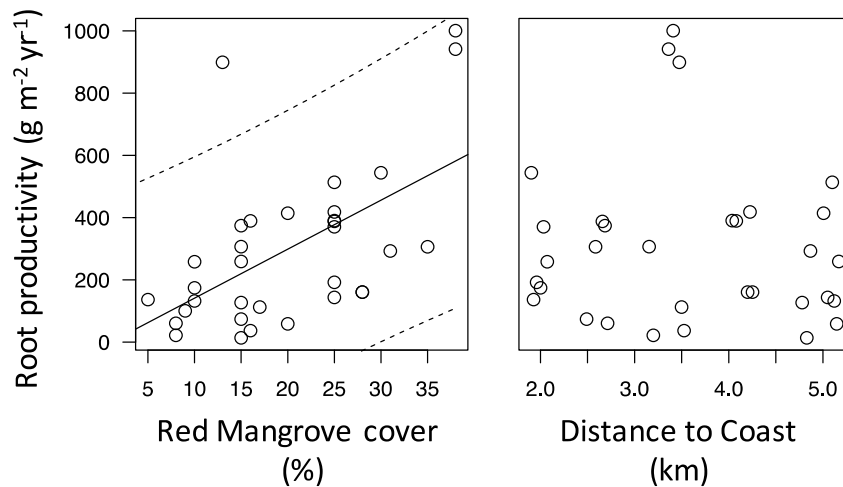
**Figure 3.2.4. a)** Root productivity was positively related to red mangrove cover, however **b)** was not related to distance to coast.

### *Breakdown of organic matter*

When incubated on the soil surface, neither cellulose nor wood standard substrate breakdown was related to mangrove cover. In this setting, wood standard substrate breakdown per degree day ($k$ dd$^{-1}$) was negatively related to %TP ($R^2 = 0.16$ ; $P = 0.02$), but the cellulose standard substrate did not show any relationship to soil characteristics ($P > 0.05$).

When incubated in the surface soil (0-15 cm), the breakdown of wood was negatively related to the C:N ratio of the surface soil ($R^2 = 0.13$; $P = 0.04$; **Figure 3.2.5a**), but not to mangrove cover, other soil characteristics, or distance from coast (**Figure 3.2.5b**). No relationships between cellulose standard substrate breakdown and vegetation, soil, or distance to coast were observed.

At the deepest soil depth (15-30 cm), wood standard substrate breakdown was unrelated to mangrove cover (**Figure 3.2.6a**). However, wood breakdown was positively related to distance from coast ($R^2 = 0.14$; $P = 0.03$), and negatively related to the the organic matter content of the soil ($R^2 = 0.3$; $P= =0.002$), TN ($R^2 = 0.27$; $P =0.003$; **Figure 3.2.6b**) and TP ($R^2 = 0.27$; $P =0.003$; Figure 5b). Cellulose standard substrate breakdown at 15-30 cm was unrelated to mangrove cover or distance to coast ($P > 0.05$), negatively related to subsoil TN ($R^2 = 0.21 : P = 0.01$), and positively related to the C:N ratio of the subsoil ($R^2 = 0.26$; $P = 0.004$).
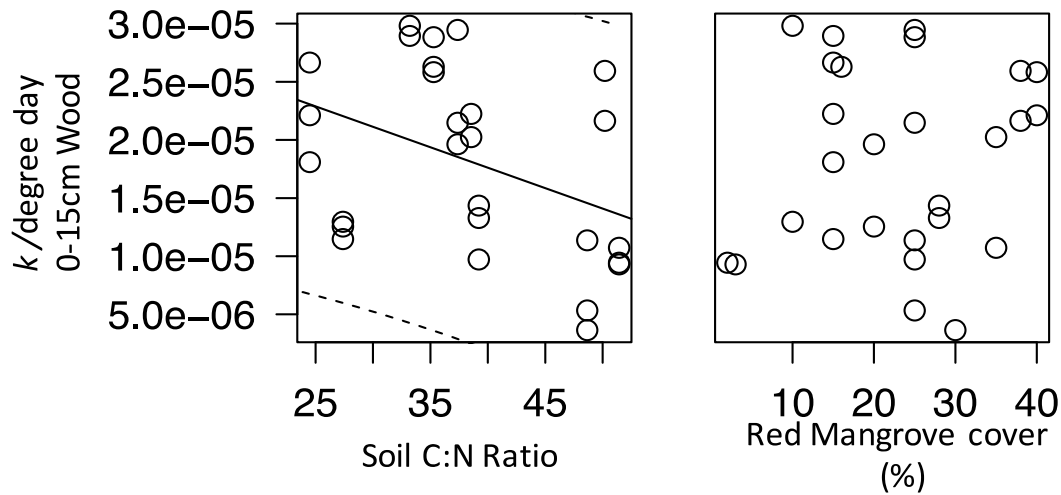
**Figure 3.2.5. a)** The breakdown of wood standard substrates was negatively related to C:N ratio and soil organic matter (SOM). **b)** There was no relationship between red mangrove cover and breakdown rate.
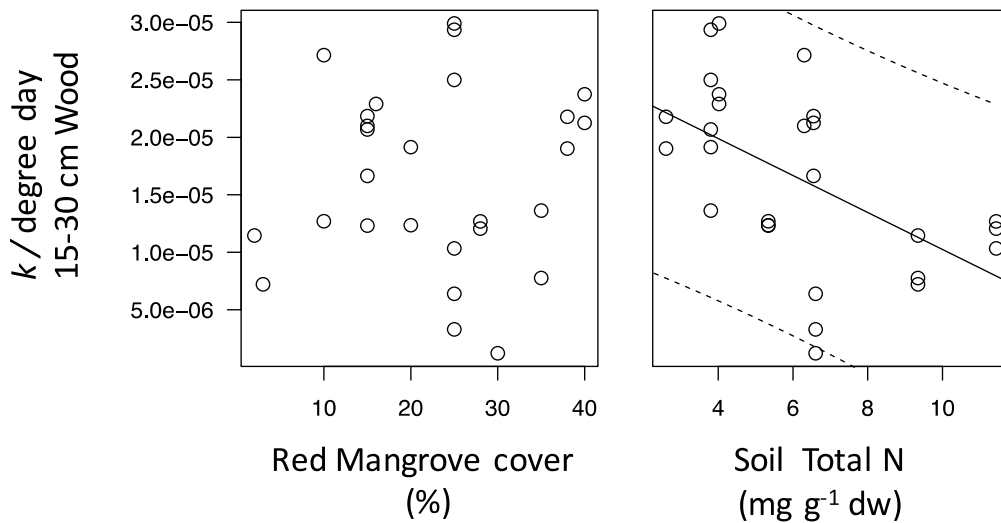


**Figure 3.2.6. a)** There was no relationship between red mangrove cover and breakdown rate. **b)** The breakdown of wood standard substrates was negatively related to C:N ratio and soil organic matter (SOM).

## Discussion

*Saltwater influence, mangrove cover and nutrient availability*

Coastal wetlands are particularly vulnerable to shifts in hydrology, because they are located at the intersection of marine and freshwater ecosystems. In this zone, saltwater intrusion is

61

generally driven by the balance of fresh and marine water (Dessu et al. 2018), and the combination of SLR and reduced freshwater availability has created widespread saltwater intrusion into freshwater and brackish wetlands (Ross et al. 2000; White and Kaplan 2017). Because much of the Everglades is less than 1.5 m above sea level (Titus and Richman 2001), the SLR rate projected for this century (1- 2 m: Haigh et al. 2014) is likely to drive widespread saltwater intrusion throughout the Everglades.

In South Florida, saltwater intrusion increases the stress of salinity but also provides nutrient subsidies, potentially driving shifts in productivity and OM breakdown. Saltwater intrusion generally drives an increase in P availability throughout the coastal Everglades (Sandoval et al. 2016), because P is more available in seawater in this "upside-down estuary" (Childers et al. 2006). Furthermore, as saltwater intrudes into freshwater marshes, P adsorbed to sediment and limestone bedrock, is rapidly released, providing a pulse of P (Price et al. 2010; Flower et al. 2016; 2017). However, we found no significant change in soil TP near the marsh-mangrove ecotone (Figure 1a); while soil phosphorus content increased within 1 km of the coast, there was no relationship between soil TP and distance to coast within 1 and 5 km, which represents the ecotone in the Southeast Saline Everglades study area.

We found that vegetation cover did not have a relationship to breakdown rates at the surface or at either tested depth. Other studies have found that mangroves can influence breakdown rates both by priming the soil and by creating shade from their canopy (Bernal et al. 2016; Kuzyakov; D'Odorico; Charles et al. in review). We found that breakdown of wood substrate was negatively related to % SOM in the 15-30 cm depth, and to a lesser extent, to %N and %P. Because much of the N and P in these oligotrophic soils is generally locked up in peat, the reduction in $k$ rates is likely driven by OM content rather than nutrients themselves.

The lack of a strong effect of soil P on the breakdown of standard carbon substrates in this study appears to contrast with results from dosing studies conducted elsewhere in the Everglades. Gaiser et al 2005 found a doubling in plant biomass through low-level nutrient inputs. Craft et al. (1992) found 50% higher OC accretion in P enriched Everglades peat marshes ($0.53$ g m$^{-2}$ yr$^{-1}$). P additions can also increase breakdown rates (Davis 1991; Qualls and Richardson 2008) in peat soils (Newman et al. 2001; Qualls and Richardson 2008). In an experimental manipulation of Everglades sawgrass peat soils, phosphorus additions increased root ingrowth (130%), but also increased breakdown rates of leaf-litter (18%), and roots (11%) (Charles et al. in prep). However, our study found the relationship between $k$ and total P to be mildly negative. Differences were identified in the recalcitrant wood substrates, but not labile cellulose. Priming of recalcitrant organic matter is a globally important process in driving organic matter breakdown (Guenet et al. 2018). There is debate on how nutrients might affect priming, with two main schools of thought, 1) nutrients *increase* soil OM breakdown by providing microbes with nutrients for growth, or 2) nutrients *decrease* soil OM breakdown, as microbes decompose OM faster in nutrient-poor conditions to "mine" for nutrients (Craine et al. 2009). However, it is recognized that differences in OM quality elicit alternative microbial responses, and that microbes with 'k' strategies often mine nutrients and thus do not increase breakdown after nutrient addition (Chen et al. 2014).

*Mangrove encroachment and C storage*

Our results show that mangrove encroachment can increase root biomass and root ingrowth, but has no impact on breakdown rates, indicating that mangrove encroachment can increase OC storage through time. Soil elevation is governed by accumulation of organic and inorganic materials (Morris et al. 2002, Nyman et al. 2006; McKee 2011), but in sediment-poor interior Everglades wetlands, the balance between inputs of organic matter (root productivity), and losses (breakdown of organic matter) largely determine soil elevation change. Roots and rhizomes are the primary sources of SOM, C storage and soil elevation change in coastal wetlands (Twilley 1999; McKee et al. 2007; Chmura 2011; Deegan et al. 2012). Therefore, an increase in mangrove root productivity and biomass storage, without an increase in breakdown rates will likely lead to OC storage.

Red mangrove cover was negatively related to distance to coast in our study (Figure.2b). Furthermore, within our study area red mangroves have increased 44% in the last twenty years while sawgrass (*Cladium jamaicense*) declined 15% (Ross et al. in prep), indicating that interior wetlands are becoming increasingly influenced by saltwater through time. Saltwater intrusion is leading to the replacement of freshwater marsh communities with salinity tolerant varieties (Sutter et al. 2013). In tropical and subtropical ecosystems, mangroves are displacing herbaceous marshes, as has been observed in Australia (Rogers et al. 2000, 2006; Winn et al. 2006), Mexico (Lopez-Medellin et al. 2011), and the United States (Ross et al. 2000; Smith et al. 2013). In the Florida Everglades *Cladium jamaicense* marshes dominate the fresher interior, while *Rhizophora mangle*-dominated mangrove forest exist in saltier areas toward the coast and the community types overlap in the ecotone (Egler 1952; Koch 1996; Ross et al. 2000). Between1927 and 2005, mangroves expanded their range inland by 35% at the expense of marsh (Krauss et al. 2011), a pattern that has been identified elsewhere in the Everglades as well (Ross et al. 2000; Smith et al. 2013).

Our results indicate that mangrove expansion is likely to increase C storage and reduce vulnerability to conversion to open water ponds. Over the past half century, saltwater intrusion has driven the interior expansion of a zone of sparse vegetation (the "white zone,") into what was previously denser-canopied freshwater marsh (Egler 1952; Ross et al. 2000). Similarly, along the ecotone, sawgrass marsh has been converted to a patchwork of open water ponds, through a poorly-understood process called "peat collapse". Saltwater intrusion is negatively related to sawgrass productivity across the Everglades landscape (Ewel et al. 2006; Macek and Rejmankova 2007; Troxler et al. 2014), but mangrove expansion may increase accretion rates (Meeder et al. 2017).

Coastal wetlands store more OC per area than other ecosystems (Chmura et al. 2003; Bouillon 2011; McLeod et al. 2011), providing a globally important feedback to climate change. The storage of OC and belowground biomass in soils often drives wetland surface elevation change (Nyman et al. 1993, 2006; Turner et al. 2000; McKee et al. 2007; Neubauer 2008), allowing many coastal wetlands to increase their surface elevation to persevere through gradual rates of SLR for thousands of years (Woodroffe et al. 1990; McKee et al. 2007). As SLR accelerates, there is concern that large portions of coastal wetlands may be lost to submergence in the coming century (Wanless et al. 2004; Cooper et al. 2008; Morris et al. 2016), however biophysical feedbacks that enhance vertical elevation gain may increase resilience and preserve some coastal wetlands (Kirwan et al. 2016). Our results suggest that the inland encroachment of mangroves may increase coastal wetland C storage and increase resilience to SLR.

## 4. SUMMARY AND FUTURE PLANS

In the next 18 months, we will complete this chapter of the White Zone research. We expect to be writing papers, making presentations, and establishing new collaborations. Most importantly, two graduate students, Rosario Vidales and Himadri Biswas, will be diving deeply into their research topics. These will involve (1) red mangrove functional traits across environmental gradients, and (2) spatial, remote sensing-based approaches to mangrove dynamics across the South Florida region.

## 5. OTHER PRODUCTS

In 2017, the following paper was published in Hydrobiologia: Meeder, J.F., R.W. Parkinson, P.L. Ruiz and M.S. Ross. Saltwater encroachment and prediction of future ecosystem response to the Anthropocene Marine Transgression, Southeast Saline Everglades, Florida. Hydrobiologia 803 (1): 29-48. Another paper was sent to be considered for publication in Solutions: Meeder, J.F., M.S. Ross, RW Parkinson and S. Castaneda. Enhancing coastal wetland resilience to SLR: just add water? Also, Mike Ross made an oral presentation: "Biphasic vegetation dynamics in the coastal Everglades" by Michael Ross, Susana Stoffella, Rosario Vidales, Himadri Biswas, Keqi Zhang, John Meeder, Jed Redwine, Joseph Park, and Dave Rudnick at the Coastal and Estuarine Research Federation (CERF) 2017 conference in Providence, RI.

## 6. LITERATURE

Bernal B, McKinley DC, Hungate BA, White PM, Mozdzer TJ, Megonigal JP. 2016. Limits to soil carbon stability; Deep, ancient soil carbon decomposition stimulated by new labile organic inputs. Soil Biology and Biochemistry 98:85-94.

Bianchi TS, Allison MA, Zhao J, Li X, Comeaux RS, Feagin RA, Kulawardhana RW. 2013. Historical reconstruction of mangrove expansion in the Gulf of Mexico: Linking climate change with carbon sequestration. Estuarine, Coastal and Shelf Science. 119: 7-16.

Brinson, M. M., R. R. Christian, and L. K. Blum. 1995. Multiple states in the sea-level induced transition from terrestrial forest to estuary. Estuaries 18(4): 648-659.

Castañeda-Moya, E., Twilley, R. R., & Rivera-Monroy, V. H. (2013). Allocation of biomass and net primary productivity of mangrove forests along environmental gradients in the Florida Coastal Everglades, USA. Forest Ecology and Management, 226-241.

Chen IC, Hill JK, Ohlemuller R, Roy DB, Thomas CD. 2011. Rapid range shifts of species associated with high levels of climate warming. Science 333:1024-1026.

Chmura GL, Anisfeld SC, Cahoon DC, Lynch JC. 2003. Global carbonsequestration in tidal, saline wetland soils. Global Biogeochemical Cycles 17: 1111 – 1114.

Clarke, KR, Warwick RM (2001). Change in marine communities: an approach to statistical analysis and interpretation, 2nd edition. PRIMER-E, Plymouth, 172pp.

Cuin, T. A., Parsons, D., & Shabala, S. (2010). Wheat cultivars can be screened for NaCl salinity tolerance by measuring leaf chlorophyll content and shoot sap potassium. *Functional Plant Biology*, *37*(7), 656-664.

DeVries, Ben, Jan Verbesselt, Lammert Kooistra, and Martin Herold. 2015. "Robust Monitoring of Small-Scale Forest Disturbances in a Tropical Montane Forest Using Landsat Time Series." *Remote Sensing of Environment* 161: 107–121

D'Odorico, P., Y. F. He, S. Collins, S. F. J. De Wekker, V. Engel, and J. D. Fuentes. 2013. Vegetation-microclimate feedbacks in woodland-grassland ecotones. Global Ecology and Biogeography 22:364-379.

Doughty CL, Langley JA, Walker WS, Feller, IC, Schaub R, Champan SK. 2015. Mangrove range expansion rapidly increases coastal wetland carbón storage.  Estuaries and Coasts 39: 385-396.

Duarte, C. M., Losada, I. J., Hendriks, I. E., Mazarrasa, I., & Marba, N. 2013. The role of coastal plant communities for climate change mitigation and adaptation. Nature Climate Change, 3, 961–968.

Duke N.,Ball M,  and Ellison J. 1998. Factors influencing biodiversity and distributional gradients in mangroves. Global Ecology and Biogeography Letters, 7, 27–47.

Egler, F. E. 1952. Southeast saline Everglades vegetation, Florida, and its management. Vegetatio 3 (4/5): 213-265.

Elridge DJ, Bowker MA, Maestre FT, Roger E, Reynolds JF and Whitford WG. 2011. Impacts of shrub encroachment on ecosystem structure and functioning: towards a global synthesis. Ecology letters 14(7): 709-722.

Ewel KC, R. R. Twilley, and J. E. Ong. 1998. Different kinds of mangrove forests provide different goods and services. Global Ecology and Biogeography Letters 7:83-94.

Fagherazzi S, L. Carniello, L. D'Alpaos, and A. Defina. 2006. Critical bifurcation of shallow microtidal landforms in tidal flats and salt marshes. Proceedings of the National Academy of Science 103:8337-8341.

Fierer N, J. M. Craine, K. McLauchlan and J. P. Schimel. 2005. Litter quality and the temperature sensitivity of decomposition.  Ecology 86:320-326.

Gaiser, E.E., Wachnicka, A., Ruiz, P., Tobias, F.A., Ross, M.S., 2005. Diatom indicators of ecosystem change in coastal wetlands. In: Bortone S. (Ed.), Estuarine Indicators. CRC Press, Boca Raton, FL, pp. 127-144.

Gill AM, Tomlinson PB. 1977.  Studies on the growth of red mangrove (*Rhizophora mangle* L.) 4. The adult root system.  Biotropica 9:145-155.

Guo H, Weaver C, Charles S, Whitt A, Dastidar S, D'Odorico P, Fuentes JD, Kominoski JS, Armitage AR, Pennings SC. 2017. Coastal regime shifts: Rapid responses of coastal wetlands to changes in mangrove cover. Ecology 98: 762-772

Henry, K. M., & Twilley, R. R. (2013). Soil development in a coastal Louisiana wetland during a climate-induced vegetation shift from salt marsh to mangrove. Journal of Coastal Research, 29: 1273–1283.

Hurvich CM, Tsai CL. 1989. Regression and time series model selection in small samples. Biometrika. 76: 297-307.

Karam A. 1993. Chemical properties of organic soils. In: Carter MR, for Canadian Society of Soil Science, Eds. Soil sampling and methods of analysis. London: Lewis Publishers. Pp 459– 71.

Kelleway JJ, Cavanaugh K, Rogers K, Feller IC, Ens E, Doughty C, Saintilan N. 2017. Review of the ecosystem service implications of mangrove encroachment into salt marshes. Global Change Biology 23: 3967-3983.

Kelleway, JJ, N. Saintilan, P. I. Macreadie, C. G. Skilbeck, A. Zawadski, P. J. Ralph. 2016. Seventy years of continuous encroachment substantially increases "blue carbon" capacity as mangroves replace intertidal salt marshes. Global Change Biology 22: 1097- 1109.

Kirwan ML, Blum LK. 2011. Enhanced decomposition offsets enhanced productivity and soil carbon accumulation in coastal wetlands responding to climate change. Biogeosciences 8: 987-993.

Kirwan ML, Megonigal JP. 2013. Tidal wetland stability in the face of human impacts and sea-level rise. Nature. 504: 53- 60.

Kirwan ML, Temmerman S, Skeehan EE, Guntenspergen GR. 2016. Overestimation of marsh vulnerability to sea level rise. Nature Climate Change 6 (3): 253-260.

Knapp AK, Briggs JM, Collins S, Archer S, Bret-Harte M, Ewers BE, Peters DP, Young DR, Shaver GR, Pendall E and Cleary MB. 2008. Shrub encroachment in North American grasslands: Shifts in growth form dominance rapidly alters control of ecosystems carbon inputs. Global Change Biology 14: 615-623.

Kominoski JS, Follstad Shah JJ, Canhoto C, Fischer DG, Giling DP, Gonzalez E, Griffiths NA, Larranaga A, LeRoy CJ, Mineau M, McElarney YR, Shirley SM, Swan CM, and Tiegs SD. 2013. Forecasting functional implications of global changes in riparian plant communities. Frontiers in Ecology and the Environment 11:423-432.

Krauss K, McKee KL, Lovelock CE, Cahoon DR, Saintilan N, Reef R, Chen L. 2013. How mangrove forests adjust to rising sea level. New Phytologist Tansley Review.

Krauss KW, Doyle TW, Twilley RR, Smith TJ III, Whelan KRT, Sullivan JK. 2005. Woody debris in mangrove forests of South Florida. Biotropica 37:9-15.

Kuzyakov, Y. 2010. Priming effects: Interactions between living and dead organic matter. Soil biology and biochemistry 42*:*1363-1371.

Li PX, Wang N, He WM, Krusi BO, Gao SQ, Zhang SM. 2008. Fertile islands under Artemisia ordosica in inland dunes of northern China, Effects of habitat and plant developmental stages. Journal of arid environments. 72: 953-963.

Lovelock CE, Cahoon DR, Friess DA, Guntenspergen GR, Krauss KW, Reef R, Rogers K, Saunders ML, Sidik F, Swales A, Saintilan N, Thuyen LX, Triet T. 2015. The vulnerability of Indo-Pacificmangrove forests to sea-level rise. Nature: 526: 559-563.

Masek, J.G., Vermote, E.F., Saleous N.E., Wolfe, R., Hall, F.G., Huemmrich, K.F., Gao, F., Kutler, J., and Lim, T-K. 2006. A Landsat surface reflectance dataset for North America, 1990–2000. *IEEE Geoscience and Remote Sensing Letters* 3(1):68-72.

McCune and Grace 2002. Analysis of ecological communities. MjM Software Design. , Gleneden Beach, Oregon, U.S.A. 300 pp.

McCune, B. and M. J. Mefford. 2011. PC-ORD.Multivariate Analysis of Ecological Data. Version 6.0. MjM Software, Gleneden Beach, Oregon, U.S.A.

McKee KL, Cahoon DR, Feller IC. 2007. Caribbean mangroves adjust to rising sea level through biotic controls on change in soil elevation. Global Ecology and Biogeography 16:545–556.

McKee KL. 2011. Biophysical controls on accretion and elevation change in Caribbean mangrove ecosystems. Estuarine, Coastal and Shelf Science 91: 475-483.

Mcleod E, Chmura GL, Bouillon S, Salm R, Björk M, Duarte CM, Lovelock CE, Schlesinger WH, Silliman BR. 2011. A blueprint for blue carbon: toward an improved understanding of the role of vegetated coastal habitats in sequestering $CO_2$. Frontiers in Ecology and the Environment 9:552-560.

Meeder, J. F. and R. W. Parkinson. 2017. SE Saline Everglades transgressive sedimentation in response to historic acceleration in sea-level rise: a viable marker for the base of the Anthropocene? Journal of Coastal Research 34 (2):490-497

Meeder, J.F., M.S. Ross, G.T. Telesnicki, P.L. Ruiz and J.P. Sah. 1996. Vegetation analysis in the C-111-Taylor Slough Basin. Document 1. The Southeast Saline Everglades revisited a half-century of coastal vegetation change, 56p. Document 2. Marine transgression in the Southeast Saline Everglades, Florida; rates, causes and plant-sediment responses. 95p. Final report to the SFWMD.

Meeder, J.F., R.W. Parkinson, P.L. Ruiz and M.S. Ross. 2017. Saltwater encroachment and prediction of future ecosystem response to the Anthropocene Marine Transgression, Southeast Saline Everglades, Florida. Hydrobiologia 803 (1): 29-48.

Middleton BA, McKee KL. 2001. Degradation of mangrove tissues and implications for peat formation in Belizean island forests. Ecology 89:818-828.

Morris JT., P. V. Sundareshwar, C. T. Nietch, B. Kjerfve. and D. R. Cahoon. 2002. Responses of coastal wetlands to rising sea level. Ecology 83:2869–2877.

Morris, J. T., Barber, D. C., Callaway, J. C., Chambers, R., Hagen, S. C., Hopkinson, C. S., Johnson, B. J., Megonigal, P., Neubauer, S. C., Troxler, T. and Wigand, C. 2016. Contributions of organic and inorganic matter to sediment volume and accretion in tidal wetlands at steady state. Earth's Future.

Nyman JA, Walters RJ, Delaune RD, Patrick WH. 2006. Marsh vertical accretion via vegetative growth. Estuarine, Coastal and Shelf Science 69: 370-380.

Olsen, S.R., and L.E. Sommers. 1982. Phosphorus. In: A.L. Page et al., editiors, Methods of soil analysis. Part 2. 2$^{nd}$ ed. Agron. Monogr.9. ASA and SSSA, Madison, WI. P. 403-430.

Olsen, S.R., C.V. Cole, F.S. Watanabe, and L.A. Dean. 1954. Estimation of available phosphorus in soils by extraction with sodium bicarbonate. USDA Circ. 939. U.S. Gov. Print. Office, Washington, DC.

Osland MJ, Enwright NM, Day RH, Gabler CA, Stagg CL, Grace JB. 2016. Beyond just sea-level rise: considering macroclimatic drivers within coastal wetland vulnerability assessments to climate change. Global Change Biology 22: 1-11.

Osland MJ, Feher LC, Griffith KT, Cavanaugh KC, Enwright NM, Day RH, Stagg CL, Krauss KW, Howard RJ, Grace JB, Rogers K. 2017. Climatic controlgs on the global distribution, abundance and species richness of mangrove forests. Ecological monographs 87: 341-359.

Osland MJ, N. Enwright, R. H. Day, and T. W. Doyle. 2013. Winter climate change and coastal wetland foundation species: salt marshes vs. mangrove forests in the southeastern United States. Global Change Biology 19:1482-1494.

Osland MJ, Spivak AC, Nestlerode JA, Lessmann JM, Almario AE, Heitmuller PT, Russell MJ, Krauss KW, Alvarez F, Dantin DD, Harvey JE, From AS, Cormier N, and Stagg CL. 2012. Ecosystem development after mangrove wetland creation: plant-soil change across a 20-year chronosequence. Ecosystems 15:848–866.

Perry, C. L., & Mendelssohn, I. A. 2009. Ecosystem effects of expanding populations of Avicennia germinans in a Louisiana salt marsh. Wetlands, 29: 396–406.

Pisani, O., L.J. Scinto, J.W. Munyon, and R. Jaffe. 2015. The respiration of flocculent detrital organic matter (floc) is driven by phosphorus limitation and substrate quality in a subtropical wetland. Geoderma. 2241-242: 272-278.

Powell, M. D., and S. H. Houston. 1996. Hurricane Andrew's landfall in south Florida. Part II: Surface wind fields and potential real- time applications. Weather and Forecasting 11:329–349.

Rejmánková E., and Sirová, D. (2007). Wetland macrophyte decomposition under different nutrient conditions: relationships between decomposition rate, enzyme activity and microbial biomass. Soil Biology and Biochemistry 39(2): 525–538.

Risser PG. 1990. The ecological importance of land-water ecotones. Man and biosphere 4: 7-21.

Rogers K, K. M. Wilton and N. Saintilan. Vegetation change and surface elevation dynamics in estuarine wetlands of southeast Australia. 2006. Estuarine, Coastal and Shelf Science 66:559-569.

Ross, M. S., Meeder, J. F., Sah, J. P., Ruiz, P. L., and Telesnicki, G. J. 2000. The southeast saline Everglades revisited: 50 years of coastal vegetation change. Journal of Vegetation Science, 11(1), 101-112.

Ross, M. S., Ruiz, P. L., Telesnicki, G. J., and Meeder, J. F. 2001. Estimating above-ground biomass and production in mangrove communities of Biscayne National Park, Florida (USA). Wetlands Ecology and Management, 9(1), 27-37.

Saintilan N, N. C. Wilson, K. Rogers, A. Rajkaran, and K. W. Krauss. 2014. Mangrove expansion and salt marsh decline at mangrove poleward limits. Global Change Biology 20:147-157.

Scholander PF, L. Van Dam and S. I. Scholander. 1955. Gas exchange in the roots of mangroves. American Journal of Botany 42:92-98.

Sims, J.T. 2009. Soil test phosphorus: Principles and methods. In: J.L. Kovar and G.M. pierzynski, editors, Methods of phosphorus analysis. 2$^{nd}$ ed. South. Coop. Ser. Bull. 408. North Carolina State University, Raleigh. P. 9-19.

Sinsabuagh, R.L. (1994). Enzymatic analysis of microbial patterns and process. Biology and Fertility of Soils 17: 69-74.

Smith III, T. J., & Whelan, K. R. (2006). Development of allometric relations for three mangrove species in South Florida for use in the Greater Everglades Ecosystem restoration. Wetlands Ecology and Management, 409-419.

Smith TJ III, Foster A, Tiling-Range G, and Jones JW. 2013. Dynamics of mangrove-marsh ecotones in subtropical coastal wetlands: fire, sea-level rise, and water levels. Fire Ecology 9:66-77.

Solorzano, L., and J.H. Sharp. 1980. Determination of total dissolved phosphorus and particulate phosphorus in natural waters. Limnol. Oceanogr: 25:754-758.

Souza Filho PW, Cohen M, Laraj CL, Lessaoo GC, Koch B, and Behling H. 2004. Holocene

coastal evolution and facies model of the Braganca Macrotidal Flat on the Amazon Mangrove Coast, Northern Brazil. Journal of Coastal Research SI, 39: 306–310.

Thieler ER Hammar-Klose ES. 2000. National Assessment of Coastal Vulnerability to Future Sea-Level Rise: Preliminary Results for the U.S. Gulf of Mexico Coast. U.S. Geological Survey, Open-File Report 00-179.

Twilley RR., Lugo AE and Patterson-Zucca C. 1986. Litter Production and Turnover in basin mangrove forests in southwest Florida. Ecology 67:670-683.

Van Auken OW. 2000. Shrub invasions of North American semiarid grasslands. Annual Review of Ecology and Systematics 31:197-215.

Verbesselt, J., A. Zeileis, and M. Herold. 2012. "Near Real-Time Disturbance Detection Using Satellite Image Time Series." Remote Sensing of Environment 123: 98–108.

Vogt KA, Vogt DJ, Bloomfield J. 1998. Analysis of some direct and indirect methods for estimating root biomass and production of forests at an ecosystem level. Plant Soil 200: 71-89.

Willard DA, Bernhardt CE. 2011. Impacts of past climate and sea level change on Everglades wetlands: placing a century of anthropogenic change into a late-Holocene context. Climatic Change. 107:59.

Wright, A.L. and K. R.Reddy. 2001. Heterotrophic microbial activity in northern Everglades wetland soils. Soil Sci. Soc. Am. J. 65:1856-1864.

Yando ES, Osland MJ, Willis JM, Day RH, Krauss KW, and Hester MW. 2016. Salt marsh-mangrove ecotones: Using structural gradients to investigate the effects of woody plant encroachment on plant-soil interactions and ecosystem carbon pools. Journal of Ecology, 104: 1020– 1031.

Young B M, Harvey LE. 1996. A spatial analysis of the relationship between mangrove (*Avicenia marina var. australasica)* physiognomy and sediment accretion in the Hauraki Plains, New Zealand. Estuarine, Coastal and Shelf Science 42: 231-246.

Zhang, K., B. Thapa, M. Ross, and D. Gann. 2016. Remote sensing of seasonal changes and disturbances in mangrove forest: a case study from South Florida. Ecosphere 7(6):e01366.

# 7. APPENDICES

## Appendix 1.2.1.

A 50 m circular buffer was created around each vegetation plot center. An area of 1 ha was gridded into 100 10 m by 10 m cells, and overlain on the buffer layer and orthophotographs. All 15 sites were analyzed at 0.8 foot resolution. Red mangroves were identified and counted manually from the orthophotographs, and crown diameters were also measured in meters. These

analyses allowed identification and measurement of minimum crown diameters of 0.24 m. Ten 10 m by 10 m cells were randomly selected for analysis. Crown area was calculated from the measured diameter. Per cent (%) cover for each mangrove shrub was calculated as:

$$\% \ cover = \frac{Crown \ area}{Grid \ area} \times 100$$

The calculated % crown cover were summed for each grid to get total % cover. Furthermore, average % cover was calculated as:

$$Average \ \% \ cover = \frac{\Sigma(Total \ \% \ cover \ from \ each \ measured \ cell)}{Total \ number \ of \ cells \ measured}$$

### *Evaluation of methodology if low resolution (3 feet) orthoimage is used:*
We calculated total crown area for each site and crown area based on trees of diameter of <1 m from 0.8 foot resolution data for all the 15 sites. Further, we calculated the percentage of crown area with diameter of <1 m, i.e., the data lost by using the lower 3 foot resolution image.

**Appendix 1.2.2.**

*Transect TKY*. The smallest crown cover along this transect was in coastal site TKYE with a median of 0.18 and median size of trees is 0.48 m. Compared to coastal site on transect TKY, the median crown cover in the intermediate and interior sites are bigger and similar to each other. On the TKY transect, crown cover increases from coast to interior while tree density declines considerably from coast to intermediate site and then increases sharply at the interior site (Table 2). Both TKYE and TKYINT have similar and high tree density, in fact TKYE has the highest tree density amongst all transect locations followed by TKYINT.

*Transect TANG*. The mean crown area of intermediate sites along transects TANG, TA2, and TA3 are larger than the coastal and interior sites. Although, the coastal and interior sites on TANG have similar mean crown area, a gradual decline in cover can be seen from coast to interior. Furthermore, the tree density at TANGLS is very high compared to TANGLI and TANGLEN. The distribution of crown sizes at all sites on transect TANG are similar to each other (Figure 2) with median varying between 0.98 – 1.21m.

*Transect TA2 and TA3*. Along transects TA2 (and to a lesser extent on TA3), mangrove cover increases from coast to intermediate and then declines at interior sites. However, the increase in cover and then the decrease is much more pronounced in transect TA2. The low cover at the coastal site on TA2 is only matched in sparseness by the coastal site on Transect TKY (TKYE). However, the low cover at TA2.6 is a function of extremely low tree density, while low cover at TKYE is a result of very small trees. The distribution of crown size of mangrove shrubs at coastal and interior sites at transect TA2 are similar with median size of 0.80 m. The crown sizes at the intermediate site are larger with a median of 1.47 m. In case of TA3, the increase in crown cover from coast to intermediate site followed by a decline from intermediate to interior site is more gradual.

*Transect TA5*. Both coastal and intermediate sites at transect TA5 have high and similar cover and mean crown area but tree density is considerably lower at the coastal site. There is a decrease in cover and tree density at the interior site as compared with the intermediate site but it has a higher tree density than the coastal site. The crown size at TA5.5 are the largest and about 50% of the crown size lie within a range of over 1m to about 2.25m.

**Appendix 1.2.3.**
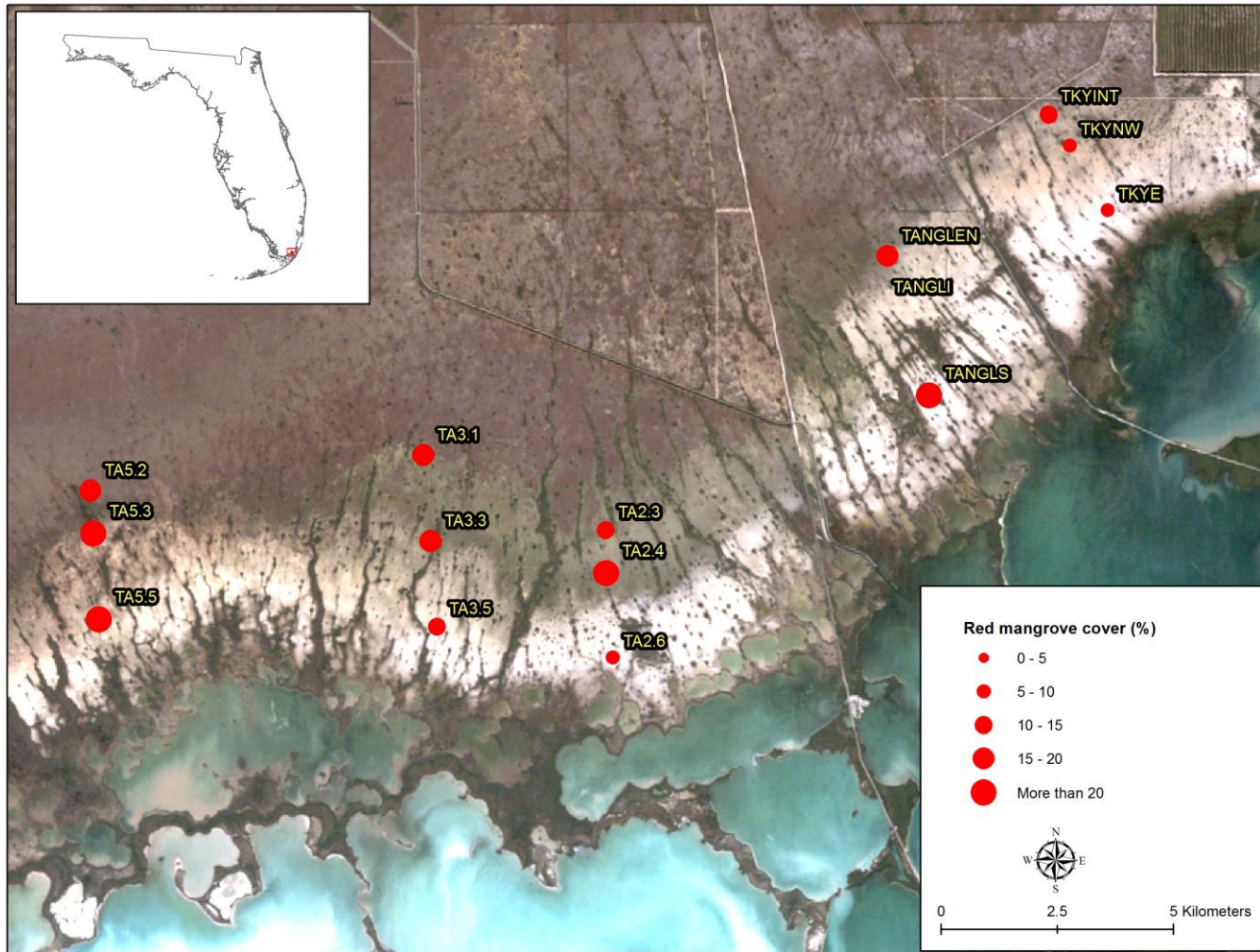


**Figure A 1.2.1. Distribution of red mangrove cover along transects.**
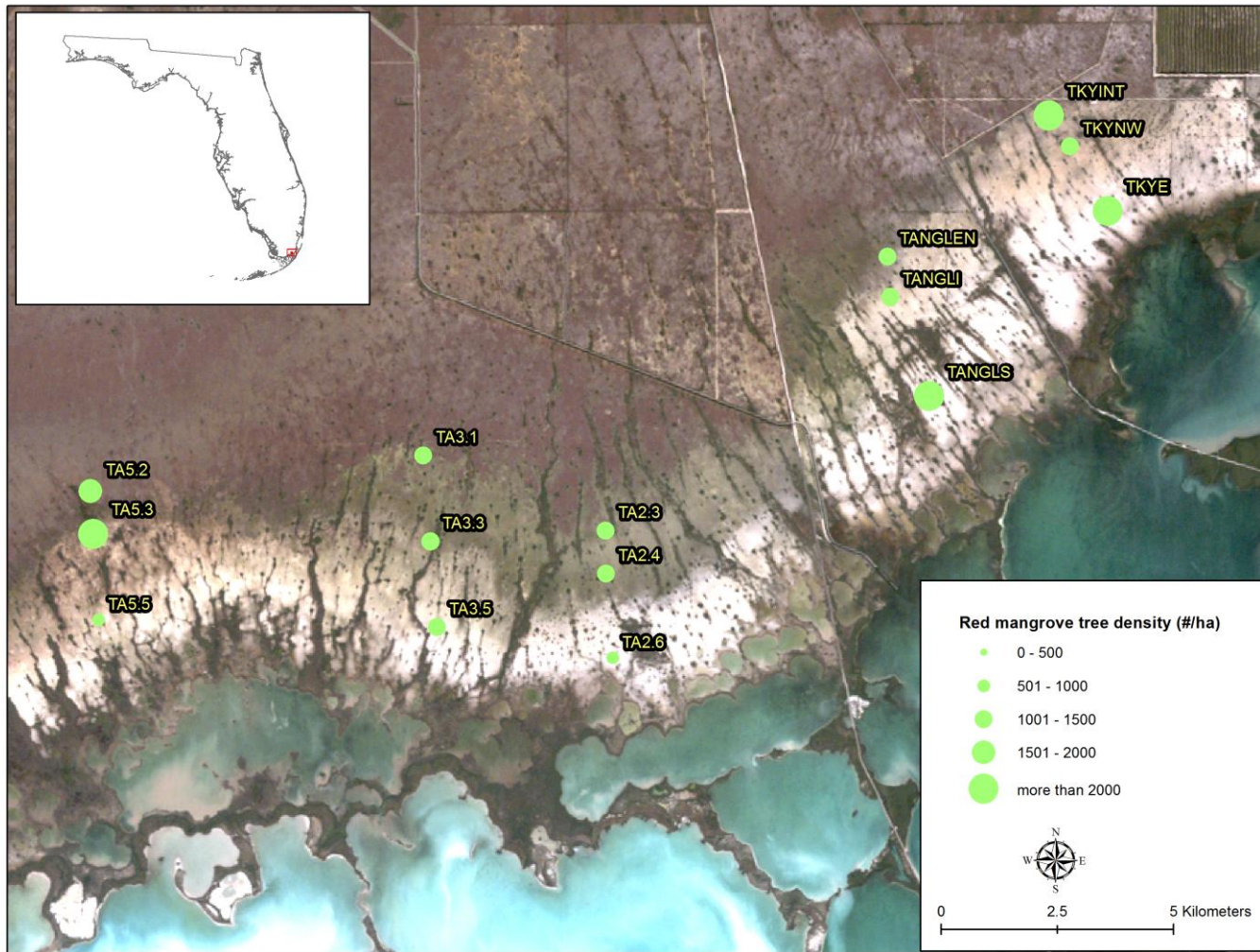
**Figure A 1.2.2. Distribution of tree density of red mangrove along transects.**

**Appendix 1.2.4.**

**Table T 2.2.1. Site-wise approximation of crown area that may not get captured in 3 feet resolution images as compared with 0.8 feet resolution images.**

| Sites | Total crown area from 0.8 feet resolution images | Crown area from diameter <1m | Crown area that will not be captured in 3 feet resolution images (%) |
|---|---|---|---|
| TKYINT | 142.09 | 63.39 | 44.61 |
| TKYNW | 92.85 | 38.39 | 41.34 |
| TKYE | 59.68 | 49.15 | 82.35 |
| TANGLEN | 155.23 | 29.76 | 19.17 |
| TANGLI | 197.10 | 24.54 | 12.45 |
| TANGLS | 226.31 | 44.29 | 19.57 |
| TA2.3 | 107.61 | 32.74 | 30.43 |
| TA2.4 | 245.02 | 8.23 | 3.36 |
| TA2.6 | 60.36 | 24.40 | 40.43 |
| TA3.1 | 152.54 | 40.25 | 26.39 |
| TA3.3 | 162.19 | 23.68 | 14.60 |
| TA3.5 | 100.34 | 29.23 | 29.13 |
| TA5.2 | 157.97 | 34.10 | 21.59 |
| TA5.3 | 213.62 | 47.57 | 22.27 |
| TA5.5 | 213.45 | 5.44 | 2.55 |

**Appendix 2.2.1**

**TKY transect**

TKYE  (DTC = 1.09 km)

No photo

0 to 9cm mangrove peat-marl with mangrove cable roots.
9 to 26 cm  white marl
26 to 49 cm saw grass peat-marl.

TKYW  (DTC = 1.93 km)

(correction 0 to 3 cm should be 0 to 4 cm)

### TKYW

0 to 3 cm mangrove peat marl.
3 to 13 cm white to grey-white marl.

13 to 18 cm mottled white and brown organic rich marl. Transitional.

18 to 62 cm dark tan to light brown Saw grass organic rich peat-marl.

TKYNW  (DTC  = 2.67 km)

No photo

0 to 2 cm mangrove peat-marl (poorly developed)
2 to 26 cm white marl with brown mottling

TKYINT  (DTC  = 3.49 km)  0 to 4 cm high SI

No photo

0 to 4 cm mangrove peat-marl (poorly developed)

4 to       white marl


  to       saw grass peat-marl


**Triangle transect**

EVER 1  (DTC = 5.15 km)

(core not processed)


TANGLEN  (DTC = 4.23 km)



Floc                              TANGLIN

Mangrove peat-marl


Marl


Saw grass peat-marl


TANGLI  (DTC = 3.5)

(core not processed)


TANGLS  (DTC = 1.5 km)

SI low for entire core.

0-27 white marl

27-48 Saw grass peat-marl

**TA 2 transect**

TA 2-2   (DTC =5.08 km)

Above 0 cm  Periphyton

0 to 8 cm  floc

8 to 17 cm

17 to 44 bioturbated white marl mottled with more organic rich tan to brown marl

TA 2.3  (DTC = 4.21 km)

(core not processed)

TA 2-4  (DTC = 3.41 km)

(core not processed)

TA 2-5  (DTC = 2.53 km)



0 to 7 floc

7 to 39 cm white marl

39 to 64 cm saw grass peat-marl, minor organic content

64 to 76 cm saw grass peat-marl, highly organic

TA 2-6  (DTC = 1.67 km)



# TA 2.6

Marl

Saw grass peat-marl

Saw grass peat

**Others**

TA 5.5

Floc

Marl

Saw grass peat-marl

0-8 peri
9-19 white marl
20-60 organic marl

T 6-4

(no core photo)

0 to 6 cm floc
6 to 28 cm white marl

# Appendix 2.2.2

Sediment data

| Mowry | | | | | | | | | | |
|---|---|---|---|---|---|---|---|---|---|---|
| 50m | core 1 | | x2 | | | TFE | | | x2 | |
| depth | sed type | SI | OM (cm3) | OM/yr/m2 | | depth | sed type | SI | OM (cm3) | Omg/m2/y |
| 0 | mpm | 2.54 | 0.040 | 133.333 | | 0 | | 3.00 | 0.099 | 164.5833 |
| 1 | | 2.28 | 0.046 | 152.667 | | 1 | mp | 2.80 | 0.198 | 330.8333 |
| 2 | | 2.75 | 0.042 | 139.500 | | 2 | | 2.60 | 0.123 | 205.0000 |
| 3 | | 2.61 | 0.108 | 359.333 | | 3 | | 2.40 | 0.132 | 220.4167 |
| 4 | | 3.15 | 0.042 | 139.500 | | 4 | | 2.20 | 0.283 | 470.9167 |
| 5 | | 2.12 | 0.072 | 241.667 | | 5 | | 2.00 | 0.224 | 373.9167 |
| 6 | | 2.26 | 0.080 | 268.167 | | 6 | | 1.80 | 0.262 | 436.5000 |
| 7 | | 1.98 | 0.112 | 372.667 | | 7 | | 1.60 | 0.189 | 315.7500 |
| 8 | | 1.53 | 0.093 | 309.500 | | 8 | | 3.00 | 0.326 | 544.0000 |
| 9 | | 1.64 | 0.076 | 252.167 | | 9 | | 2.80 | 0.295 | 491.1667 |
| 10 | | 1.36 | 0.438 | nd | | 10 | | 2.60 | 0.241 | 402.0000 |
| 11 | | 1.38 | nd | nd | | 11 | | 2.40 | 0.192 | 320.6667 |
| 12 | | 1.44 | 0.070 | 116.417 | | 12 | | 2.20 | 2.000 | 489.1667 |
| 13 | ml | 1.38 | 0.092 | 57.781 | | 13 | | 2.00 | 0.205 | 341.2500 |
| 14 | | 1.36 | 0.056 | 35.062 | | 14 | | 1.80 | 0.206 | 342.8333 |
| 15 | | 1.36 | 0.123 | 76.969 | | 15 | | 1.60 | 0.165 | 275.4167 |
| 16 | | 1.31 | 0.100 | 62.500 | | 16 | | 1.07 | 0.250 | 416.3333 |
| 17 | | 0.00 | 0.061 | 38.250 | | 17 | | 4.00 | 0.437 | 728.1667 |
| 18 | | 0.00 | 0.066 | 41.406 | | 18 | | 3.37 | 0.564 | 940.5833 |
| 19 | | 1.40 | 0.061 | 38.437 | | 19 | | 2.67 | 0.562 | 937.3333 |
| 20 | | 1.38 | 0.039 | 24.500 | | 20 | | 2.37 | 0.680 | ######## |
| 21 | | 1.36 | 0.083 | 51.688 | | 21 | | 3.44 | 0.650 | ######## |
| 22 | | 1.36 | 0.075 | 46.875 | | 22 | | 1.87 | 0.356 | 593.9167 |
| 23 | | 1.50 | 0.052 | 32.438 | | 23 | | 1.50 | 0.640 | ######## |
| 24 | | 1.39 | 0.063 | 39.250 | | 24 | | 2.00 | 0.328 | 547.4167 |
| 25 | | 1.41 | 0.083 | 52.094 | | 25 | | | | |
| 26 | | 1.41 | 0.071 | 44.188 | | | | | | |
| 27 | | 1.33 | nd | #VALUE! | | | | | | |
| 28 | | 1.36 | 0.091 | 57.031 | | | | | | |
| 29 | | 1.43 | 0.119 | 74.187 | | | | | | |
| | | 1.38 | | | | | | | | |
| | | 1.27 | | | | | | | | |

| TDE | | | x2 | | | TDWW | 400M | | x2 | |
|---|---|---|---|---|---|---|---|---|---|---|
| depth | sed type | SI | OM (cm3) | OM/yr/m2 | | depth | sed type | SI | OM (cm3) | Omg/m2/y |
| 0 | mp | 3.10 | 0.137 | 569.375 | | 0 | mpm | 1.80 | 0.595 | nd |
| 1 | | 2.90 | 0.164 | 681.667 | | 1 | | 1.52 | 0.046 | 114.500 |
| 2 | | 2.70 | 0.107 | 446.875 | | 2 | | 1.60 | 0.042 | 104.625 |
| 3 | | 2.50 | 0.181 | 752.292 | | 3 | | 1.69 | 0.108 | 269.500 |
| 4 | | 2.30 | 0.094 | 389.792 | | 4 | | 1.62 | 0.042 | 104.625 |
| 5 | | 2.10 | 0.140 | 583.750 | | 5 | | 1.62 | 0.073 | 181.250 |
| 6 | | 1.90 | 0.092 | 382.292 | | 6 | | 1.99 | 0.080 | 201.125 |
| 7 | | 1.70 | 0.110 | 459.583 | | 7 | | 2.30 | 0.112 | 279.500 |
| 8 | | 3.10 | 0.143 | 594.167 | | 8 | | 1.86 | 0.093 | 232.125 |
| 9 | | 2.90 | 0.120 | 500.833 | | 9 | | 1.76 | 0.076 | 189.125 |
| 10 | | 2.70 | 0.098 | 406.458 | | 10 | | nd | 0.070 | 174.625 |
| 11 | | 2.50 | 0.128 | 535.000 | | 11 | | 1.68 | 0.092 | 231.125 |
| 12 | | 2.30 | 0.115 | 478.750 | | 12 | | 1.59 | 0.056 | 140.250 |
| 13 | | 2.10 | 0.100 | 417.083 | | 13 | | 1.68 | 0.123 | 307.875 |
| 14 | | 2.03 | 0.106 | 440.625 | | 14 | | 1.59 | 0.100 | 250.000 |
| 15 | mpm | 2.18 | 0.089 | 286.613 | | 15 | | 1.37 | 0.061 | 153.000 |
| 16 | | 1.83 | 0.096 | 310.806 | | 16 | | 1.29 | 0.066 | 165.625 |
| 17 | | 2.10 | 0.080 | 257.581 | | 17 | | 1.37 | 0.062 | 153.750 |
| 18 | | 2.68 | 0.040 | 128.387 | | 18 | | 1.43 | 0.039 | 98.000 |
| 19 | | 1.62 | 0.129 | 415.323 | | 19 | ml | 1.41 | 0.083 | 51.688 |
| 20 | | 1.58 | 0.044 | 143.226 | | 20 | | 1.35 | 0.075 | 46.875 |
| 21 | | 2.09 | 0.055 | 178.226 | | 21 | | 1.41 | 0.052 | 32.438 |
| 22 | | 1.58 | 0.094 | 303.226 | | 22 | | 1.41 | 0.063 | 39.250 |
| 23 | | 1.39 | 0.054 | 173.548 | | 23 | | 1.42 | 0.083 | 52.094 |
| 24 | | 1.39 | 0.095 | 306.935 | | 24 | | 1.39 | 0.071 | 44.188 |
| 25 | | 1.51 | 0.089 | 286.613 | | 25 | | 1.42 | 0.091 | 57.031 |
| 26 | | 1.57 | 0.097 | 313.387 | | 26 | | 1.40 | 0.119 | 74.188 |
| 27 | | 1.54 | 0.122 | 393.387 | | 27 | | 1.36 | 0.104 | 64.906 |
| 28 | mpm | 1.32 | 0.073 | 236.290 | | 28 | | 1.36 | 0.091 | 56.906 |
| 29 | | 1.40 | 0.072 | 231.129 | | 29 | | 1.46 | 0.133 | 82.938 |
| 30 | | 1.33 | 0.084 | 271.935 | | 30 | | | 0.100 | |
| 31 | | 1.59 | 0.070 | 227.097 | | 31 | | | 0.107 | |

| Turkey Point | | | | | | TKYW | | | | |
|---|---|---|---|---|---|---|---|---|---|---|
| Coast | | | | | | | | | | |
| depth | sed type | SI | OM (cm3) | OM/yr/m2 | | depth | sed type | SI | OM (cm3) | OM/yr/m2 |
| 0 | mpm | 3.39 | 0.038 | 245.833 | | 0 | mpm | 2.40 | no data for core | |
| 1 | | 2.18 | 0.046 | 297.115 | | 1 | | 2.72 | | |
| 2 | | 3.08 | 0.040 | 254.487 | | 2 | | 1.91 | | |
| 3 | | 3.39 | 0.029 | 186.859 | | 3 | ml | 1.33 | | |
| 4 | | 2.88 | 0.045 | 287.821 | | 4 | | 1.60 | | |
| 5 | | 2.21 | 0.033 | 210.897 | | 5 | | 1.38 | | |
| 6 | | 3.00 | 0.055 | 355.449 | | 6 | | 1.32 | | |
| 7 | | 1.98 | 0.043 | 272.756 | | 7 | | 1.92 | | |
| 8 | | 1.68 | 0.047 | 301.603 | | 8 | | 1.00 | | |
| 9 | | 1.94 | 0.045 | 285.256 | | 9 | | 1.29 | | |
| 10 | ml | | 0.042 | 26.063 | | 10 | | 1.26 | | |
| 11 | | | 0.061 | 37.844 | | 11 | | 1.46 | | |
| 12 | | | 0.040 | 24.844 | | 12 | | 1.40 | | |
| 13 | | | 0.063 | 39.125 | | 13 | | 1.47 | | |
| 14 | | | 0.078 | 48.875 | | 14 | | 1.36 | | |
| 15 | | | 0.073 | 45.406 | | 15 | | 1.46 | | |
| 16 | | | 0.091 | 56.875 | | 16 | | 1.65 | | |
| 17 | | | 0.061 | 37.875 | | 17 | | 1.39 | | |
| 18 | | | 0.080 | 50.187 | | 18 | | 1.33 | | |
| 19 | | 1.40 | 0.092 | 57.219 | | 19 | | 1.43 | | |
| 20 | | 1.38 | 0.064 | 39.781 | | 20 | | 1.45 | | |
| 21 | | 1.36 | 0.046 | 28.687 | | 21 | sgpm | 1.36 | | |
| 22 | | 1.36 | 0.057 | 35.781 | | 22 | | 1.45 | | |
| 23 | | 1.50 | 0.067 | 42.125 | | 23 | | 1.41 | | |
| 24 | | 1.39 | 0.069 | 43.344 | | 24 | | nd | | |
| 25 | | 1.41 | 0.081 | 50.406 | | 25 | | 1.31 | | |
| 26 | | 1.41 | 0.096 | 60.125 | | 26 | | 1.33 | | |
| 27 | | 1.33 | 0.105 | 65.531 | | 27 | | 1.27 | | |
| 28 | | 1.36 | 0.075 | 46.625 | | 28 | | 1.24 | | |
| 29 | | 1.43 | 0.066 | 41.344 | | 29 | | 1.41 | | |
| 30 | | 1.38 | 0.078 | 48.750 | | 30 | | 1.32 | | |
| 31 | | 1.27 | 0.079 | 49.563 | | 31 | | 1.35 | | |

TKYNW

| depth | sed type | SI | OM (cm3) | OM/yr/m2 |
|---|---|---|---|---|
| 0 | mpm | 3.5 | 0.038 | 122.917 |
| 1 | | 1.9 | 0.023 | 75.160 |
| 2 | ml | 1.4 | 0.030 | 37.250 |
| 3 | | 1.5 | 0.026 | 31.875 |
| 4 | | 1.1 | 0.046 | 57.563 |
| 5 | | 1.4 | 0.041 | 51.750 |
| 6 | | 1.4 | 0.036 | 45.500 |
| 7 | | 1.5 | 0.049 | 61.281 |
| 8 | | 1.4 | 0.041 | 51.813 |
| 9 | | 1.4 | 0.051 | 64.062 |
| 10 | | 1.3 | 0.067 | 83.875 |
| 11 | | 1.4 | 0.076 | 94.688 |
| 12 | | 1.4 | 0.067 | 84.375 |
| 13 | | 1.4 | 0.073 | 91.375 |
| 14 | sgpm | 1.4 | 0.086 | 198.264 |
| 15 | | 1.4 | 0.096 | 221.759 |
| 16 | | 1.4 | nd | nd |
| 17 | | 1.4 | 0.071 | 163.657 |
| 18 | | 1.4 | 0.097 | 224.306 |
| 19 | | 1.4 | 0.111 | 257.639 |
| 20 | | 1.4 | 0.102 | 235.301 |
| 21 | | 1.4 | 0.055 | |
| 22 | | 1.4 | 0.064 | |
| 23 | | 1.3 | 0.048 | |
| 24 | | 1.4 | 0.047 | |
| 25 | | | | |
| 26 | | | | |
| 27 | | | | |
| 28 | | | | |
| 29 | | | | |
| 30 | | | | |
| 31 | | | | |

TKYINT

| depth | sed type | SI | OM (cm3) | OM/yr/m2 |
|---|---|---|---|---|
| 0 | mpm | 1.60 | 0.048 | 152.548 |
| 1 | | 1.94 | 0.052 | 165.224 |
| 2 | | 2.00 | 0.050 | 160.737 |
| 3 | | 1.67 | 0.055 | 175.481 |
| 4 | ml | 1.34 | 0.055 | 68.500 |
| 5 | | 1.42 | 0.060 | 74.625 |
| 6 | | 1.32 | 0.073 | 91.313 |
| 7 | | 1.55 | 0.051 | 64.063 |
| 8 | | 1.31 | 0.071 | 88.938 |
| 9 | sgpm | 1.18 | 0.099 | 228.009 |
| 10 | | 1.29 | 0.111 | 256.134 |
| 11 | | 1.29 | 0.114 | 264.583 |
| 12 | | 1.27 | 0.091 | 210.995 |
| 13 | | 1.34 | 0.106 | 244.676 |
| 14 | | 1.34 | 5.069 | |
| 15 | | 1.43 | 0.099 | 230.093 |
| 16 | | 1.38 | 0.113 | 261.111 |
| 17 | | 1.43 | 0.150 | 346.065 |
| 18 | | 1.36 | 0.073 | 168.866 |
| 19 | | 1.35 | 0.105 | 244.097 |
| 20 | | 1.33 | 0.144 | sp highly compacted |
| 21 | | 1.50 | 0.153 | |
| 22 | | nd | 0.202 | |
| 23 | | nd | 0.202 | |
| 24 | | nd | 0.234 | |
| 25 | | 1.50 | 0.206 | |
| 26 | | 1.42 | 0.291 | |
| 27 | | 0.83 | 0.266 | |
| 28 | | 1.29 | 0.244 | |
| 29 | | | 0.292 | |

32
33
34
35
36
37
38
39
40
41
42
43
44
45
Triangle

| TRANGLS | | | | | TANGLIN | | | | |
|---|---|---|---|---|---|---|---|---|---|
| depth | sed type | SI | OM (cm3) | OM/yr/m2 | depth | sed type | SI | OM (cm3) | OM/yr/m2 |
| 0-1 | | | 0.051 | 64.125 | 0 | peri | 0 | 0.000 | 0.000 |
| 1 | | | 0.051 | 63.188 | 1 | marl | 1 | 0.046 | 57.313 |
| 2 | | | 0.017 | 21.375 | 2 | | 1.5 | 0.044 | 54.688 |
| 3 | | | 0.027 | 33.938 | 3 | | 2.1 | 0.064 | 79.375 |
| 4 | | | 0.033 | 40.813 | 4 | | 1.9 | 0.054 | 68.063 |
| 5 | | | 0.036 | 45.188 | 5 | | 1.2 | 0.054 | 67.250 |
| 6 | | | 0.034 | 42.313 | 6 | | 1.8 | 0.036 | 45.062 |
| 7 | | | 0.044 | 55.000 | 7 | | 1.4 | 0.029 | 36.812 |
| 8 | | | 0.044 | 54.750 | 8 | | 1.3 | 0.024 | 29.500 |
| 9 | | | 0.055 | 69.125 | 9 | | 1.3 | 0.021 | 25.625 |
| 10 | | 1.37 | 0.085 | 106.000 | 10 | | 1.4 | 0.030 | 37.938 |
| 11 | | 1.40 | 0.109 | 136.750 | 11 | | 1.4 | 0.025 | 31.375 |
| 12 | | 1.36 | 0.087 | 108.938 | 12 | | 1.4 | 0.030 | 37.313 |
| 13 | | 1.40 | 0.069 | 85.812 | 13 | | 1.3 | 0.034 | 41.875 |
| 14 | | 1.42 | 0.083 | 104.375 | 14 | | 1.3 | 0.023 | 28.187 |
| 15 | | 1.39 | 0.052 | 65.375 | 15 | | 1.3 | 0.015 | 19.063 |
| 16 | | 1.31 | -0.061 | nd | 16 | | 1.4 | 0.021 | 26.812 |
| 17 | | 1.34 | 0.058 | 72.625 | 17 | | 1.4 | 0.029 | 35.625 |

| depth | SI | OM (cm3) | OM/yr/m2 |
|---|---|---|---|
| 18 | 1.27 | 0.042 | 52.000 |
| 19 | 1.46 | 0.044 | 54.750 |
| 20 | 1.29 | 0.541 | nd |
| 21 | 1.36 | 0.049 | 61.625 |
| 22 | 1.38 | 0.047 | 58.125 |
| 23 | 1.17 | 0.053 | 65.875 |
| 24 | 1.50 | 0.048 | 60.312 |
| 25 | 1.00 | 0.059 | 74.375 |
| 26 | 1.30 | 0.067 | 83.125 |
| 27 | 1.28 | 0.058 | 72.250 |
| 28 | 1.37 | 0.116 | |
| 29 | 1.35 | 0.092 | |
| 30 | 1.43 | 0.114 | |
| 31 | 1.36 | 0.145 | |
| 32 | 1.38 | 0.148 | |
| 33 | 1.50 | 0.422 | |
| 34 | 1.35 | 0.117 | |
| 35 | 1.23 | 0.178 | |
| 36 | 1.28 | 0.118 | |
| 37 | 1.22 | 0.092 | |
| 38 | 1.12 | 0.097 | |
| 39 | 1.25 | 0.103 | |
| 40 | 1.45 | 0.145 | |
| 41 | 1.36 | 0.130 | |
| 42 | 1.21 | 0.162 | |
| 43 | 1.28 | 0.181 | |
| 44 | 1.27 | 0.119 | |
| 45 | 1.23 | 0.135 | |
| 46 | 1.29 | 0.116 | |

| depth | sed type | SI | OM (cm3) | OM/yr/m2 |
|---|---|---|---|---|
| 18 | | 1.3 | 0.031 | 38.187 |
| 19 | | 1.4 | 0.032 | 40.375 |
| 20 | | 1.4 | 0.029 | 36.188 |
| 21 | | 1.3 | 0.029 | 36.812 |
| 22 | | 1.5 | 0.035 | 44.250 |
| 23 | | 1.3 | 0.045 | 55.813 |
| 24 | sgpm | 1.6 | 0.082 | 189.767 |
| 25 | | 1.4 | 0.053 | 122.907 |
| 26 | | 1.3 | 0.051 | 119.767 |
| 27 | | 1.6 | 0.114 | 264.535 |
| 28 | | 1.3 | 0.070 | 162.791 |
| 29 | | 1.3 | 0.074 | 172.558 |
| 30 | | 1.4 | 0.051 | 119.302 |
| 31 | | 1.4 | 0.069 | 159.535 |
| 32 | | 1.5 | 0.075 | 173.721 |
| 33 | | 1.7 | 0.069 | 160.349 |
| 34 | | 1.4 | 0.073 | 169.535 |
| 35 | | 1.4 | 0.053 | 122.326 |
| 36 | | 1.7 | 0.061 | 140.930 |
| 37 | | 1.6 | 0.054 | 126.512 |
| 38 | | 1.4 | 0.070 | 162.326 |
| 39 | | 1.3 | 0.078 | 182.209 |
| 40 | | 1.4 | 0.061 | 142.093 |
| 41 | | 1.5 | 0.045 | 105.581 |
| 42 | | 1.2 | 0.061 | 141.512 |
| 43 | | 1.4 | 0.059 | 137.791 |
| 44 | | 1.5 | 0.068 | 157.442 |
| 45 | | 1.1 | 0.086 | 200.930 |
| 46 | | 1.4 | 0.057 | 132.674 |

T2

T2.2

| depth | sed type | SI | OM (cm3) | OM/yr/m2 |
|---|---|---|---|---|
| 0-1 | peri | nd | 0.060 | |
| 1 | | | 0.055 | |
| 2 | | | 0.068 | |

T2.5

| depth | sed type | SI | OM (cm3) | OM/yr/m2 |
|---|---|---|---|---|
| 0-1 | peri | nd | 0.045 | 0.000 |
| 1 | | | 0.047 | 0.000 |
| 2 | | | 0.061 | 0.000 |

| # | | | | # | | | |
|---|---|---|---|---|---|---|---|
| 3 | | 0.077 | | 3 | ml | 0.044 | 55.500 |
| 4 | | 0.071 | | 4 | | 0.060 | 74.875 |
| 5 | | 0.069 | | 5 | | 0.067 | 83.250 |
| 6 | | 0.090 | | 6 | | 0.058 | 73.062 |
| 7 | | 0.085 | | 7 | | 0.053 | 66.312 |
| 8 | ml | 0.076 | 112.625 | 8 | | 0.043 | 53.437 |
| 9 | | 0.051 | 105.938 | 9 | | -0.194 | nd |
| 10 | | 0.062 | 94.875 | 10 | | 0.025 | 31.000 |
| 11 | | 0.063 | 63.375 | 11 | | 0.033 | 41.562 |
| 12 | | 0.070 | 77.875 | 12 | | 0.037 | 46.563 |
| 13 | | 0.065 | 78.687 | 13 | | 0.038 | 47.563 |
| 14 | | -0.445 | 87.750 | 14 | | 0.035 | 44.375 |
| 15 | | 0.064 | 81.375 | 15 | | 0.053 | 65.937 |
| 16 | | 0.035 | nd | 16 | | 0.063 | 79.250 |
| 17 | | 0.040 | 80.000 | 17 | | 0.068 | 84.937 |
| 18 | | 0.045 | 43.750 | 18 | | 0.063 | 78.625 |
| 19 | | 0.043 | 50.500 | 19 | | 0.061 | 75.875 |
| 20 | | 0.053 | 56.750 | 20 | | 0.077 | 96.000 |
| 21 | | 0.038 | 53.625 | 21 | | 0.071 | 88.250 |
| 22 | | 0.027 | 66.250 | 22 | | 0.093 | 116.438 |
| 23 | | 0.033 | 48.063 | 23 | | 0.045 | 56.625 |
| 24 | | 0.000 | 33.250 | 24 | | 0.044 | 54.438 |
| 25 | sgpm | 0.000 | 41.687 | 25 | | 0.054 | 67.562 |
| 26 | | 0.000 | 0.000 | 26 | | 0.042 | 52.250 |
| 27 | | 0.000 | 0.000 | 27 | | 0.048 | 60.438 |
| 28 | | 0.000 | 0.000 | 28 | | 0.042 | 52.313 |
| 29 | | 0.000 | 0.000 | 29 | | 0.050 | 62.187 |
| 30 | | 0.000 | 0.000 | 30 | | 0.076 | 94.625 |
| 31 | | 0.000 | 0.000 | 31 | | 0.071 | 88.187 |
| 32 | | 0.000 | 0.000 | 32 | sgpm | 0.079 | 183.488 |
| 33 | | 0.000 | 0.000 | 33 | | 0.081 | 188.023 |
| 34 | | 0.000 | 0.000 | 34 | | 0.069 | 160.581 |
| 35 | | 0.000 | 0.000 | 35 | | 0.088 | 204.186 |
| 36 | | 0.000 | 0.000 | 36 | | 0.105 | 243.023 |
| 37 | | 0.000 | 0.000 | 37 | | 0.091 | 212.209 |
| 38 | | | 0.000 | 38 | | 0.072 | 168.372 |

| depth | SI | OM (cm3) | OM/yr/m2 | | depth | SI | OMcm3 | Omg/m2/y |
|---|---|---|---|---|---|---|---|---|
| 39 | | | 0.000 | | 39 | | 0.075 | 174.651 |
| 40 | | | | | 40 | | 0.069 | 161.279 |
| 41 | | | | | 41 | | 0.075 | 174.884 |
| 42 | | | | | 42 | | -0.430 | nd |
| 43 | | | | | 43 | | 0.082 | 189.651 |
| 44 | | | | | 44 | | 0.080 | 185.581 |
| 45 | | | | | | | | |
| 46 | | | | | | | | |

Transect 5

T2.6 5.5

| depth | sed type | SI | OM (cm3) | OM/yr/m2 | depth | sed type | SI | OMcm3 | Omg/m2/y |
|---|---|---|---|---|---|---|---|---|---|
| 0-1 | peri | nd | 0.039 | 0.000 | 0 | floc | nd | 0.000 | 0.000 |
| 1 | | | 0.041 | 0.000 | 1 | floc | nd | 0.000 | 0.000 |
| 2 | ml | | 0.044 | 54.750 | 2 | floc | nd | 0.000 | 0.000 |
| 3 | | | 0.041 | 51.313 | 3 | ml | 1.25 | 0.018 | 23.062 |
| 4 | | | 0.043 | 53.375 | 4 | | nd | 0.018 | 22.375 |
| 5 | | nd | nd | | 5 | | 1.33 | 0.026 | 32.062 |
| 6 | | | 0.048 | 59.688 | 6 | | 1.25 | 0.025 | 31.125 |
| 7 | | | 0.041 | 51.500 | 7 | | 1.57 | 0.033 | 41.438 |
| 8 | | | 0.048 | 60.062 | 8 | | 1.80 | 0.044 | 54.812 |
| 9 | | | 0.050 | 62.375 | 9 | | 1.98 | 0.041 | 50.750 |
| 10 | | | 0.050 | 62.625 | 10 | | 1.81 | 0.055 | 68.875 |
| 11 | | | 0.070 | 87.563 | 11 | | 1.67 | 0.035 | 44.125 |
| 12 | | | 0.070 | 88.063 | 12 | | 1.17 | 0.042 | 52.250 |
| 13 | | | 0.055 | 68.437 | 13 | | 1.17 | 0.039 | 48.938 |
| 14 | | | 0.068 | 85.375 | 14 | | 1.30 | 0.042 | 52.375 |
| 15 | | | 0.057 | 71.250 | 15 | | 1.20 | 0.539 | nd |
| 16 | | | 0.071 | 88.563 | 16 | | 1.07 | 0.043 | 53.438 |
| 17 | sgpm | | 0.092 | 214.070 | 17 | | 1.13 | 0.045 | 56.500 |
| 18 | | | 0.096 | 223.605 | 18 | | 1.21 | 0.069 | 86.813 |
| 19 | | | 0.097 | 225.349 | 19 | | 1.36 | 0.061 | 75.813 |
| 20 | | | 0.111 | 258.140 | 20 | | 1.23 | 0.061 | 76.875 |
| 21 | | nd | nd | | 21 | | 1.32 | 0.057 | 70.875 |
| 22 | | | 0.106 | 246.047 | 22 | | 1.18 | 0.069 | 86.625 |
| 23 | | | 0.110 | 255.930 | 23 | | 1.27 | 0.067 | 83.688 |

| | | |
|---|---|---|
| 24 | 0.113 | 263.605 |
| 25 | 0.096 | 224.419 |
| 26 | nd | nd |
| 27 | 0.109 | 252.326 |
| 28 | 0.086 | 200.349 |
| 29 | 0.103 | 240.349 |
| 30 | 0.069 | 160.116 |
| 31 | 0.078 | 180.581 |
| 32 | 0.078 | 181.047 |
| 33 | 0.090 | 208.256 |
| 34 | 0.124 | 288.605 |
| 35 | 0.117 | 272.442 |
| 36 | 0.102 | 236.628 |
| 37 | 0.104 | |
| 38 | 0.102 | |
| 39 | 0.100 | |
| 40 | 0.117 | |
| 41 | 0.120 | |
| 42 | 0.129 | |
| 43 | 0.120 | |
| 44 | 0.094 | |
| 45 | 0.098 | |
| 46 | 0.127 | |

| | | | | |
|---|---|---|---|---|
| 24 | | 1.10 | 0.051 | 63.437 |
| 25 | | 1.31 | 0.070 | 87.500 |
| 26 | swpm | 1.29 | 0.080 | 194.390 |
| 27 | swpm | 1.26 | 0.080 | 196.098 |
| 28 | swpm | 1.20 | 0.085 | 206.341 |
| 29 | ml | 1.17 | 0.064 | 79.875 |
| 30 | ml | 1.29 | 0.064 | 80.438 |
| 31 | ml | 1.29 | 0.057 | 71.250 |
| 32 | ml | 1.22 | 0.057 | 71.500 |
| 33 | ml | 1.25 | 0.052 | 65.562 |
| 34 | ml | 1.21 | 0.055 | 68.563 |
| 35 | | 1.21 | 0.072 | 90.312 |
| 36 | | 1.17 | 0.069 | 86.375 |
| 37 | | 1.23 | 0.075 | 93.437 |
| 38 | | 1.27 | 0.075 | 93.313 |
| 39 | | 1.23 | 0.073 | 91.000 |
| 40 | | 1.33 | 0.081 | 100.937 |
| 41 | | 1.25 | 0.071 | 88.563 |
| 42 | sgpm | 1.34 | 0.076 | 185.976 |
| 43 | sgpm | 1.26 | 0.069 | 167.683 |
| 44 | sgpm | 1.20 | 0.062 | 151.220 |
| 45 | sgpm | 1.34 | 0.068 | 165.366 |
| 46 | sgpm | 1.20 | 0.067 | 163.293 |

Transect 6

6.4

| depth | sed type | SI | OMcm3 | Omg/m2/y |
|---|---|---|---|---|
| 0 | floc | 0.00 | 0.000 | 0.000 |
| 1 | floc | 0.00 | 0.021 | 26.312 |
| 2 | floc | 0.00 | 0.021 | 25.688 |
| 3 | ml | 0.00 | 0.037 | 46.000 |
| 4 | ml | 0.00 | 0.066 | 82.812 |
| 5 | ml | 0.00 | 0.079 | 98.875 |
| 6 | ml | 0.00 | 0.064 | 80.250 |
| 7 | ml | 1.00 | 0.050 | 63.000 |

| | | | | |
|---|---|---|---|---|
| 8 | ml | 0.00 | 0.060 | 75.062 |
| 9 | ml | 1.30 | 0.057 | 70.813 |
| 10 | ml | 1.30 | 0.050 | 62.250 |
| 11 | ml | 1.30 | 0.068 | 84.875 |
| 12 | ml | 1.40 | 0.068 | 84.750 |
| 13 | ml | 1.31 | 0.070 | 87.375 |
| 14 | ml | 1.30 | 0.048 | 59.625 |
| 15 | ml | 1.20 | 0.047 | 58.875 |
| 16 | ml | 1.00 | 0.044 | 54.500 |
| 17 | ml | 1.10 | 0.038 | 47.687 |
| 18 | ml | 1.30 | 0.040 | 49.875 |
| 19 | ml | 1.50 | 0.045 | 56.812 |
| 20 | ml | 1.20 | 0.038 | 48.000 |
| 21 | ml | 1.20 | 0.045 | 56.250 |
| 22 | ml | 1.32 | 0.040 | 50.000 |
| 23 | ml | 1.20 | 0.542 | 677.687 |
| 24 | ml | 1.10 | 0.067 | 84.062 |
| 25 | ml | 1.35 | 0.070 | 88.063 |
| 26 | ml | 1.40 | 0.071 | 88.875 |
| 27 | ml | 1.30 | 0.066 | 82.937 |
| 28 | ml | 1.50 | 0.033 | 41.375 |
| 29 | ml | 0.00 | 0.060 | 74.437 |
| 30 | ml | 0.00 | 0.034 | 42.375 |
| 31 | ml | 0.00 | 0.040 | 49.812 |
| 32 | | 0.00 | | |
| 33 | | | | |

**Appendix 2.2.3**

Relationship between SI and OM (g/m2/yr)

Scatter plots incorporated all SI OM data pairs

Box and whisker plots incorporated SI OM data pairs by sediment type

OM in this data set always refers to grams of organic matter in one square meter accumulated in one year.

Locator
First number is transect number which  is followed by a period
Transect key

2 = Mowry
3 = Turkey Point
4 = TANGLIN
5 = Transect 5
6 = Transect 6

The second number is the Core number which is followed by a period
Core key for HistCk
1 = 850m
2 = 600m
3 = 400m
4 = 150m
5 = 40m

Core key for Mowry
6 = CDW=Core 1 =50m
7 = TFE
8 = TDE
9 = TDWW

Core key for Turkey Point
10 = coast=TKYE

11 = TKYNW
12 = TKYINT

transect # core # depth;  written as 1.2.12

| Depth | SI | Om |
|---|---|---|
| 2 | 12 | |

green data = produced not calculated

| Mangrove peat | | | | | | | | | | |
|---|---|---|---|---|---|---|---|---|---|---|
| Core | depth | SI | OM | locator | | Core | depth | SI | OM | locator |
| TFE | 0 | 3.00 | 164.583 | 2.7.0 | | TFE | 22 | 1.87 | 593.917 | 2.7.22 |
| TFE | 1 | 2.80 | 330.833 | 2.7.1 | | TFE | 23 | 1.50 | 1066.000 | 2.7.23 |
| TFE | 2 | 2.60 | 205.000 | 2.7.2 | | TFE | 24 | 2.00 | 547.417 | 2.7.24 |
| TFE | 3 | 2.40 | 220.417 | 2.7.3 | | TDE | 0 | 3.10 | 569.375 | 2.8.0 |
| TFE | 4 | 2.20 | 470.917 | 2.7.4 | | TDE | 1 | 2.90 | 681.667 | 2.8.1 |
| TFE | 5 | 2.00 | 373.917 | 2.7.5 | | TDE | 2 | 2.70 | 446.875 | 2.8.2 |
| TFE | 6 | 1.80 | 436.500 | 2.7.6 | | TDE | 3 | 2.50 | 752.292 | 2.8.3 |
| TFE | 7 | 1.60 | 315.750 | 2.7.7 | | TDE | 4 | 2.30 | 389.792 | 2.8.4 |
| TFE | 8 | 3.00 | 544.000 | 2.7.8 | | TDE | 5 | 2.10 | 583.750 | 2.8.5 |
| TFE | 9 | 2.80 | 491.167 | 2.7.9 | | TDE | 6 | 1.90 | 382.292 | 2.8.6 |
| TFE | 10 | 2.60 | 402.000 | 2.7.10 | | TDE | 7 | 1.70 | 459.583 | 2.8.7 |
| TFE | 11 | 2.40 | 320.667 | 2.7.11 | | TDE | 8 | 3.10 | 594.167 | 2.8.8 |
| TFE | 12 | 2.20 | 489.167 | 2.7.12 | | TDE | 9 | 2.90 | 500.833 | 2.8.9 |
| TFE | 13 | 2.00 | 341.250 | 2.7.13 | | TDE | 10 | 2.70 | 406.458 | 2.8.10 |
| TFE | 14 | 1.80 | 342.833 | 2.7.14 | | TDE | 11 | 2.50 | 535.000 | 2.8.11 |
| TFE | 15 | 1.60 | 275.417 | 2.7.15 | | TDE | 12 | 2.30 | 478.750 | 2.8.12 |
| TFE | 16 | 1.07 | 416.333 | 2.7.16 | | TDE | 13 | 2.10 | 417.083 | 2.8.13 |
| TFE | 17 | 4.00 | 728.167 | 2.7.17 | | TDE | 14 | 2.03 | 440.625 | 2.8.14 |
| TFE | 18 | 3.37 | 940.583 | 2.7.18 | | | | | | |

| | | | | | | | | | | |
|---|---|---|---|---|---|---|---|---|---|---|
| TFE | 19 | 2.67 | 937.333 | 2.7.19 | | | | N | 58.000 | |
| TFE | 20 | 2.37 | 1133.083 | 2.7.20 | | | | Mean | 520.224 | |
| TFE | 21 | 3.44 | 1083.167 | 2.7.21 | | | | Max | 1133.083 | |
| TFE | 22 | 1.87 | 593.917 | 2.7.22 | | | | Min | 164.5833 | |
| TFE | 23 | 1.50 | 1066.000 | 2.7.23 | | | | | | |
| TFE | 24 | 2.00 | 547.417 | 2.7.24 | | | | | | |
| TDE | 0 | 3.10 | 569.375 | 2.8.0 | | | | | | |
| TDE | 1 | 2.90 | 681.667 | 2.8.1 | | | | | | |
| TDE | 2 | 2.70 | 446.875 | 2.8.2 | | | | | | |
| TDE | 3 | 2.50 | 752.292 | 2.8.3 | | | | | | |
| TDE | 4 | 2.30 | 389.792 | 2.8.4 | | | | | | |
| TDE | 5 | 2.10 | 583.750 | 2.8.5 | | | | | | |
| TDE | 6 | 1.90 | 382.292 | 2.8.6 | | | | | | |
| TDE | 7 | 1.70 | 459.583 | 2.8.7 | | | | | | |
| TDE | 8 | 3.10 | 594.167 | 2.8.8 | | | | | | |
| TDE | 9 | 2.90 | 500.833 | 2.8.9 | | | | | | |
| TDE | 10 | 2.70 | 406.458 | 2.8.10 | | | | | | |
| TDE | 11 | 2.50 | 535.000 | 2.8.11 | | | | | | |
| TDE | 12 | 2.30 | 478.750 | 2.8.12 | | | | | | |
| TDE | 13 | 2.10 | 417.083 | 2.8.13 | | | | | | |
| TDE | 14 | 2.03 | 440.625 | 2.8.14 | | | | | | |
| | | | | | | | | | | |

| Mangrove peat marl | | | | | | | | | | |
|---|---|---|---|---|---|---|---|---|---|---|
| | | | | | | | | | | |
| Core | depth | SI | OM | locator | | Core | Depth | SI | OM | locator |
| Mowry 50m | 0 | 2.54 | 133.333 | 2.6.0 | | TDWW | 8 | 1.86 | 232.125 | 2.9.8 |
| Mowry 50m | 1 | 2.28 | 152.667 | 2.6.1 | | TDWW | 9 | 1.76 | 189.125 | 2.9.9 |
| Mowry 50m | 2 | 2.75 | 139.500 | 2.6.2 | | TDWW | 10 | 1.72 | 174.625 | 2.9.10 |
| Mowry 50m | 3 | 2.61 | 359.333 | 2.6.3 | | TDWW | 11 | 1.68 | 231.125 | 2.9.11 |
| Mowry 50m | 4 | 3.15 | 139.500 | 2.6.4 | | TDWW | 12 | 1.59 | 140.250 | 2.9.12 |
| Mowry 50m | 5 | 2.12 | 241.667 | 2.6.5 | | TDWW | 13 | 1.68 | 307.875 | 2.9.13 |
| Mowry 50m | 6 | 2.26 | 268.167 | 2.6.6 | | TDWW | 14 | 1.59 | 250.000 | 2.9.14 |
| Mowry 50m | 7 | 1.98 | 372.667 | 2.6.7 | | TDWW | 15 | 1.37 | 153.000 | 2.9.15 |
| Mowry 50m | 8 | 1.53 | 309.500 | 2.6.8 | | TDWW | 16 | 1.29 | 165.625 | 2.9.16 |
| Mowry 50m | 9 | 1.64 | 252.167 | 2.6.9 | | TDWW | 17 | 1.37 | 153.750 | 2.9.17 |
| Mowry 50m | 12 | 1.44 | 116.417 | 2.6.10 | | TDWW | 18 | 1.43 | 98.000 | 2.9.18 |
| TDE | 15 | 2.18 | 286.613 | 2.8.15 | | TKYE | 0 | 3.39 | 245.833 | 3.10.0 |
| TDE | 16 | 1.83 | 310.806 | 2.8.16 | | TKYE | 1 | 2.18 | 297.115 | 3.10.1 |
| TDE | 17 | 2.10 | 257.581 | 2.6.11 | | TKYE | 2 | 3.08 | 254.487 | 3.10.2 |
| TDE | 18 | 2.68 | 128.387 | 2.8.17 | | TKYE | 3 | 3.39 | 186.859 | 3.10.3 |
| TDE | 19 | 1.62 | 415.323 | 2.8.18 | | TKYE | 4 | 2.88 | 287.821 | 3.10.4 |
| TDE | 20 | 1.58 | 143.226 | 2.6.12 | | TKYE | 5 | 2.21 | 210.897 | 3.10.5 |
| TDE | 21 | 2.09 | 178.226 | 2.8.19 | | TKYE | 6 | 3.00 | 355.449 | 3.10.6 |
| TDE | 22 | 1.58 | 303.226 | 2.8.20 | | TKYE | 7 | 1.98 | 272.756 | 3.10.7 |
| TDE | 23 | 1.39 | 173.548 | 2.6.13 | | TKYE | 8 | 1.68 | 301.603 | 3.10.8 |
| TDE | 24 | 1.39 | 306.935 | 2.8.21 | | TKYE | 9 | 1.94 | 285.256 | 3.10.9 |
| TDE | 25 | 1.51 | 286.613 | 2.8.22 | | TKYNW | 0 | 3.45 | 122.917 | 3.11.0 |
| TDE | 26 | 1.57 | 313.387 | 2.6.14 | | TKYNW | 1 | 1.92 | 75.160 | 3.11.1 |
| TDE | 27 | 1.54 | 393.387 | 2.8.23 | | TKYINT | 0 | 1.60 | 152.548 | 3.12.0 |
| TDE | 28 | 1.32 | 236.290 | 2.8.24 | | TKYINT | 1 | 1.94 | 165.224 | 3.12.1 |
| TDE | 29 | 1.40 | 231.129 | 2.6.15 | | TKYINT | 2 | 2.00 | 160.737 | 3.12.2 |
| TDE | 30 | 1.33 | 271.935 | 2.8.25 | | TKYINT | 3 | 1.67 | 175.481 | 3.12.3 |
| TDE | 31 | 1.59 | 227.097 | 2.8.26 | | | | | | |
| TDWW | 1 | 1.52 | 114.500 | 2.9.1 | | | | | | |
| TDWW | 2 | 1.60 | 104.625 | 2.9.2 | | | | N | 62.000 | |

| TDWW | 3 | 1.69 | 269.500 | 2.9.3 | | | | Mean | 223.377 | |
|------|---|------|---------|-------|--|--|--|------|---------|--|
| TDWW | 4 | 1.62 | 104.625 | 2.9.4 | | | | Max | 415.323 | |
| TDWW | 5 | 1.62 | 181.250 | 2.9.5 | | | | Min | 75.1603 | |
| TDWW | 6 | 1.99 | 201.125 | 2.9.6 | | | | | | |
| TDWW | 7 | 2.30 | 279.500 | 2.9.7 | | | | | | |
| | | | | | | | | | | |

| Marl | | | | | | | | | |
|---|---|---|---|---|---|---|---|---|---|
| Core | Depth | SI | OM | locator | | Core | Depth | SI | OM | locator |
| Mowry 50m | 13 | 1.38 | 57.781 | 2.6.13 | | TKYE | 26 | 1.41 | 60.125 | 3.10.26 |
| Mowry 50m | 14 | 1.36 | 35.062 | 2.6.14 | | TKYE | 27 | 1.33 | 65.531 | 3.10.27 |
| Mowry 50m | 15 | 1.36 | 76.969 | 2.6.15 | | TKYE | 28 | 1.36 | 46.625 | 3.10.28 |
| Mowry 50m | 16 | 1.31 | 62.500 | 2.6.16 | | TKYE | 29 | 1.43 | 41.344 | 3.10.29 |
| Mowry 50m | 17 | 1.36 | 38.250 | 2.6.17 | | TKYE | 30 | 1.38 | 48.750 | 3.10.30 |
| Mowry 50m | 18 | 1.36 | 41.406 | 2.6.18 | | TKYE | 31 | 1.27 | 49.563 | 3.10.31 |
| Mowry 50m | 19 | 1.40 | 38.437 | 2.6.19 | | TKYNW | 2 | 1.42 | 37.250 | 3.11.2 |
| Mowry 50m | 20 | 1.38 | 24.500 | 2.6.20 | | TKYNW | 3 | 1.50 | 31.875 | 3.11.3 |
| Mowry 50m | 21 | 1.36 | 51.688 | 2.6.21 | | TKYNW | 4 | 1.08 | 57.563 | 3.11.4 |
| Mowry 50m | 22 | 1.36 | 46.875 | 2.6.22 | | TKYNW | 5 | 1.42 | 51.750 | 3.11.5 |
| Mowry 50m | 23 | 1.50 | 32.438 | 2.6.23 | | TKYNW | 6 | 1.43 | 45.500 | 3.11.6 |
| Mowry 50m | 24 | 1.39 | 39.250 | 2.6.24 | | TKYNW | 7 | 1.46 | 61.281 | 3.11.7 |
| Mowry 50m | 25 | 1.41 | 52.094 | 2.6.25 | | TKYNW | 8 | 1.41 | 51.813 | 3.11.8 |
| Mowry 50m | 26 | 1.41 | 44.188 | 2.6.26 | | TKYNW | 9 | 1.38 | 64.062 | 3.11.9 |
| Mowry 50m | 28 | 1.36 | 57.031 | 2.6.27 | | TKYNW | 10 | 1.28 | 83.875 | 3.11.10 |
| Mowry 50m | 29 | 1.43 | 74.187 | 2.6.28 | | TKYNW | 11 | 1.39 | 94.688 | 3.11.11 |
| TDWW | 19 | 1.41 | 51.688 | 2.9.19 | | TKYNW | 12 | 1.38 | 84.375 | 3.11.12 |
| TDWW | 20 | 1.35 | 46.875 | 2.9.20 | | TKYNW | 13 | 1.36 | 91.375 | 3.11.13 |
| TDWW | 21 | 1.41 | 32.438 | 2.9.21 | | TKYINT | 4 | 1.34 | 68.500 | 3.12.4 |
| TDWW | 22 | 1.41 | 39.250 | 2.9.22 | | TKYINT | 5 | 1.42 | 74.625 | 3.12.5 |
| TDWW | 23 | 1.42 | 52.094 | 2.9.23 | | TKYINT | 6 | 1.32 | 91.313 | 3.12.6 |
| TDWW | 24 | 1.39 | 44.188 | 2.9.24 | | TKYINT | 7 | 1.55 | 64.063 | 3.12.7 |
| TDWW | 25 | 1.42 | 57.031 | 2.9.25 | | TKYINT | 8 | 1.31 | 88.938 | 3.12.8 |
| TDWW | 26 | 1.40 | 74.188 | 2.9.26 | | TANGLIN | 1 | 1.00 | 57.313 | 4.0.1 |
| TDWW | 27 | 1.36 | 64.906 | 2.9.27 | | TANGLIN | 2 | 1.50 | 54.688 | 4.0.2 |
| TDWW | 28 | 1.36 | 56.906 | 2.9.28 | | TANGLIN | 3 | 2.13 | 79.375 | 4.0.3 |
| TDWW | 29 | 1.46 | 82.938 | 2.9.29 | | TANGLIN | 4 | 1.92 | 68.063 | 4.0.4 |
| TKYE | 10 | 1.36 | 26.063 | 3.10.10 | | TANGLIN | 5 | 1.17 | 67.250 | 4.0.5 |
| TKYE | 11 | 1.38 | 37.844 | 3.10.11 | | TANGLIN | 6 | 1.83 | 45.062 | 4.0.6 |
| TKYE | 12 | 1.44 | 24.844 | 3.10.12 | | TANGLIN | 7 | 1.38 | 36.812 | 4.0.7 |
| TKYE | 13 | 1.38 | 39.125 | 3.10.13 | | TANGLIN | 8 | 1.32 | 29.500 | 4.0.8 |
| TKYE | 14 | 1.36 | 48.875 | 3.10.14 | | TANGLIN | 9 | 1.33 | 25.625 | 4.0.9 |
| TKYE | 15 | 1.36 | 45.406 | 3.10.15 | | TANGLIN | 10 | 1.35 | 37.938 | 4.0.10 |
| TKYE | 16 | 1.31 | 56.875 | 3.10.16 | | TANGLIN | 11 | 1.43 | 31.375 | 4.0.11 |
| TKYE | 17 | 1.36 | 37.875 | 3.10.17 | | TANGLIN | 12 | 1.42 | 37.313 | 4.0.12 |
| TKYE | 18 | 1.36 | 50.187 | 3.10.18 | | TANGLIN | 13 | 1.33 | 41.875 | 4.0.13 |
| TKYE | 19 | 1.40 | 57.219 | 3.10.19 | | TANGLIN | 14 | 1.33 | 28.187 | 4.0.14 |
| TKYE | 20 | 1.38 | 39.781 | 3.10.20 | | TANGLIN | 15 | 1.31 | 19.063 | 4.0.15 |
| TKYE | 21 | 1.36 | 28.687 | 3.10.21 | | TANGLIN | 16 | 1.38 | 26.812 | 4.0.16 |
| TKYE | 22 | 1.36 | 35.781 | 3.10.22 | | TANGLIN | 17 | 1.42 | 35.625 | 4.0.17 |
| TKYE | 23 | 1.50 | 42.125 | 3.10.23 | | TANGLIN | 18 | 1.28 | 38.187 | 4.0.18 |
| TKYE | 24 | 1.39 | 43.344 | 3.10.24 | | TANGLIN | 19 | 1.44 | 40.375 | 4.0.19 |
| TKYE | 25 | 1.41 | 50.406 | 3.10.25 | | TANGLIN | 20 | 1.43 | 36.188 | 4.0.20 |
| | | | | | | TANGLIN | 21 | 1.33 | 36.812 | 4.0.21 |
| | | | | | | TANGLIN | 22 | 1.50 | 44.250 | 4.0.22 |
| | | | | | | | | | | |

Marl continued

| Core | Depth | SI | OM | locator | | Core | Depth | SI | OM | locator | |
|---|---|---|---|---|---|---|---|---|---|---|---|---|
| TANGLIN | 23 | 1.25 | 55.813 | 4.0.23 | | sixfour | 10 | 1.30 | 62.250 | 6.0.10 | |
| fivefive | 3 | 1.25 | 23.062 | 5.0.3 | | sixfour | 11 | 1.30 | 84.875 | 6.0.11 | |
| fivefive | 4 | 1.29 | 22.375 | 5.0.4 | | sixfour | 12 | 1.40 | 84.750 | 6.0.12 | |
| fivefive | 5 | 1.33 | 32.062 | 5.0.5 | | sixfour | 13 | 1.31 | 87.375 | 6.0.13 | |
| fivefive | 6 | 1.25 | 31.125 | 5.0.6 | | sixfour | 14 | 1.30 | 59.625 | 6.0.14 | |
| fivefive | 7 | 1.57 | 41.438 | 5.0.7 | | sixfour | 15 | 1.20 | 58.875 | 6.0.15 | |
| fivefive | 8 | 1.80 | 54.812 | 5.0.8 | | sixfour | 16 | 1.00 | 54.500 | 6.0.16 | |
| fivefive | 9 | 1.98 | 50.750 | 5.0.9 | | sixfour | 17 | 1.10 | 47.687 | 6.0.17 | |
| fivefive | 10 | 1.81 | 68.875 | 5.0.10 | | sixfour | 18 | 1.30 | 49.875 | 6.0.18 | |
| fivefive | 11 | 1.67 | 44.125 | 5.0.11 | | sixfour | 19 | 1.50 | 56.812 | 6.0.19 | |
| fivefive | 12 | 1.17 | 52.250 | 5.0.12 | | sixfour | 20 | 1.20 | 48.000 | 6.0.20 | |
| fivefive | 13 | 1.17 | 48.938 | 5.0.13 | | sixfour | 21 | 1.20 | 56.250 | 6.0.21 | |
| fivefive | 14 | 1.30 | 52.375 | 5.0.14 | | sixfour | 22 | 1.32 | 50.000 | 6.0.22 | |
| fivefive | 16 | 1.07 | 53.438 | 5.0.16 | | sixfour | 24 | 1.10 | 84.062 | 6.0.24 | |
| fivefive | 17 | 1.13 | 56.500 | 5.0.17 | | sixfour | 25 | 1.35 | 88.063 | 6.0.25 | |
| fivefive | 18 | 1.21 | 86.813 | 5.0.18 | | sixfour | 26 | 1.40 | 88.875 | 6.0.26 | |
| fivefive | 19 | 1.36 | 75.813 | 5.0.19 | | sixfour | 27 | 1.30 | 82.937 | 6.0.27 | |
| fivefive | 20 | 1.23 | 76.875 | 5.0.20 | | sixfour | 28 | 1.50 | 41.375 | 6.0.28 | |
| fivefive | 21 | 1.32 | 70.875 | 5.0.21 | | sixfour | 29 | 0.00 | 74.437 | 6.0.29 | |
| fivefive | 22 | 1.18 | 86.625 | 5.0.22 | | sixfour | 30 | 0.00 | 42.375 | 6.0.30 | |
| fivefive | 23 | 1.27 | 83.688 | 5.0.23 | | sixfour | 31 | 0.00 | 49.812 | 6.0.31 | |
| fivefive | 24 | 1.10 | 63.437 | 5.0.24 | | | | | | | |
| fivefive | 25 | 1.31 | 87.500 | 5.0.25 | | | | | | | |
| sixfour | 3 | 0.00 | 46.000 | 6.0.3 | | | | N | 141.000 | | |
| sixfour | 4 | 0.00 | 82.812 | 6.0.4 | | | | Mean | 54.685 | | |

Marl continued

| | | | | | | | | | | | |
|---|---|---|---|---|---|---|---|---|---|---|---|
| sixfour | 5 | 0.00 | 98.875 | 6.0.5 | | | | Max | 98.875 | | |
| sixfour | 6 | 0.00 | 80.250 | 6.0.6 | | | | Min | 19.063 | | |
| sixfour | 7 | 1.00 | 63.000 | 6.0.7 | | | | | | | |
| sixfour | 8 | 0.00 | 75.062 | 6.0.8 | | | | | | | |
| sixfour | 9 | 1.30 | 70.813 | 6.0.9 | | | | | | | |
| | | | | | | | | | | | |

| Saw grass peat marl | | | | | | | | | | |
|---|---|---|---|---|---|---|---|---|---|---|
| Core | Depth | SI | OM | locator | | Core | Depth | SI | OM | locator |
| TKYNW | 14 | 1.36 | 198.264 | 3.11.14 | | TANGLIN | 51 | 1.25 | 165.698 | 4.0.51 |
| TKYNW | 15 | 1.37 | 221.759 | 3.11.15 | | TANGLIN | 52 | 1.25 | 146.860 | 4.0.52 |
| TKYNW | 17 | 1.38 | 163.657 | 3.11.16 | | TANGLIN | 53 | 1.38 | 200.349 | 4.0.53 |
| TKYNW | 18 | 1.39 | 224.306 | 3.11.17 | | TANGLIN | 54 | 1.17 | 144.767 | 4.0.54 |
| TKYNW | 19 | 1.40 | 257.639 | 3.11.18 | | TANGLIN | 55 | 1.19 | 198.256 | 4.0.55 |
| TKYNW | 20 | 1.35 | 235.301 | 3.11.19 | | TANGLIN | 56 | 1.17 | 238.372 | 4.0.56 |
| TKYINT | 9 | 1.18 | 228.009 | 3.12.9 | | TANGLIN | 57 | 1.20 | 165.930 | 4.0.57 |
| TKYINT | 10 | 1.29 | 256.134 | 3.12.10 | | fivefive | 26 | 1.29 | 194.390 | 5.0.26 |
| TKYINT | 11 | 1.29 | 264.583 | 3.12.11 | | fivefive | 27 | 1.26 | 196.098 | 5.0.27 |
| TKYINT | 12 | 1.27 | 210.995 | 3.12.12 | | fivefive | 28 | 1.20 | 206.341 | 5.0.28 |
| TKYINT | 13 | 1.34 | 244.676 | 3.12.13 | | fivefive | 42 | 1.34 | 185.976 | 5.0.29 |
| TKYINT | 15 | 1.43 | 230.093 | 3.12.14 | | fivefive | 43 | 1.26 | 167.683 | 5.0.30 |
| TKYINT | 16 | 1.38 | 261.111 | 3.12.15 | | fivefive | 44 | 1.20 | 151.220 | 5.0.31 |
| TKYINT | 17 | 1.43 | 346.065 | 3.12.16 | | fivefive | 45 | 1.34 | 165.366 | 5.0.32 |
| TKYINT | 18 | 1.36 | 168.866 | 3.12.17 | | fivefive | 46 | 1.20 | 163.293 | 5.0.33 |
| TKYINT | 19 | 1.35 | 244.097 | 3.12.18 | | fivefive | 47 | 1.13 | 124.390 | 5.0.34 |
| TANGLIN | 24 | 1.56 | 189.767 | 4.0.24 | | fivefive | 48 | 1.19 | 163.293 | 5.0.35 |
| TANGLIN | 25 | 1.42 | 122.907 | 4.0.25 | | fivefive | 49 | 1.22 | 140.732 | 5.0.36 |
| TANGLIN | 26 | 1.30 | 119.767 | 4.0.26 | | fivefive | 50 | 1.20 | 159.512 | 5.0.37 |
| TANGLIN | 27 | 1.63 | 264.535 | 4.0.27 | | fivefive | 51 | 1.30 | 129.756 | 5.0.38 |
| TANGLIN | 28 | 1.33 | 162.791 | 4.0.28 | | fivefive | 52 | 1.33 | 188.049 | 5.0.39 |
| TANGLIN | 29 | 1.29 | 172.558 | 4.0.29 | | fivefive | 53 | 1.26 | 219.512 | 5.0.40 |
| TANGLIN | 30 | 1.42 | 119.302 | 4.0.30 | | fivefive | 54 | 1.30 | 240.976 | 5.0.41 |
| TANGLIN | 31 | 1.40 | 159.535 | 4.0.31 | | fivefive | 55 | 1.27 | 262.439 | 5.0.42 |
| TANGLIN | 32 | 1.45 | 173.721 | 4.0.32 | | fivefive | 56 | 1.27 | 267.073 | 5.0.43 |
| TANGLIN | 33 | 1.73 | 160.349 | 4.0.33 | | fivefive | 57 | 1.21 | 274.268 | 5.0.44 |
| TANGLIN | 34 | 1.42 | 169.535 | 4.0.34 | | fivefive | 58 | 1.39 | 217.683 | 5.0.45 |
| TANGLIN | 35 | 1.40 | 122.326 | 4.0.35 | | fivefive | 59 | 1.00 | 205.610 | 5.0.46 |
| TANGLIN | 36 | 1.73 | 140.930 | 4.0.36 | | fivefive | 60 | 1.23 | 199.756 | 5.0.47 |
| TANGLIN | 37 | 1.64 | 126.512 | 4.0.37 | | fivefive | 61 | 1.25 | 226.585 | 5.0.48 |
| TANGLIN | 38 | 1.38 | 162.326 | 4.0.38 | | fivefive | 62 | 1.25 | 177.805 | 5.0.49 |
| TANGLIN | 39 | 1.33 | 182.209 | 4.0.39 | | | | | | |
| TANGLIN | 40 | 1.44 | 142.093 | 4.0.40 | | | | | | |
| TANGLIN | 41 | 1.50 | 105.581 | 4.0.41 | | | | | | |
| TANGLIN | 42 | 1.15 | 141.512 | 4.0.42 | | | | N | 74 | |
| TANGLIN | 43 | 1.38 | 137.791 | 4.0.43 | | | | Mean | 185.152 | |
| TANGLIN | 44 | 1.50 | 157.442 | 4.0.44 | | | | Max | 346.065 | |
| TANGLIN | 45 | 1.13 | 200.930 | 4.0.45 | | | | Min | 104.419 | |
| TANGLIN | 46 | 1.43 | 132.674 | 4.0.46 | | | | | | |
| TANGLIN | 47 | 1.00 | 104.419 | 4.0.47 | | | | | | |
| TANGLIN | 48 | 1.33 | 111.047 | 4.0.48 | | | | | | |
| TANGLIN | 49 | 1.23 | 147.791 | 4.0.49 | | | | | | |
| TANGLIN | 50 | 1.38 | 127.326 | 4.0.50 | | | | | | |

# Appendix 3.2.1.

## Sediment accumulation rates

### Part 1. TANGLIN CORE

**Sedimentation rate 0.6-0.8 mm/yr as shown in figures**

| Lab # | Core | Depth cm | Dry Mass g | Wet Mass g | Po-210 dpm | Po-210 +/- dpm | Po-210 dpm/g | Po-210 dpm/cm3 | Depth Midpoint |
|---|---|---|---|---|---|---|---|---|---|
| 2563 | TANGLIN | 0-1 | 0.8232 | | 8.4859 | 0.342 | 10.308 | 2.828644 | 0.5 |
| 2564 | TANGLIN | 1-2 | 1.4315 | | 15.351 | 0.656 | 10.723 | 5.116852 | 1.5 |
| 2565 | TANGLIN | 2-3 | 1.6409 | | 16.73 | 0.693 | 10.196 | 5.576766 | 2.5 |
| 2566 | TANGLIN | 3-4 | 1.5918 | | 18.655 | 1.121 | 11.72 | 6.218472 | 3.5 |
| 2567 | TANGLIN | 4-5 | 1.979 | | 27.676 | 1.094 | 13.985 | 9.22545 | 4.5 |
| 2568 | TANGLIN | 5-6 | 1.7135 | | 21.885 | 0.845 | 12.772 | 7.294898 | 5.5 |
| 2569 | TANGLIN | 6-7 | 1.8794 | | 14.69 | 0.512 | 7.8161 | 4.896528 | 6.5 |
| 2570 | TANGLIN | 7-8 | 1.8121 | | 10.027 | 0.314 | 5.5335 | 3.342404 | 7.5 |
| 2571 | TANGLIN | 8-9 | 2.1982 | | 7.7346 | 0.261 | 3.5186 | 2.578186 | 8.5 |
| 2572 | TANGLIN | 9-10 | 1.8376 | | 8.7394 | 0.289 | 4.7559 | 2.913118 | 9.5 |
| 2573 | TANGLIN | 10-11 | 1.7091 | | 7.001 | 0.268 | 4.0963 | 2.333656 | 10.5 |
| 2574 | TANGLIN | 11-12 | 2.216 | | 5.5041 | 0.224 | 2.4838 | 1.834716 | 11.5 |
| 2575 | TANGLIN | 12-13 | 2.4322 | 4.7372 | 3.499 | 0.104 | 1.4386 | 1.166334 | 12.5 |
| 2576 | TANGLIN | 13-14 | 2.219 | 4.3974 | 3.7495 | 0.116 | 1.6897 | 1.24982 | 13.5 |
| 2577 | TANGLIN | 14-15 | 2.237 | 4.4937 | 2.6795 | 0.107 | 1.1978 | 0.893152 | 14.5 |
| 2578 | TANGLIN | 15-16 | 2.0675 | 4.3153 | 2.4112 | 0.078 | 1.1662 | 0.803738 | 15.5 |
| 2579 | TANGLIN | 16-17 | 2.231 | 4.5077 | 2.4601 | 0.078 | 1.1027 | 0.82004 | 16.5 |
| 2580 | TANGLIN | 17-18 | 2.3363 | 4.7884 | 2.7639 | 0.093 | 1.183 | 0.92131 | 17.5 |
| 2581 | TANGLIN | 18-19 | 2.1417 | 4.3315 | 3.3345 | 0.104 | 1.5569 | 1.1115 | 18.5 |
| 2582 | TANGLIN | 19-20 | 1.9312 | 3.9327 | 2.3045 | 0.072 | 1.1933 | 0.76817 | 19.5 |
| 2583 | TANGLIN | 20-21 | 2.233 | 4.5945 | 2.6528 | 0.111 | 1.188 | 0.88426 | 20.5 |
| 2586 | TANGLIN | 23-24 | 2.1942 | 4.7304 | 3.5568 | 0.156 | 1.621 | 1.1856 | 23.5 |
| 2587 | TANGLIN | 24-25 | 1.2606 | 3.6172 | 2.5772 | 0.149 | 2.0444 | 0.859066 | 24.5 |
| 2588 | TANGLIN | 25-26 | 1.5768 | 4.2654 | 2.5683 | 0.136 | 1.6288 | 0.856102 | 25.5 |
| 2627 | TANGLIN | 38-29 | 1.5973 | 3.2895 | 2.3756 | 0.104 | 1.4873 | 0.791882 | 28.5 |
| 2628 | TANGLIN | 30-31 | 1.3698 | 3.1837 | 1.9755 | 0.13 | 1.4422 | 0.658502 | 30.5 |

**Part 2. T6-4 core**

**Upper core Periphyton. Not analyzed for Pb-210.**
**Sedimentation rate 0.6-0.8 mm/yr as shown in figures**

| Lab # | Core | Depth | Dry Mass | Wet Mass | Po-210 | Po-210 | Po-210 | Po-210 | Depth |
|---|---|---|---|---|---|---|---|---|---|
| | | cm | g | g | dpm | +/- dpm | dpm/g | dpm/cm3 | Midpoint |
| | T6-4 | 0-1 | | | | | | | 0.5 |
| | T6-4 | 1-2 | | | | | | | 1.5 |
| | T6-4 | 2-3 | | | | | | | 2.5 |
| 2589 | T6-4 | 3-4 | 0.4404 | 3.0863 | 5.3382 | 0.153 | 12.121 | 1.779388 | 3.5 |
| 2590 | T6-4 | 4-5 | 1.4687 | 3.5329 | 20.791 | 0.608 | 14.156 | 6.930326 | 4.5 |
| 2591 | T6-4 | 5-6 | 1.4392 | 3.6394 | 26.129 | 0.704 | 18.155 | 8.709714 | 5.5 |
| 2592 | T6-4 | 6-7 | 1.7541 | 3.599 | 13.397 | 0.357 | 7.6377 | 4.46576 | 6.5 |
| 2593 | T6-4 | 7-8 | 2.042 | 4.5577 | 13.786 | 0.372 | 6.751 | 4.595188 | 7.5 |
| 2594 | T6-4 | 8-9 | 1.9485 | 4.2954 | 15.548 | 0.387 | 7.9793 | 5.182554 | 8.5 |
| 2595 | T6-4 | 9-10 | 1.9786 | 4.3243 | 12.112 | 0.323 | 6.1217 | 4.037462 | 9.5 |
| 2596 | T6-4 | 10-11 | 2.0546 | 4.2018 | 8.7319 | 0.291 | 4.2499 | 2.910648 | 10.5 |
| 2597 | T6-4 | 11-12 | 2.2477 | 4.1681 | 7.0425 | 0.189 | 3.1332 | 2.347488 | 11.5 |
| 2598 | T6-4 | 12-13 | 1.7241 | 3.5726 | 5.1144 | 0.171 | 2.9664 | 1.704794 | 12.5 |
| 2599 | T6-4 | 13-14 | 2.3862 | 4.4567 | 4.0459 | 0.128 | 1.6955 | 1.34862 | 13.5 |
| 2600 | T6-4 | 14-15 | 2.101 | 3.911 | 3.3152 | 0.127 | 1.5779 | 1.105078 | 14.5 |
| 2601 | T6-4 | 15-16 | 2.1426 | 3.7766 | 3.2782 | 0.112 | 1.53 | 1.092728 | 15.5 |
| 2602 | T6-4 | 16-17 | 2.6067 | 4.7182 | 3.3864 | 0.106 | 1.2991 | 1.12879 | 16.5 |
| 2603 | T6-4 | 17-18 | 2.6345 | 4.3513 | 3.4931 | 0.096 | 1.3259 | 1.164358 | 17.5 |
| 2604 | T6-4 | 18-19 | 2.6567 | 4.8618 | 3.6635 | 0.113 | 1.379 | 1.221168 | 18.5 |
| 2605 | T6-4 | 19-20 | 2.6567 | 4.8618 | 3.4886 | 0.111 | 1.3131 | 1.162876 | 19.5 |
| 2606 | T6-4 | 20-21 | 2.36 | 4.0636 | 3.3967 | 0.106 | 1.4393 | 1.132248 | 20.5 |
| 2607 | T6-4 | 21-22 | 2.118 | 0.09 | 3.3123 | 0.287 | 1.5639 | 1.10409 | 21.5 |
| 2608 | T6-4 | 22-23 | 2.0632 | 4.5079 | 3.0292 | 0.095 | 1.4682 | 1.009736 | 22.5 |
| 2609 | T6-4 | 23-24 | 2.2123 | 3.3323 | 3.2693 | 0.11 | 1.4778 | 1.089764 | 23.5 |